Department of Applied Geology

Basin Record of Mesozoic Tectonic Events in Southeast South China

Chongjin Pang

This thesis is presented for the Degree of
Doctor of Philosophy
of
Curtin University

March 2014

Declaration

To the best of my knowledge and belief this thesis contains no material previously published by any other person except where due acknowledgment has been made. This thesis contains no material which has been accepted for the award of any other degree or diploma in any university.

Chongjin Pang

Date: 21-03-2014

Abstract

Upper Triassic to Middle Jurassic strata in southeastern South China were deposited on top of the Indosinian Orogen, a northwest-verging fold-and-thrust belt that spanned ~250 to ~200 Ma. The strata are preserved over a wide area, thereby preserving much of the Mesozoic tectonic history of southeastern South China. The sedimentary basin represented by those strata evolved in time from intracontinental terrestrial to shallow-marine and back to terrestrial environments. The basin was subsequently inverted and succeeded by a basin-and-range province, signifying continental-scale vertical movements. Several competing tectonic models have been proposed to explain the formation of the basin and contemporaneous magmatic events. The subsidence mechanism of this synorogenic to post-orogenic Late Triassic to Middle Jurassic basin is enigmatic.

In this study, field-based basin analysis supplemented by geochronology was carried out. Stratigraphic, palaeontological and geochronological data are analysed to establish the three-dimensional geometry of the basin and continental vertical movements. Results are then applied to understand the Mesozoic tectonic evolution and test the related geodynamics of South China.

An overall fining-upward basal sequence and three overlying coarsening-upward sequences (>2400 m-thick) are recorded in the Daxi-Zhuyuan sections. Four facies associations (prodelta, delta-front, delta-plain, fluvial) are recognised based on lithology, sedimentary structures and palaeontology. The facies associations are interpreted to represent a Carnian to early Toarcian fluvial to marine-influenced, fluvial-dominated deltaic succession. Tectonic controls, rather than eustasy and climate, are interpreted to have played a primary role in the cyclic development of the Daxi-Zhuyuan succession. Four regional-scale tectonostratigraphic stages are recognised. Stage 1 is a retrogradational-progradational cycle characterised by increasing then slowly decreasing subsidence rates, accompanied by slow to medium sedimentation rates, possibly in a compressive tectonic setting. Stage 2 is mainly an aggradational cycle responding to a complex interplay between moderate subsidence rates, high sedimentation rates and eustasy. Stage 3 represents a retrogradational-aggradational-progradational cycle reflecting changes of high sedimentation and high

subsidence rates to lower subsidence and sedimentation rates prior to intracontinental uplift. Stage 4 records continued uplift and subsequent development of a Late Jurassic-Cretaceous basin-and-range province.

A Carnian to Bajocian sedimentary succession (>2700 m-thick) is preserved in the Gaosi-Songxi sections. Diverse facies associations (deltaic, fluvial, shallow-marine, interdistributary bay and lacustrine) are recognised. The influence of palaeoclimate on sedimentary structure, variation of river-style, and sediment supply are identified, particularly for the Middle Jurassic strata. Nevertheless, the occurrence of volcanic rocks, the change of depositional environments and the cyclic development of stratigraphic stacking patterns through time imply that tectonics played an important role on the stratigraphic evolution.

Basin-scale chronostratigraphic results show that the southeastern South China basin was formed during the Carnian to the Bajocian, lasting ~70 Myrs, along with occasional volumes of coeval magmatic rocks between ~200 and 190 Ma. Five basin-wide depositional sequences are defined on the basis of long-term stacking pattern of lithofacies assemblages. Sequence 1 records an overall retrogradation of fluvial deposits. Sequence 2 documents aggradation to progradation and to aggradation of shallow-marine influenced deltaic systems, and aggradation or retrogradation of fluvial deposits. Sequence 3 preserves shallow-marine influenced deltaic and fluvial deposits, showing more complicated stacking patterns that depend on where they were within the depositional systems, e.g., distal or proximal parts. Sequence 4 also documents shallow-marine influenced deltaic and fluvial deposits, but showing an overall progradational stacking pattern. Sequence 5 is dominated by lacustrine, deltaic and fluvial deposits, and is broadly progradational.

Isopachs indicate that loci of subsidence and accumulation varied through time. Those isopachs and palaeocurrents are consistent with detrital zircon U-Pb age populations of sandstones, which show spatial and temporal variations for the Upper Triassic sandstones, implying heterogeneous provenances. However, detrital zircon U-Pb age distributions for the Lower Jurassic sandstones are comparable basin-wide, indicating common provenances. The combined results indicated pre-isolated depositional systems were gradually coalesced, implying basin enlargement.

Tectonostratigraphic analysis shows that the Middle Permian to Lower Triassic siliciclastic and carbonate strata represent foreland basin packages that prograded westward as a result of the cratonward migration of associated fold-and-thrust belts during the Indosinian Orogeny. Orogeny was succeeded by synorogenic to post-orogenic sedimentary rocks of the Late Triassic to Middle Jurassic basin that initiated on the orogen that was still active to the northwest. The initiation of this basin during the Late Triassic appears to have been caused by crustal flexure (i.e. sagging). Stratigraphic evolution and the onset of anorogenic magmatism during the Early Jurassic imply that the subsidence involved a whole lithospheric process. If lithospheric extension is excluded, one interpretation is that rapid subsidence and resulting sediment accumulation were induced by increased but differentiated gravitational pull force of a subducted flat-slab, while subsequent slab break-off produced anorogenic magmatism. Subsequent termination of the basin and development of a basin-and-range province can be explained by lithospheric rebound due to the break-up and foundering of the subducted flat-slab.

Keywords: Mesozoic, intracontinental basin, basin record, synorogenic to post-orogenic, vertical movement, flat subduction, tectonics, South China

Acknowledgements

First and foremost, I would like to express sincere thanks to my supervisors, Professors Zheng-Xiang Li, Bryan Krapež and Yi-Gang Xu, without whom this thesis could not have been completed. Thank you for your endless guidance, tireless editing, patience and encouragement. I thank Professor Zheng-Xiang Li for the weekly discussions on data analysis and interpretation, and on PhD direction in general, pulling me back on track when I got lost, and training me to understand plate tectonics. I am also fortunate to have worked with Professor Bryan Krapež during my PhD study. I particularly thank him for patiently teaching me how to log and understand sedimentary rocks in the field and how to do the field-based basin analysis, tireless editing my written English, and encouraging me to think differently when interpreting sedimentary rocks. I am also grateful to Professor Yi-Gang Xu for supporting my fieldwork in South China, and his invaluable suggestions and discussions on my thesis and paper throughout this project. Thank you all for everything.

I would like to thank Dr. Hai-Quan Liu, Mr Jun Cao, and my girlfriend Dr. Shunv Wen for the many months of field assistance. Without your help, I could not have obtained such fruitful, first-hand field data. I also thank Drs. Wu-Xian Li, Xuan-Ce Wang, Ji-Hua Tao, Ming-Dao Sun, and Mr Juan-Peng Guan, for assisting fieldwork at times. I thank Profs. Zhuo-Ting Liao, Chu-Zhen Chen, Xiang-Wu Wu, and Shi-Xuan Wen from the Nanjing Institute of Geology and Palaeontology, Chinese Academy of Sciences for fossil identification.

I would like to thank Drs. Allen Kennedy, Richard Taylor and Mr Hao Gao for assisting SHIRMIP zircon U-Pb age analysis and Ms. Elaine Miller for CL imaging at Curtin University. I also thank Drs. Shunv Wen, Hong-Xia Li, He Li and Hong Zhang for assisting LA-ICPMS zircon U-Pb age dating and Prof. Xiao-Long Huang and Ms. Lin-Li Chen for CL imaging at the Guangzhou Institute of Geochemistry, Chinese Academy of Sciences.

Thank you to Mr Ying-Chao (Leo) Liu for teaching me ArcGIS. Without your help I would not have been able to draw such great geological maps. Thank you Drs. Xuan-Ce Wang, Hui-Qing Huang, Li-Feng Meng, and Robert Madden, Mr

Kong-Yang Zhu and Jia-Wen Niu, and Ms. Wei-Hua Yao, Li-Ping Liu, Ni Tao, Qian Wang, Ying Jia Teoh, and Fiona Mothersole at Curtin University, Drs. Hong-Yan Li, Yu-Ting Zhong, and Xun Wei at the Guangzhou Institute of Geochemistry, and Mr Mao Luo, Mr Ben Li, Drs. Jian-Wei Zi, and Yong-Jun Lv at University of Western Australia, for your helps and academic discussions.

I thank Profs. Xiao-Long Huang, Bin He, Lai-Xi Tong, Tou-Ping Peng, Wei-Guang Zhu, and Dr. Shan Li for helpful discussions during their visit to Western Australia, and Thank you to Prof. Simon Wilde for constructive suggestions and comments on my work.

I would like to thank my friends Mr Wai How Low, Ms Cheau May Lo, and Ms Ee Wah Chang for making my life enjoyable.

Finally, I would like to thank my parents, my brothers and sister for great encouragement and support during my entire PhD study.

This PhD work was supported by the CAS/SAFEA International Partnership Program for Creative Research Teams (KZCX2-YW-Q04-06) and by the Australian Research Council (grants DP110104799). I appreciate the TIGeR Top-Up Award and the China Scholarship Council–Curtin International Postgraduate Research Scholarship (CSC-CIPRS) that support my PhD study at Curtin University.

Table of Contents

Table of Figures

Table of Tables

Chapter 1: Introduction

1.1. Background

Sedimentary basins are sensitive recorders of dynamic processes controlling the deformation of the lithosphere and its interaction with the deep mantle and surfaces processes (Cloetingh and Ziegler, 2007). The stratigraphic record is controlled by: 1) sediment supply from the eroding source region, 2) grain size distribution of that sediment supply; and 3) area available (i.e. accommodation) for sediment accumulation in the downstream regions (Armitage et al., 2011). These factors are in turn influenced by external or 'allogenic' controls, such as eustatic change, climate change and tectonic activity (Yang et al., 1998; Blum and Törnqvist, 2000; Rasmussen, 2004; Hampson et al., 2012). In particular, for intracontinental basins, tectonic activity or climate change is generally the primary control on sediment supply and accommodation creation.

Stratigraphic patterns (aggradation, progradation and retrogradation) of sedimentation units are reliable indicators of relationships between factors that controlled sediment supply and factors that controlled accommodation generation (e.g., Posamentier et al., 1988; Van Wagoner et al., 1990; Krapez, 1996; Catuneanu et al., 2009). For instance, an aggradational stacking pattern implies that the factors are balanced, whereas retrogradational and progradational stacking patterns imply that the factors are imbalanced respectively in favour of accommodation and sediment supply (Van Wagoner et al., 1990; Krapez, 1996). The longer-term stacking pattern of basin-scale sequence packages can further be applied to define basin geometry (e.g., foreland, rift or strike-slip basin) and evolution, by combining with associated fault pattern and magmatism.

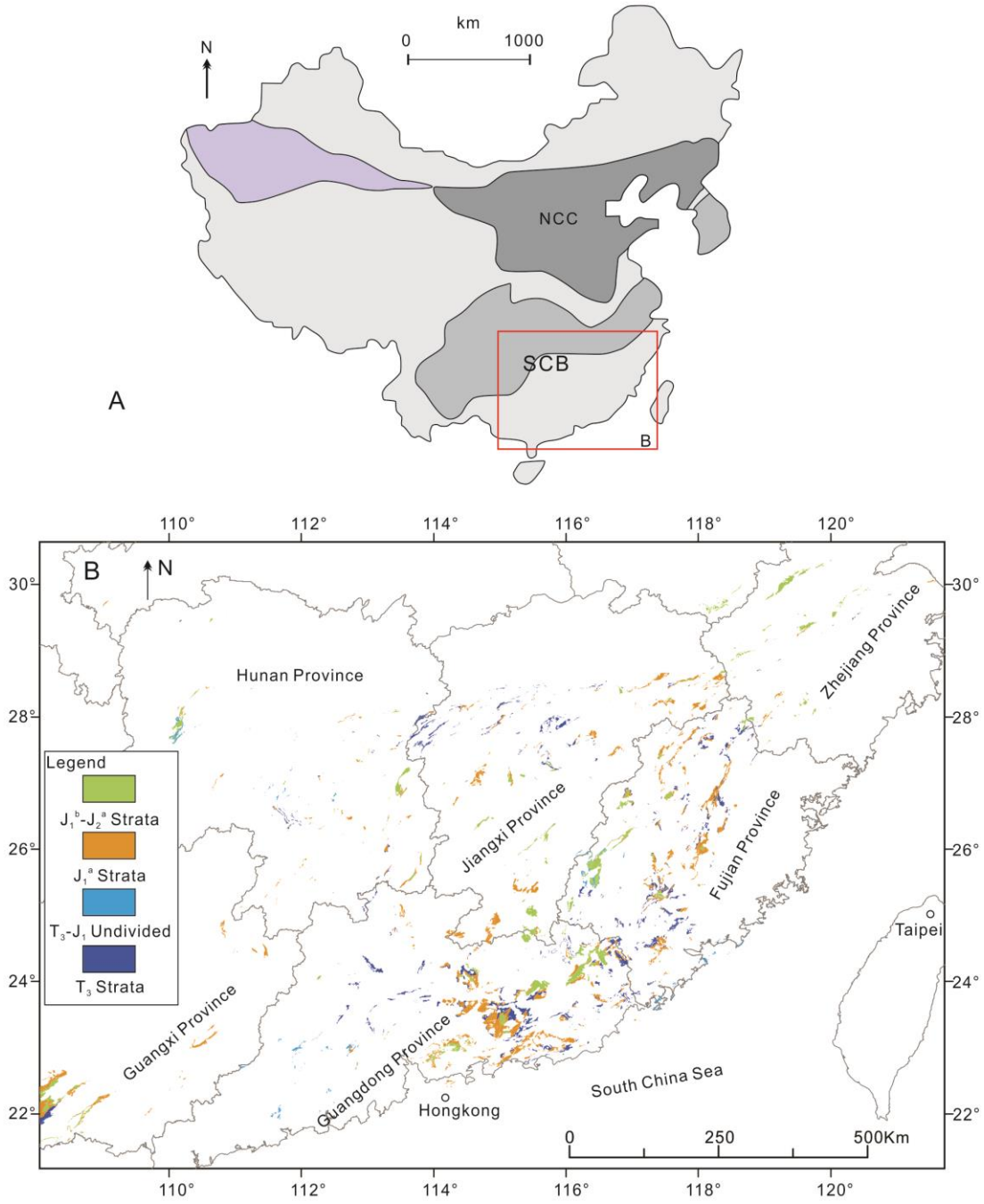

Figure 1.1 Distribution of the Upper Triassic to Middle Jurassic strata in southeastern South China. (A) Location of the studied basin within China (modified after Zhu et al., 2012). SCB = South China Block; NCC = North China Craton. (B) Distribution of the Upper Triassic to Middle Jurassic Strata in southeastern South China (modified after 1:200,000 scale maps). T_3 = Late Triassic; J_1^a = early-Early Jurassic, J_1^b = late-Early Jurassic, J_2^a = early-Middle Jurassic.

Sedimentary basins are formed in varied tectonic settings, such as divergent, convergent and transform settings (Ingersoll, 1988; Allen and Allen, 2005; Ingersoll, 2012). It is commonly recognised that tectonic setting exerts first-order control on basin formation (Xie and Heller, 2009). Basins in similar tectonic settings could

show similar patterns of subsidence, and thus differences in subsidence histories between basins may reflect how fundamental driving mechanisms vary as well as secondary controls, such as sea-level change and sediment loading (Xie and Heller, 2009). The driving mechanisms of subsidence are principally related to processes within the lithosphere (Allen and Allen, 2005). The mechanisms of subsidence in most sedimentary basin systems have been defined (McKenzie, 1981; DeCelles and Giles, 1996; Allen and Allen, 2005; Cloetingh and Ziegler, 2007; Xie and Heller, 2009; Ingersoll, 2012), whereas the subsidence mechanism of synconvergent basins formed on active orogens related to low-angle subduction is poorly understood (e.g., Dalmayrac and Molnar, 1981; Allmendinger et al., 1997; Druschke et al., 2009b). Strata of the Late Triassic to Middle Jurassic age formed on top of the orogenic belt during the Indosinian Orogeny (Li and Li, 2007) are widely preserved in southeastern South China (**Fig. 1.1**). The basin record of Mesozoic South China here will serve as an example to show how a synorogenic basin formed and evolved through time and associated geodynamics.

The South China Block was formed due to the collision between the Yangtze Craton to the northwest and the Cathaysia Block to the southeast during the Early Neoproterozoic time (~1200–880 Ma) (Li et al., 2002; Li et al., 2008; Li et al., 2014b) (see **Chapter 2**). The South China Block had undergone a series of tectonic events from the Early Neoproterozoic to the Early Paleozoic (Li et al., 2008; Li et al., 2010b). Since the Late Paleozoic, a shallow-marine carbonate platform covered the entire South China Block. This was followed by the development of a ~1300 km-wide fold-and-thrust belt in response to the Indosinian Orogeny during the Permo-Middle Triassic time, which is interpreted to be formed by the cratonward migration of flat subduction of an oceanic plateau (Li and Li, 2007; Li et al., 2012b) (**Fig. 1.2**). A broad but shallow basin formed during the late stage of the orogeny since the Late Triassic, and evolved into a shallow-marine basin during the Early Jurassic, followed by the basin uplift and the development of a basin-and-range province during the Middle Jurassic (Li and Li, 2007) (**Fig. 1.2**), implying significant vertical movements of the continent (Li et al., 2014b). The formation of this Late Triassic to Early Jurassic basin is enigmatic. This basin was interpreted to be an intracontinental sag formed during the gravitational pull of the eclogitising, flat-subducted oceanic slab (Li and Li, 2007) (**Fig. 1.2**), whereas others recognized its post-orogenic nature but

give no tectonic mechanism for its formation (e.g., Shu et al., 2009). To better understand the basin formation, this project focuses on the stratigraphic record, palaeontology and geochronological data of the Late Triassic to Middle Jurassic basin(s) to: 1) establish the 3D geometry and history of the basin(s) and continental vertical movements; 2) understand the Mesozoic tectonic evolution in this region; 3) test the flat subduction hypothesis as well as other tectonic models.

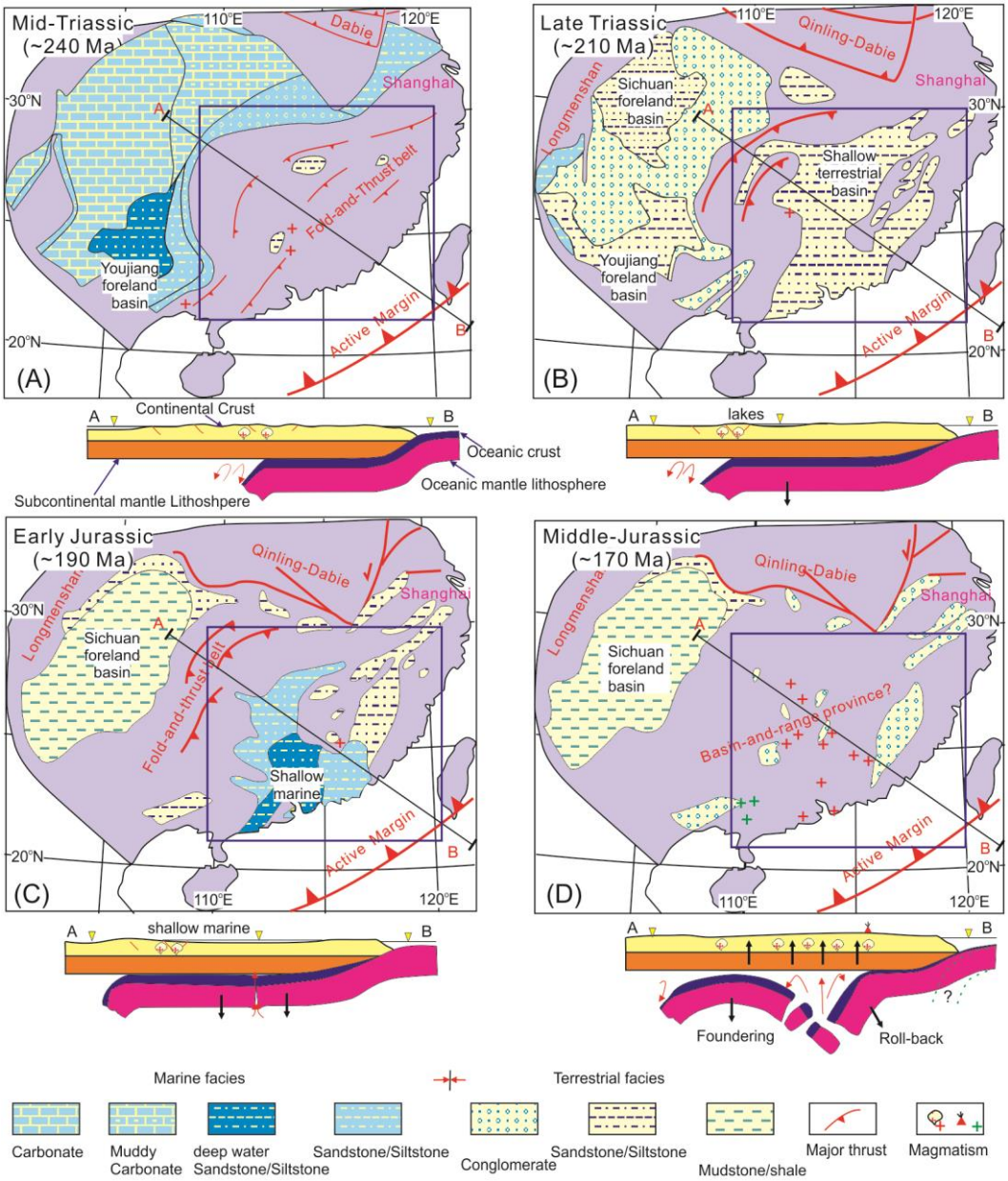

Figure 1.2 Palaeogeography of Middle Triassic to Middle Jurassic age in South China and a proposed flat-slab subduction model (Li and Li, 2007). The blue box marked the studied basin.

1.2. Significance

How the subduction of an oceanic plateau impacts on continental tectonics, and consequences of the subduction of oceanic plateaux in particular, is still a developing field in geosciences. The flat subduction model has been used to explain the post-80 Ma Laramide Orogen in western North America (Coney and Reynolds, 1977; Livaccari et al., 1981) and the Andes (Ramos and Folguera, 2009) along the eastern Pacific margin. In the western Pacific margin, Li and Li (2007) first proposed the Mesozoic flat-slab subduction beneath the South China Block. If such model is correct, it would help to understand how the older flat subduction form and its geotectonic consequences. The basin record of Mesozoic South China (shallow marine → orogenic uplift → shallow marine again → basin-and-range type province; Li and Li, 2007; **Fig. 1.2**) will provide unique insights into the spatial and temporal variations of this large-scale continental vertical movements that may have been caused by flat-slab subduction.

This basin analysis study will thus not only help to better understand the Mesozoic basin evolution and associated tectonic events in South China, but also to promote our understanding of fundamental tectonic processes such as the flat subduction of oceanic plateaux (Li and Li, 2007). A systematic analysis of the evolutionary history of the Mesozoic basins, especially the basin between the Late Triassic and the Middle Jurassic in southeastern South China, can help to reconstruct the magnitude and timing of the regional continental vertical movements and test the potential sub-continental lithospheric geodynamic processes such as flat-slab subduction and foundering. If correct, the flat-slab subduction model would help to explain the formation mechanism of the broad (commonly >700 km-wide) orogenic belts and associated magmatic provinces around the world. There is a large Mesozoic mineral province in South China, enriched in copper, iron, gold, lead-zinc, and rare-earth elements, that has been associated with the Mesozoic tectono-magmatic events. This study will therefore help to understand how tectonic processes controlled the formation of such major mineral provinces.

1.3. Research methods

This thesis is based on field-based sedimentary and basin analysis and laboratory studies.

1.3.1. Field techniques

Nearly five months were spent in the field to collect sedimentary data from outcrops, involving two fieldtrips: one from October 2010 to December 2010, and the other from October 2011 to January 2012. Nearly thirty-five sections of Upper Triassic to Middle Jurassic strata were measured. Information collected includes: 1) spatial and temporal lithofacies variations; 2) thickness of the various units; 3) fossil features; 4) sedimentary structures, including palaeocurrent data; and 5) conformities or unconformities that define different rock packages. Special attention was paid to the transitions between terrestrial facies and marine facies identified through a combination of fossil evidences (flora and fauna) and sedimentological analysis (e.g. alluvial fan deposits, river channels, and basin geometry), the maximum sedimentary thickness at the depocentre of the sag basin, and lateral changes and thickness. Stratigraphic columns are plotted and correlated in five cross-sections. The study area is broad, ranging from coastal region to continental interior in southeastern South China, covering the Guangdong, Fujian, Jiangxi, Hunan, Zhejiang and Guangxi provinces (**Fig. 1.1**).

1.3.2. Laboratory techniques

Samples, including tuff, tuffaceous mudrocks, and fine- to coarse-grained sandstones were collected for zircon U-Pb analysis to document spatial and temporal variations of the provenance and to constrain depositional ages. Detrital zircon U-Pb ages of twenty-two fine- to coarse-grained sandstone samples were obtained for provenance analysis. Zircon U-Pb ages of three tuff and tuffaceous mudrock samples, and one granite sample were obtained to constrain depositional ages. Zircon U-Pb dating was carried out using the SHRIMP facility at the John de Later Centre of Mass Spectrometry (JdLMS), Curtin University, and the LA-ICPMS facility at the State Key Laboratory of Isotope Geochemistry, Guangzhou Institute of Geochemistry, Chinese Academy of Sciences (CAS).

1.4. Structure of thesis

This thesis consists of seven chapters. They will be presented as follows:

Chapter 1 presents fundamental background information, proposes scientific questions to be addressed, and highlights the significance of this project.

Chapter 2 introduces the geology of the South China Block and broadly reviews the Permian to Cretaceous stratigraphic data in southeastern South China.

Chapter 3 presents detail facies analysis of the Daxi-Zhuyuan succession in northern Guangdong Province to identify facies associations and influence of control factors (autogenic vs. allogenic) on sedimentation, and shows stratigraphic correlation between the Daxi-Zhuyuan succession and three other published successions to discuss region-scale basin history and associated geodynamics.

Chapter 4 presents detail facies analysis of the Gaosi-Songxi succession in northeastern Guangdong Province to identify facies associations and influence of control factors, especially climate, and correlates with the Daxi-Zhuyuan succession to unravel regional depositional history.

Chapter 5 presents chronostratigraphic data across the basin, divides depositional sequences of individual successions, and reconstructs palaeogeographic and basin geometry.

Chapter 6 presents detrital zircon U-Pb age populations of sandstones of the basin to uncover the provenance sources and reconstruct the dispersal systems.

Chapter 7 summarises tectonostratigraphic data of the basin, correlates its sedimentary pattern with those of basins in North Atlantic and North America, and discusses mechanism of basin formation and geodynamics.

Chapter 2: Geological background

2.1. Introduction

The South China Block is bounded by the Qinling-Dabie-Sulu orogenic belt to the north, and by the Longmenshan and the Ailaoshan-Red river faults belts respectively to the west and to the southwest (**Fig. 2.1A**). A series of geological events from the Neoproterozoic to the present have been well documented.

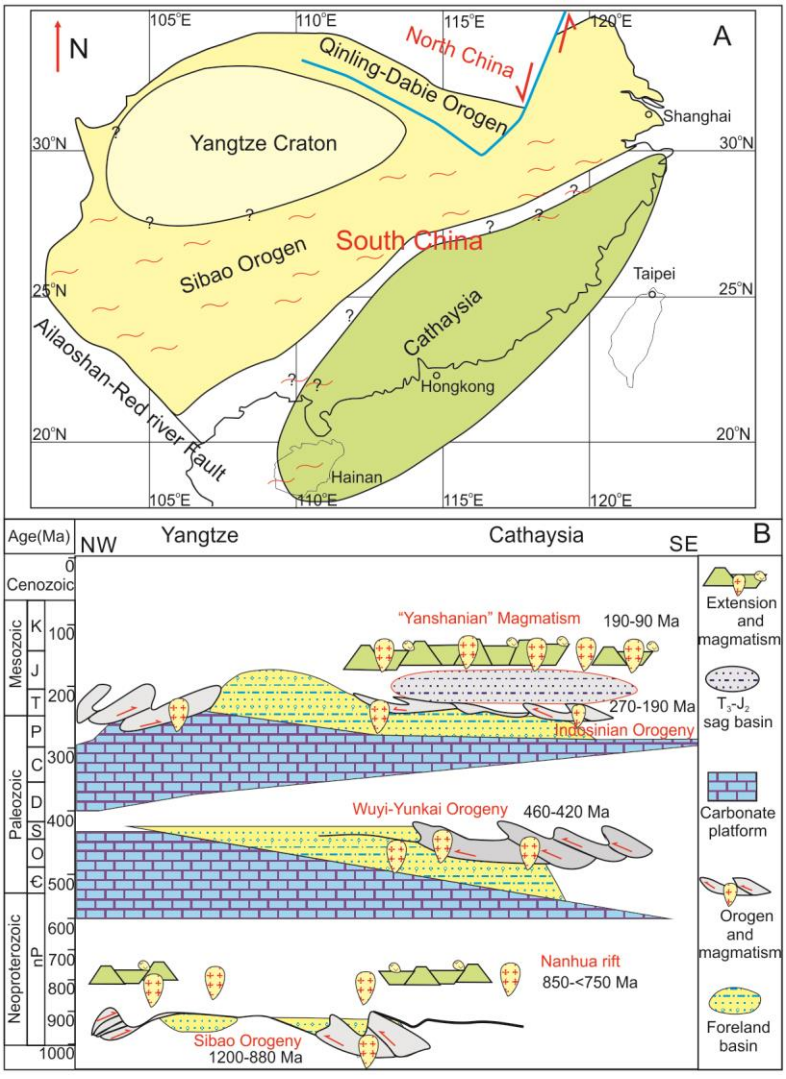

Figure 2.1 Geological history of the South China Block. (A) Tectonic components of the South China Block (after Li et al., 2002). (B) A brief history of the South China Block since the Early Neoproterozoic (Li et al., 2014b).

2.2. Tectonic Evolution of the South China Block

2.2.1. Neoproterozoic Assemblage and Subsequent Rifting

The South China Block comprises the Yangtze Block to the northwest and the Cathaysia Block to the southeast (**Fig. 2.1A**). The Cathaysia Block has a basement of ~1830-1430 Ma that were metamorphosed at ~1300-1000 Ma, making it a potential extension of southwestern Laurentia (Li et al., 2002; Li et al., 2008). The Yangtze Block has an Archean-Palaeoproterozoic (~3500-2000 Ga) basement in the northern Kongling area, and underwent a tectonothermal event at ~2000-1800 Ma (Qiu et al., 2000; Zhang et al., 2006a). Collision between the Yangtze and the Cathaysia blocks (also called the Huanan terrane) during the Early Neoproterozoic (~1200-880 Ma) shaped the present-day South China Block (**Fig. 2.1**). This event was locally named the Sibao Orogeny (**Fig. 2.1B**), one of the "Grenvillian" orogenic events during the assembly of the Rodinia Supercontinent (Li et al., 2002; Li et al., 2008; Li et al., 2009a).

The building of the South China Block was followed by deposition of an ~850-820 Ma volcanic-sedimentary succession (Sequence-I), an ~820-720 Ma rift succession (Sequence-II), and an ~720-635 Ma glacial and interglacial succession (Sequence-III) in the continental NE-SW-trending Nanhua Rift (basin) across central South China (**Fig. 2.1B**), the N-S trending Kangdian Rift in the western side of the Yangtze Block, and the E-W trending Bikou-Hanan Rift in the northwestern side of the Yangtze Block (Wang et al., 2012). Sequence-I in the Nanhua basin contains bimodal volcanism (i.e. part of the Shuangqiaoshan Group) that records the initiation of intracontinental rifting at ~850 Ma (Li et al., 2010a). Sequence-II can be divided into two sequence-sets, respectively representing: 1) an early-rifting facies association of continental alluvial/fluvial and volcaniclastic deposits overlain by drowned carbonate-platform and carbonaceous shale, and 2) the main rift facies associations of continental volcanic and shallow-marine deposits (Wang and Li, 2003). The glacial and interglacial deposits of Sequence-III (the Nantuo glaciation) are followed by deposition of platform carbonate, carbonaceous shale and siliceous rock, implying the continental rift basins evolved into a post-glaciation sag phase (Wang and Li, 2003). The Hf-Nd isotope analysis of the rift deposits reveals that there was a dominant ~825-800 Ma mafic provenance, likely linked to a

contemporaneous continental flood basalt province in South China (Wang et al., 2011).

Neoproterozoic syn-rift magmatism, including volcanics, dyke swarms and plutons have been well studied and interpreted to be represent four major episodes, that is, ~825 Ma, ~800 Ma, ~780 Ma, and ~750 Ma (Li et al., 2003b). Eruptions of high temperature OIB-type basalts during this time interval were interpreted to be related to the upwelling of a mantle plume starting at ~825 Ma beneath South China (Wang et al., 2007a; Wang et al., 2008; Wang et al., 2009b). The large scale intra-plate magmatism and associated continental rifting that occurred during the mid-Neoproterozoic (~850 to <750 Ma) were interpreted to represent the breakup of the Rodinia supercontinent caused by a long-lived mantle plume (Wang et al., 2007a; Li et al., 2008; Wang et al., 2009b; Li et al., 2010a).

In an alternative tectonic interpretation, Zhao et al. (2011) proposed that collision between the Yangtze and the Cathaysia blocks occurred at ~830 Ma, and the Early Neoproterozoic strata (>830 Ma) were deposited on an active continental margin, whereas the Late Neoproterozoic strata (820-730 Ma) were formed in the continental Nanhua rift basin during back-arc spreading above a long-lived flat subduction zone. However, the proposed flat subduction (Zhao et al., 2011) is supported by little geological evidence and the associated back-arc spreading model cannot explain the formation of high temperature (>1500 ℃) komatiitic basalts (~825 Ma; Wang et al., 2007). In addition, back-arc extension is inconsistent with their proposed low-angle subduction, which instead should have caused intracontinental orogenic events. It has been suggested that back-arc spreading develops for subduction dips larger than 50 °, whereas back-arc shortening occurs for deep dips less than 30 °(Lallemand et al., 2005; Sdrolias and Müller, 2006).

2.2.2. The Early Paleozoic Wuyi-Yunkai Orogeny

After the Nantuo glaciation, the Nanhua rift basin continued to be filled with platform carbonate, carbonaceous shale and chert on the Yangtze side but dominantly terrestrial clastic rocks on the Cathaysia side (Wang, 1985; Liu and Xu, 1994; Li, 1998a; Wang and Li, 2003). The Nanhua Rift converted into a foreland basin from the Middle to Late Ordovician, and was almost closed by the end of the

Silurian during the Wuyi-Yunkai Orogeny in southeastern South China (~>460 to 420-415 Ma; **Fig. 2.1B**) (Li, 1998a; Li et al., 2010b). This orogenic event was traditionally named the "Caledonian movement" (e.g., Ren, 1991), and also the "Kwangsian Movement/Orogeny" by others (Ting, 1929; Chen et al., 2010; Wang et al., 2010b). Facies changes from deep-water graptolite-bearing black shales to thick clastic, shallow-water deposits, along with the rapid increase in depositional rates from ~28.7 to ~647.5 m/Myr between the late Darriwilian and the early Katian (~460 to ~450 Ma) in southern Jiangxi Province (the Chongyi-Yongxin area) well document the onset of the Orogeny (Chen et al., 2010).

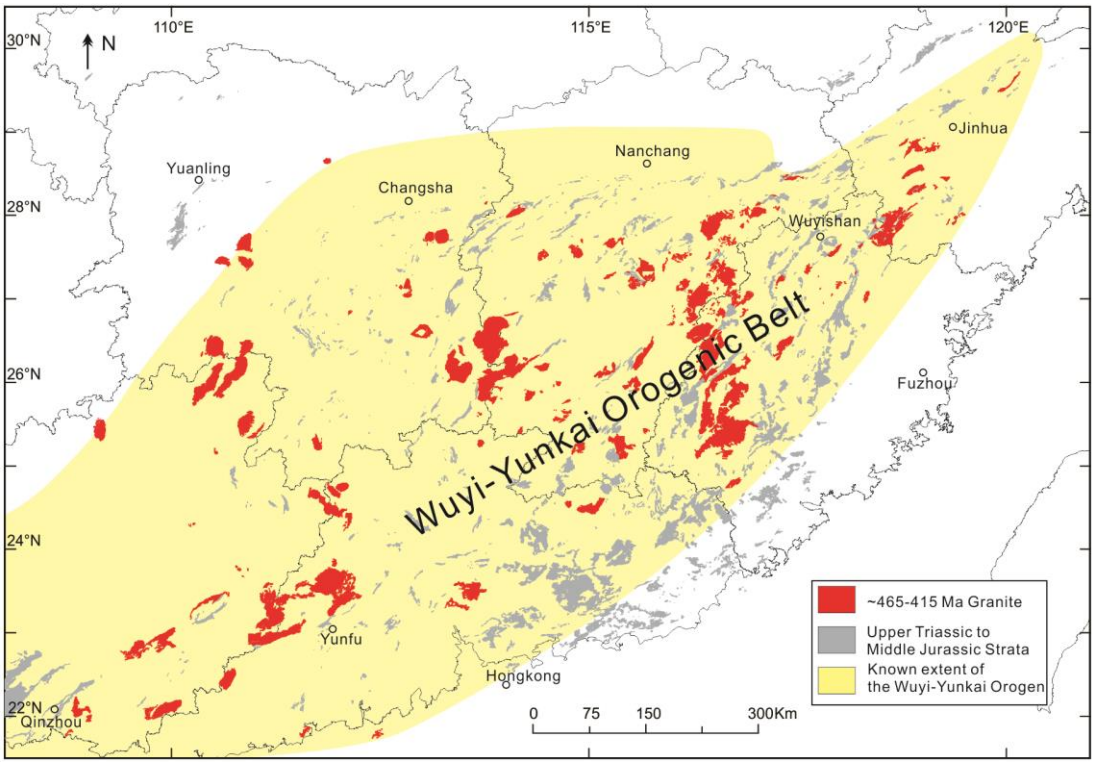

Figure 2.2 Geological features of the Wuyi-Yunkai orogenic belt. Spatial extent of the Wuyi-Yunkai orogen (after Li et al., 2010b) and distribution of associated granitic rocks (after Li et al., 2010b; Wang et al., 2013).

The Orogeny strongly deformed pre-Devonian strata that underlie younger strata with an angular unconformity, and the Orogen covers an area of 2000 × 600 km^2, extending from the Wuyi Mountains in the northeast to the Yunkai Mountains in the southwest (**Fig. 2.2**), from which the name Wuyi-Yunkai Orogeny was suggested (Li et al., 2010b). Liu and Xu (1994) suggested that the Orogeny resulted from the closure of a small oceanic basin between the Yangtze and the Cathaysia blocks. However, detrital zircon U-Pb results reveal that Cambrian to Silurian

sandstones on the western Cathaysia Block and the eastern Yangtze Block have similar provenance, which argues against there being an open ocean between these two blocks during the Early Paleozoic (Wang et al., 2010b). Based on the basin records, deformation and magmatism, it is generally accepted that the Wuyi-Yunkai Orogeny represents an Early Paleozoic intra-plate orogenic event in South China (Ren, 1991; Li, 1998; Li et al., 2010b; Wang et al., 2010b).

Granitic rocks intruding pre-Silurian strata are widespread, and have an age range of ~465 to 415 Ma, peaking at ~435 Ma (**Fig. 2.2**) (Li et al., 2010b; Wang et al., 2013). High zircon saturation temperatures between 784 ℃ and 845 ℃ of the ~435 Ma granites and the non-deformed nature for most of them imply they were derived from dehydration melting of the Proterozoic crust with a high geotherm during the relaxation phase of the Orogeny (Li et al., 2010b). The Wuyi-Yunkai orogen experienced a phase of rapid pressure drop from >8 kbar at ~460-440 Ma to ~4 kbar by ~440 Ma in the Wuyi region, showing a clockwise *P-T* path, followed by a relatively quick cooling to 500-300 ℃ by ~420 Ma, as indicated by the $^{40}Ar/^{39}Ar$ ages of hornblende and biotite from the metamorphic rocks (Li et al., 2010b).

2.2.3. The Early Mesozoic Indosinian Orogeny

After the Wuyi-Yunkai Orogeny, the South China Block evolved into a relatively steady stage from the Devonian to the Middle Permian. The Devonian to Middle Permian strata can be correlated in terms of biotas and lithologies, for instance, the Permian Qixia Formation of carbonate facies was deposited across the Block (Ren, 1991; Liu and Xu, 1994; Li, 1998a), and thus can be treated as a stratigraphic marker bed (see **Section 2.2.1**). Carbonate facies of the Qixia Formation were gradually overlain conformably by siliciclastic sedimentary rocks from east to west, recording the westward progradation of a Permian foreland basin, followed by the development of an ~1300 km-wide fold-and-thrust belt (an orogenic event named the Indosinian Orogeny in Chinese literature; **Fig. 2.3**) (Li and Li, 2007). This orogenic event is also documented by an angular unconformity between pre-Middle Triassic strata and Upper Triassic-Lower Jurassic strata, and by intrusion of Late Permian to Middle Triassic granitic rocks (**Fig. 2.3**) (HBGMR, 1984; JBGMR, 1984; FBGMR, 1985; GBGMR, 1988; Ren, 1991; Zhou et al., 2006; Li and Li, 2007; Shu et al., 2009; Wang et al., 2013).

Li et al. (2006) reported that ~267-262 Ma Wuzhishan granitic rocks on Hainan Island are calc-alkaline I-type granites, whereas Wang et al. (2005a) recognized ~254-242 Ma alkaline syenite plutons with high-K in the Fujian Province in the eastern Cathaysia Block (**Fig. 2.3**). Triassic granites, mainly ranging from ~250 to ~210 Ma (Li and Li, 2007), are peraluminous-dominated showing an affinity of S-type granites, along with calc-alkaline I-type granites (Zhou et al., 2006; Wang et al., 2013). On the other hand, the deformation of this orogenic belt (**Fig. 2.3**) is a series of top-to-NW crustal-scale to thin-skinned thrusts (NE-trending folds and faults), and a small number of top-to-SE back thrusts (Li and Li, 2007; Li et al., 2010b), which were suggested to be formed at ~217-195 Ma (Wang et al., 2005e). During the Late Triassic, a broad basin started to form on the orogenic belt, and evolved from continental lacustrine to shallow-marine during the Early Jurassic (**Fig. 2.1B**) (Wang, 1985; Liu and Xu, 1994; Li and Li, 2007).

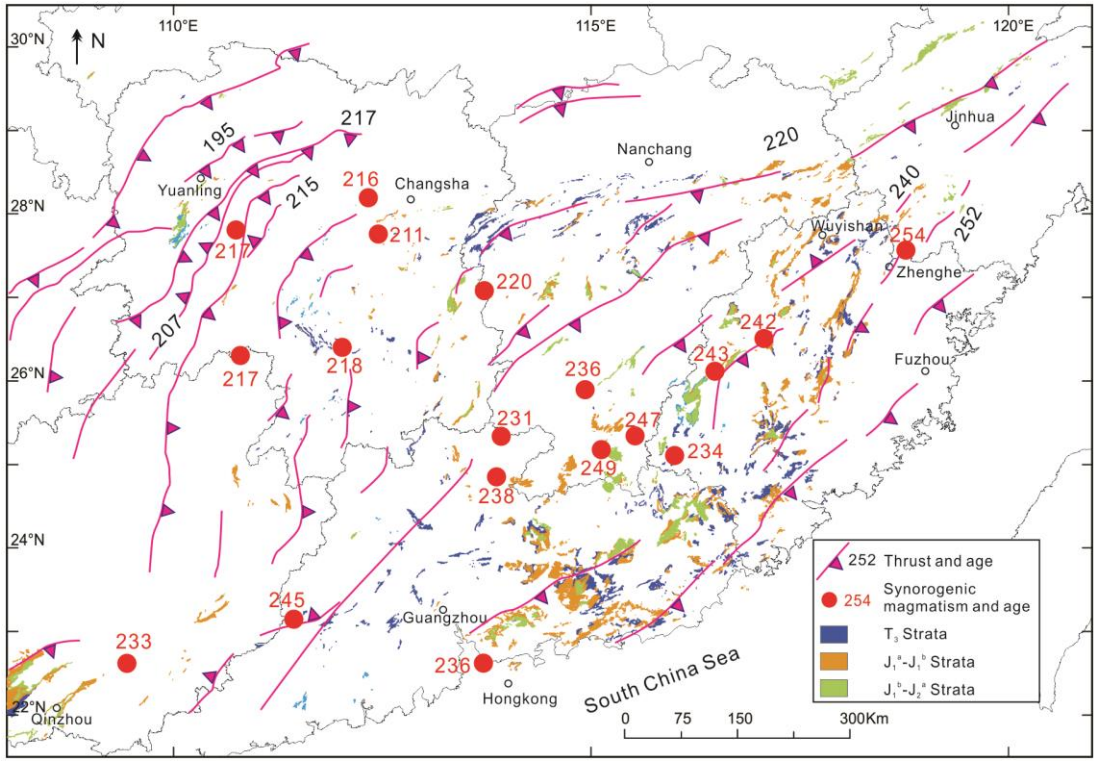

Figure 2.3 Geological features of the Indosinian orogenic belt (The South China Fold Belt). Spatial distributions and ages of fold-and-thrust belts are after Li and Li (2007). Ages of representative syn-orogenic granites are from Li and Li (2007) and Wang et al. (2013). The Late Triassic to Middle Jurassic basin sits on the orogen, which prograded from the coastal region to the continental interior (NW). The youngest age of the fold-and-thrust belts, from its northwest frontal zone, overlaps with the age of the basin.

The presence of the ~265 Ma calc-alkaline granitic rocks (syn-tectonic granites) on Hainan Island (Li et al., 2006a) implies that the Indosinian Orogeny initiated during the Middle Permian, caused by the subduction of the palaeo-Pacific plate, which is consistent with the first appearance of siliciclastic deposits in the eastern Cathaysia Block (Li and Li, 2007; Li et al., 2012a). Li and Li (2007) further proposed a flat-slab subduction model to explain the following events from the Permian to the Cretaceous: 1) cratonward migration of thrusting, metamorphism, and syn-orogenic magmatism between ~250 and ~190 Ma (**Fig. 2.3**), 2) cratonward propagation of the orogenic front and associated foreland basin by 235-230 Ma, and 3) a Late Triassic-Early Jurassic (T_3-J_1) broad sag basin formed in the wake of the migrating foreland fold-and-thrust belt, followed by a late-Mesozoic basin-and-range style province after the Orogeny ceased at ~200-190 Ma.

Alternatively, Zhou et al. (2006) argued that the southeastern South China was tectonically influenced by Tethyan tectonics (subduction of the Indochina Block) before the Early Jurassic, but has been controlled by Pacific tectonics (subduction of the palaeo-Pacific plate) since the Middle Jurassic (Shu et al., 2009). Wang et al. (2013) argued against the presence of a younging-trend in the Triassic magmatism towards the continental interior. They considered that the Indosinian orogenic event was controlled by subduction of the Indochina Block during the Middle to Late Triassic, and the southeastern South China was not influenced by the subduction of the palaeo-Pacific plate until the Early Jurassic.

2.2.4. The Late Mesozoic basin-and-range province

The Indosinian orogenic event was followed by a post-orogenic extension and widespread magmatism between the late Early Jurassic and the Cretaceous (~180-80 Ma, also called the Yanshanian magmatism; **Fig. 2.1B**). The magmatism of this period is characterized by bimodal intrusions and volcanism, including granitoid, A-type granite, gabbro, syenite, rhyolite, and basalts (Li and McCulloch, 1998; Zhou and Li, 2000; Li et al., 2003a; Chen et al., 2004; Wang et al., 2005c; Li et al., 2007a; Hsieh et al., 2008; Li et al., 2009b; Meng et al., 2012). Previously, the Yanshanian magmatism was divided into the Early Yanshanian episode (180-140 Ma) and the Late Yanshanian episode (140-80 Ma; e.g., Zhou and Li, 2000; Hsieh et al., 2008). Recently, however, A-type granite and gabbro of ~194 Ma with positive $\varepsilon Nd_{(t)}$

signatures ($\varepsilon Nd_{(t)} > 0$) were reported in northeastern Guangdong Province (Zhu et al., 2010), whereas contemporaneous granodiorite and gabbro-diabase were dated in southern Jiangxi Province (Yu et al., 2010c). This implies that the anorogenic magmatism initiated much earlier than those previously dated.

On the other hand, the T_3-J_1 broad basin was broken up into NE-trending graben from the Middle Jurassic (e.g., Wang et al., 1985; Li and Li, 2007). Volcanic rocks of Middle Jurassic age, emplacing along the rifting system, are preserved in western Fujian Province, southern Jiangxi Province, southern Hunan Province and northern Guangdong Province (e.g., Zhou et al., 2006; Shu et al., 2009; Meng et al., 2012). The region further evolved into a series of NE-trending extensional or rift basins during the Cretaceous, filled with basaltic rocks and gypsiferous red sandstones and mudstones (e.g., Shu et al., 2009). Basin evolution and synchronous bimodal magmatism imply that southeastern South China underwent continental-scale lithospheric extension from the Middle Jurassic to the Cretaceous, which was previously defined as a basin-and-range type province (Gilder et al., 1991; Li, 2000; Li and Li, 2007).

2.3. Mesozoic sedimentation in southeastern South China

2.3.1. Middle Permian to Lower Triassic strata: foreland basin deposits?

Permian to Lower Triassic sedimentary records are well preserved in southeastern South China, whereas Middle Triassic strata are widely scattered, i.e., in northern Guangdong Province, western Fujian Province and southern Hunan Province (HBGMR, 1984; FBGMR, 1985; GBGMR, 1988). As discussed above, the mid-Permian Qixia Formation is carbonate facies and can be correlated across the South China Block (e.g., HBGMR, 1984; FBGMR, 1985; GBGMR, 1988; Liu and Xu, 1994; **Fig. 2.4**). The Qixia Formation was gradually overlain by siliciclastic deposits of the Wenbishan Formation and the Dangchong Formation in the eastern side of the Cathaysia Block (coastal regions), whereas it was covered by the Maokou Formation of carbonate-dominated facies in the western Cathaysia Block and the eastern Yangtze Block (continental interior; e.g., HBGMR, 1984; FJBGMR, 1985;

GBGMR, 1988; **Fig. 2.4**). The Wenbishan Formation consists of siliceous rock, shale, siltstone, mudstone and sandstone from the lower to the upper parts, about 150-300 m-thick (FBGMR, 1985; GBGMR, 1988; **Fig. 2.4**), and is interpreted to be formed in fluvial to deltaic environments. The overlying Tongziyan Formation is characterized by coal-bearing mudstone, siltstone, shale and sandstone, ranging from 260 to 550 m-thick (**Fig. 2.4**). In contrast, to the west, the Dangchong Formation consists of only shale, whereas the Maokou Formation comprises predominately marine carbonate and subordinately shale (HBGMR, 1984; **Fig. 2.4**), implying a continental platform setting. Therefore, during the late Middle Permian, the eastern part of the southeastern South China was first to be covered by siliciclastic sediments, which propagated gradually into the continental interior (e.g., Liu and Xu, 1994; Li and Li, 2007; **Figs 2.1** and **2.4**), implying an eastern source region.

During the Wuchiapingian, coal-bearing siliciclastic sediments propagated further into the continental interior (**Fig. 2.4**), indicating that the source region was uplifted and migrated westward. For instance, the Cuipingshan Formation represents the fluvial strata in the Fujian Province, whereas the Geding and Dong Formations are of coal-bearing deltaic-fluvial deposits in northern Guangdong Province (FBGMR, 1985; GBGMR, 1988; **Fig. 2.4**). The Longtan Formation is a sequence of thick (~700 m) coal-bearing fluvial siliciclastic rocks preserved in eastern Hunan Province, and it is correlated with the Wujiaping Formation of carbonate facies in western Hunan Province (**Fig. 2.4**).

During the Changhsingian to the Early Triassic, coarse-grained sediments interbedded with carbonates (the Dalong and Xikou Formations) were mainly deposited in the Fujian Province in eastern Cathaysia Block, whereas marine carbonates and shales overlying the older coal-bearing sedimentary rocks are preserved in the northern Guangdong Province, Jiangxi Province and Hunan Province (**Fig. 2.4**), showing a fining-upwards trend. This implies that the southeastern South China may be subjected to rejuvenated subsidence prior to the uplift of the continent recorded by an angular unconformity relationship between the Upper and Lower Triassic strata (**Fig. 2.4**). Indeed, strata of the early Middle Triassic, although widely scattered, document change from marine sedimentary basins to continental deposits or erosion in the southeastern South China (Tong and Liu, 2000).

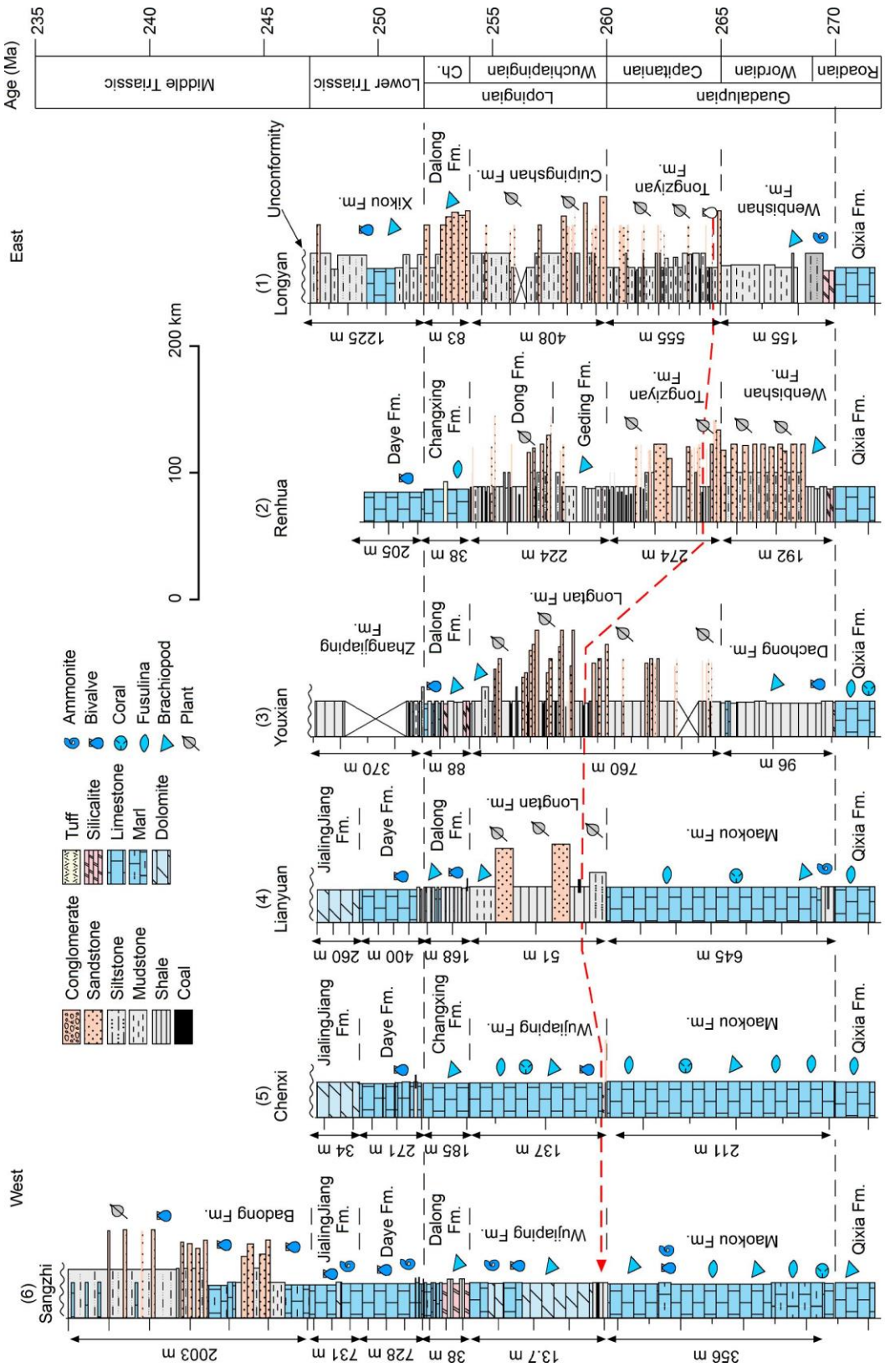
Age (Ma)
235
240
245
250
255
260
265
270
Middle Triassic
Lower Triassic
Ch.
Wuchiapingian
Lopingian
Capitanian
Wordian
Guadalupian
Roadian
East
West
(1) Longyan
(2) Renhua
(3) Youxian
(4) Lianyuan
(5) Chenxi
(6) Sangzhi
Unconformity
Xikou Fm.
Dalong Fm.
Cuipingshan Fm.
Tongziyan Fm.
Wenbishan Fm.
Qixia Fm.
Daye Fm.
Changxing Fm.
Dong Fm.
Geding Fm.
Zhangjiaping Fm.
Longtan Fm.
Dachong Fm.
JialingJiang Fm.
Maokou Fm.
Wujiaping Fm.
Badong Fm.
1225 m
83 m
408 m
555 m
155 m
205 m
38 m
224 m
274 m
192 m
370 m
88 m
760 m
96 m
260 m
400 m
168 m
51 m
645 m
34 m
271 m
185 m
137 m
211 m
2003 m
731 m
728 m
38 m
13.7 m
356 m
0
100
200 km
Ammonite
Bivalve
Coral
Fusulina
Brachiopod
Plant
Tuff
Silicalite
Limestone
Marl
Dolomite
Conglomerate
Sandstone
Siltstone
Mudstone
Shale
Coal

Figure 2.4 Chronostratigraphic evolution of the Middle Permian to Lower Triassic strata in southeastern South China. Stratigraphic and palaeontological data are from published geological reports (HBGMR, 1984; FBGMR, 1985; GBGMR, 1988). Red dashed line indicates that the first occurrence of coal deposits at individual sections. Section 1 locates in the Fujian Province; Section 2 in the Guangdong Province; Section 3 to 6 in the Hunan Province. See **Figure 2.5** for locations of the provinces.

Reconstructed palaeogeographic maps show that the continent was uplifted during the late Middle Triassic (e.g., Liu and Xu, 1994). These sedimentary deposits were interpreted to represent a foreland basin that resulted from an Andean-type subduction of the palaeo-Pacific plate beneath South China from the Middle Permian (Li and Li, 2007; Li et al., 2012b). Detrital zircon U-Pb and isotopic analysis of Middle to Upper Permian strata in the coastal region reveal that there was an ~280 Ma magmatic event in this region, possibly reflecting the formation of a continental arc by the subduction of the palaeo-Pacific plate during the Early Permian (Li et al., 2012a), although there are no exposures of ~280 Ma magmatic rocks.

2.3.2. Upper Triassic to Upper Jurassic strata: intracontinental deposits

Following the depositional hiatus, southeastern South China commenced to subside and receive sediments again during the Late Triassic (**Fig. 2.5**; e.g., HBGMR, 1984; FBGMR, 1985; JBGMR, 1985; GBGMR, 1988). The present-day residual strata are mainly distributed in the Guangdong, Hunan, Jiangxi and Fujian provinces, but scatter in the Guangxi and southern Zhejiang provinces (**Fig. 2.3**).

Upper Triassic units were assigned using different formal names in different provinces (**Fig. 2.5**). Some groups were subdivided into several formations, for instance, the Genkou Group in the Guangdong Province was divided into the Hongweikeng, Xiaoshui and Toumuchong formations; the Anyuan Group in the Jiangxi Province includes the Zijiachong, Sanjiachong, Sanqiutian and Duojiang formations in an ascending age order (**Fig. 2.5**). Basically, these units are coal-bearing siliciclastic sedimentary rocks interbedded with brackish to shallow-marine deposits in the Jiangxi, Guangdong and southern Hunan provinces, whereas only coal-bearing siliciclastic sedimentary rocks were deposited in the Fujian and western Hunan provinces (**Fig. 2.5**) (HBGMR, 1984; JBGMR, 1984; FBGMR, 1985; Qian et al., 1987; GBGMR, 1988). These deposits, ranging from ~200 to ~3000 m-thick, recorded first a deepening and then shallowing depositional process.

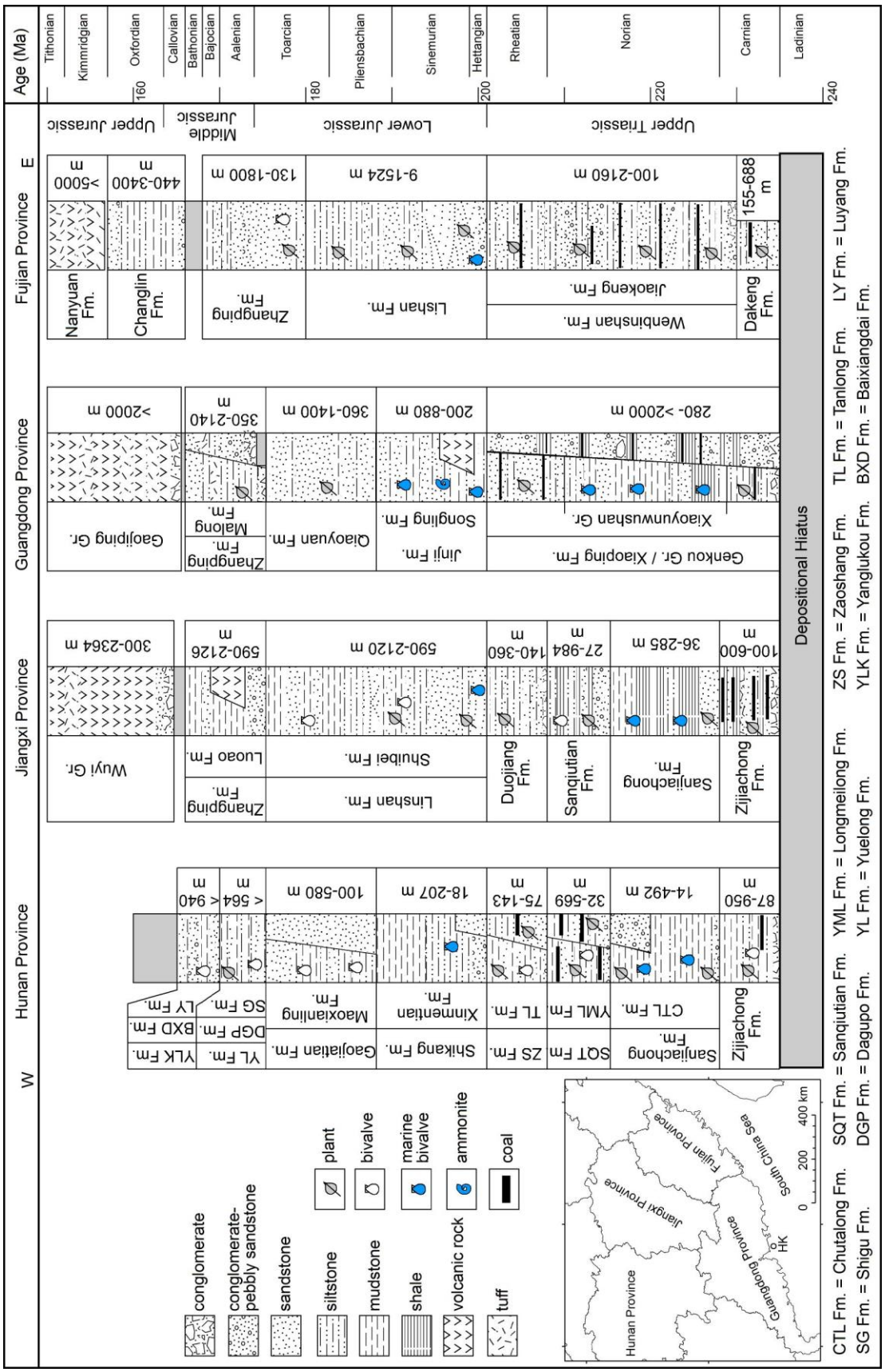
Age (Ma)
Tithonian
Kimmridgian
Oxfordian
Callovian
Bathonian
Bajocian
Aalenian
Toarcian
Pliensbachian
Sinemurian
Hettangian
Rheatian
Norian
Carnian
Ladinian
160
180
200
220
240
Upper Jurassic
Middle Jurassic
Lower Jurassic
Upper Triassic
W
Hunan Province
Jiangxi Province
Guangdong Province
Fujian Province
E
Depositional Hiatus
Wuyi Gr.
Zhangping Fm.
Luoao Fm.
Linshan Fm.
Shuibei Fm.
Duojiang Fm.
Sanqiutian Fm.
Sanjiachong Fm.
Zijiachong Fm.
Gaojiping Gr.
Qiaoyuan Fm.
Jinji Fm.
Songling Fm.
Genkou Gr. / Xiaoping Fm.
Xiaoyunwushan Gr.
Nanyuan Fm.
Changlin Fm.
Lishan Fm.
Wenbinshan Fm.
Jiaokeng Fm.
Dakeng Fm.
300-2364 m
590-2126 m
590-2120 m
140-360 m
27-984 m
36-285 m
100-600 m
>2000 m
350-2140 m
360-1400 m
200-880 m
280- >2000 m
>5000 m
440-3400 m
130-1800 m
9-1524 m
100-2160 m
155-688 m
YLK Fm.
DGP Fm.
BXD Fm.
YL Fm.
LY Fm.
SG Fm.
Gaojiatian Fm.
Maoxianling Fm.
Shikang Fm.
Xinmentian Fm.
ZS Fm.
TL Fm.
SQT Fm.
YML Fm.
CTL Fm.
Sanjiachong Fm.
Zijiachong Fm.
< 940 m
< 564 m
100-580 m
18-207 m
75-143 m
32-569 m
14-492 m
87-950 m
conglomerate
conglomerate-pebbly sandstone
sandstone
siltstone
mudstone
shale
volcanic rock
tuff
plant
bivalve
marine bivalve
ammonite
coal
Hunan Province
Jiangxi Province
Guangdong Province
Fujian Province
South China Sea
HK
0
200
400 km
CTL Fm. = Chutalong Fm.
SQT Fm. = Sanqiutian Fm.
YML Fm. = Longmeilong Fm.
ZS Fm. = Zaoshang Fm.
TL Fm. = Tanlong Fm.
LY Fm. = Luyang Fm.
SG Fm. = Shigu Fm.
DGP Fm. = Dagupo Fm.
YL Fm. = Yuelong Fm.
YLK Fm. = Yanglukou Fm.
BXD Fm. = Baixiangdai Fm.

Figure 2.5 Stratigraphic overview of the Upper Triassic to Upper Jurassic strata in southeastern South China. Lithologies, palaeontological data and formation divisions are based on published reports (HBGMR, 1984; JBGMR, 1984; FBGMR, 1985; GBGMR, 1988).

Early Jurassic sedimentary rocks are widely documented in southeastern South China, and can be correlated across the region. These deposits are characterized by marine sandstone, mudstone, siltstone and shale in the lower part, but by coal-bearing terrestrial sandstone, siltstone and mudstone in the upper part in the Guangdong and Hunan provinces, whereas coal-bearing conglomerate, sandstone, siltstone, and mudstone are dominant in the Fujian and Jiangxi provinces (**Fig. 2.5**; HBGMR, 1984; GBGMR, 1988). The deposits are generally ~120 to ~2100 m-thick, and vary from places to places. Volcanic rocks of Early Jurassic age are reported from the Guangdong Province (GBGMR, 1988, 1996). Overall, the Lower Jurassic strata document another cycle of deepening to shallowing sedimentation (**Fig. 2.5**).

Middle Jurassic strata are preserved mainly in the Fujian and eastern Guangdong provinces, and are sporadically distributed in the Jiangxi and Hunan provinces (**Figs 2.3** and **2.5**). These deposits, ranging from ~130 to >3000 m-thick, are dominated by multicoloured terrestrial tuffaceous sandstone, siltstone, mudstone and tuff, and are represented by the Zhangping Formation (e.g., FBGMR, 1985; GBGMR, 1988; **Fig. 2.5**). Previously, the age of the Zhangping Formation was poorly constrained due to the lack of index fossils. However, the basal unit of the Gaojiping Group overlying the Zhangping Formation on an angular unconformity in the eastern Guangdong Province was reported to be between ~168 Ma and ~145 Ma in age (Guo et al., 2012), implying that the Zhangping Formation was deposited before ~168 Ma, between the Toarcian and the Bajocian. In this study, sample from the lowermost part of the Zhangping Formation in the Fujian Province was dated and gave a maximum depositional age of ~189 Ma (see **Chapter 5**), which is much older than published age (e.g., FBGMR, 1985). The implication is that the Zhangping Formation could be late Pliensbachian to Bajocian age in the Fujian Province.

Upper Jurassic strata consist mainly of volcanic and volcaniclastic rocks, and overlie the Upper Triassic to Middle Jurassic strata on an angular unconformity (**Fig. 2.5**). These rocks are dominantly distributed along the coastal region, such as the eastern Guangdong and Fujian provinces (**Fig. 2.5**).

2.3.3. Cretaceous strata: extensional/rift basin deposits

Cretaceous strata are widespread in southeastern South China, and comprise a sequence of very thick terrestrial reddish clastic sedimentary rocks, distributing in NE-trending grabben. The lower unit consists of variegated siliciclastic rocks, interlayered by volcaniclastic and minor volcanic lava, with fossil plant, bivalve, ostracoda and conchostracans, ranging from ~220 to ~3000 m-thick, whereas the upper unit contains brown reddish, reddish siliciclastic sedimentary rocks and interbedded evaporate beds, with vertebrate fossils (e.g., dinosaur), varying from ~1000 to ~9000 m-thick (e.g., HBGMR, 1984; JBGMR, 1984; FBGMR, 1985; GBGMR, 1988). It generally accepted that the Cretaceous basins (i.e., half-grabben, grabben) were formed in an extensional setting or rifting, and a basin-and-range type province was invoked to depict the palaeogeography and tectonic setting of the Cretaceous southeastern South China (e.g., Gilder, 1991; Li and Li, 2007).

Chapter 3: Facies analysis and tectonic implication of the Daxi-Zhuyuan succession in north Guangdong Province

(This chapter contains contents published in the following paper:

Pang, C.-J., Krapež, B., Li, Z.-X., Xu, Y.-G., Liu, H.-Q., and Cao, J., 2014, Stratigraphic evolution of a Late Triassic to Early Jurassic intracontinental basin in southeastern South China: A consequence of flat-slab subduction? Sedimentary Geology, v. 302, p. 44-63.

All results and conclusions, unless otherwise acknowledged in this paper, were done by myself under supervision.)

3.1. Introduction

Sedimentary response to early Mesozoic post-orogenic tectonism was widely recorded in intracontinental sedimentary basins along the Atlantic. For instance, during the Late Triassic-Early Jurassic, extensional basins formed on collapsed Palaeozoic orogenic belts in the Newfoundland and Iberian regions (e.g., the Jeanne D'Arc, Fundy and Lusitanian basins), representing the initial phase of continental breakup and opening of the Atlantic Ocean (Sinclair, 1995; Færseth, 1996; Torsvik et al., 2001; Alves et al., 2003; Tucholke et al., 2007; Alves et al., 2009). A coeval basin that formed on a Permo-Triassic orogenic belt has been documented in the southeastern part of South China (e.g., Wang, 1985; Sun et al., 1989; Liu and Xu, 1994; Li and Li, 2007; Shu et al., 2009). However, the mechanism for the formation of the basin has not attracted much attention until recently, and stratigraphic information about the basin has been insufficient to warrant correlation with the Newfoundland-Iberian basins in terms of origin and evolution of the basin fill.

The southeastern part of the South China Block experienced extensive Late Permian to early Mesozoic deformation, metamorphism and magmatism, collectively known as the Indosinian Orogeny (Cui and Li, 1983; Hsu et al., 1990; Li, 1998b; Wang et al., 2005e; Zhou et al., 2006; Li and Li, 2007). A broad Late Triassic to Early Jurassic (T_3-J_1) sedimentary basin formed over the orogen in the southeastern

half of the South China Block (Wang, 1985; Sun et al., 1989; Liu and Xu, 1994; **Fig. 3.1A**). This basin was interpreted by Li and Li (2007) to be an intracontinental sag formed during the gravitational pull of an eclogitising, flat-subducted oceanic slab underneath the region, whereas other authors recognise its post-orogenic nature but give no tectonic mechanism for its formation (e.g., Shu et al., 2009).

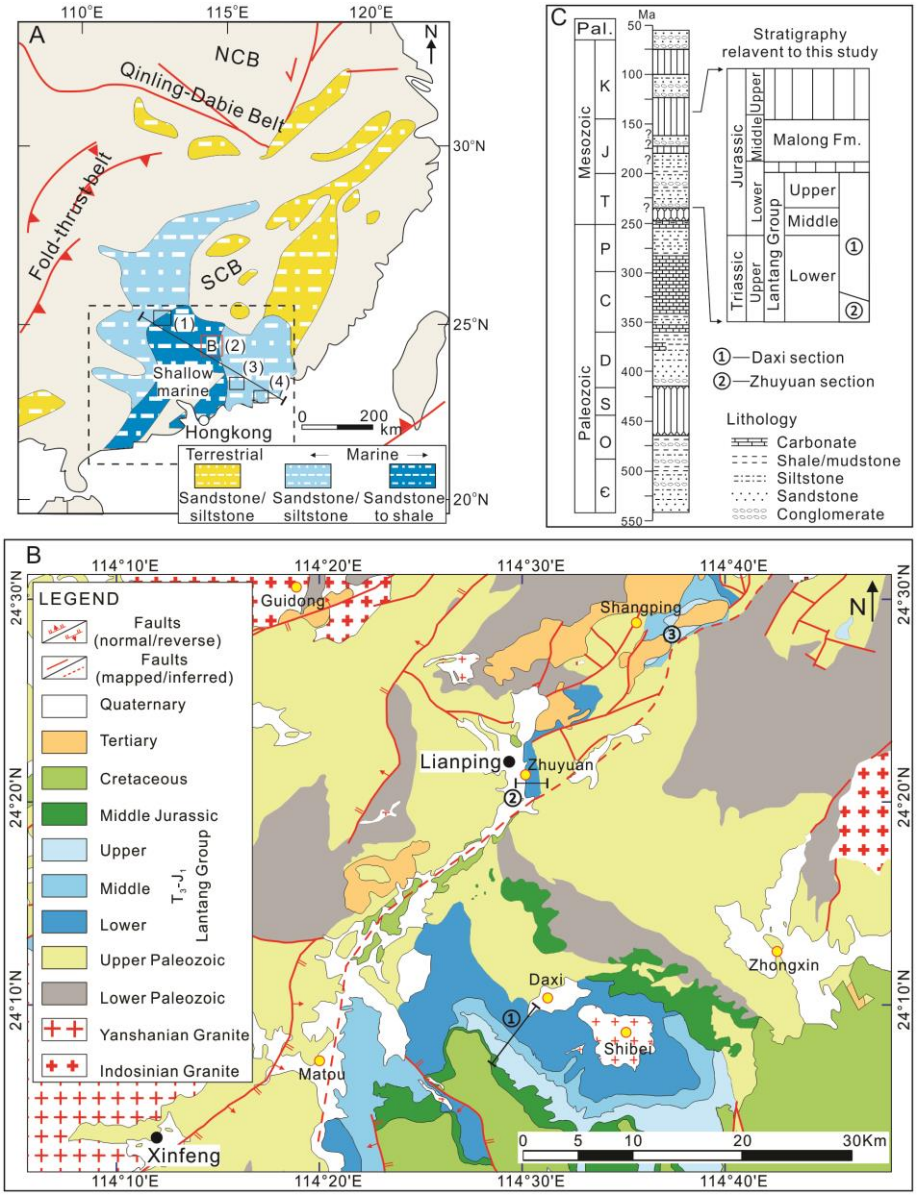

Figure 3.1 Geological maps of the study area. (A) Palaeogeography of the Early Jurassic in southeastern South China (modified after Li and Li, 2007). NCB = North China Block, SCB = South China Block. White areas are the ocean, while grey areas represent the present-day shape of Chinese continent and islands. Dash-line box marks the spatial range in **Fig. 3.11A**, in which (1), (2), (3) and (4) number the correlated sections. (B) Geological map of the Daxi-Zhuyuan area (modified after 1: 200,000 scale map; GBGMR, 1964). ① marks the Daxi section, ② the Zhuyuan section, and ③ the Shangping section. (C) Lower Palaeozoic to Cenozoic

stratigraphy in the study area (GBGMR, 1988). Fm = Formation, Pal. = Paleogene, K = Cretaceous, J = Jurassic, T = Triassic, P = Permian, C = Carboniferous, D = Devonian, S = Silurian, O = Ordovician, Є = Cambrian.

This chapter documents the evolutionary history of the T_3-J_1 sedimentary basin in southeastern South China by examining the sedimentary succession (herein named the Daxi section, marked as '1' in **Fig. 3.1B**) accumulated in the estimated depocentre of the basin (**Fig. 3.1A**). Our results are combined with those from published work on the Zhuyuan section ('2' in **Fig. 3.1B**; Qian et al., 1987) and with those along a northwestern to southeastern cross section (**Fig. 3.1A**) in order to: 1) define the Late Triassic to Early Jurassic basin history in southeastern South China, 2) to discuss possible basin-forming mechanisms, and 3) to compare and contrast the South China basin to time equivalents in the North Atlantic.

3.2. Geological setting

Prior to the formation of the T_3-J_1 basin, a 1300 km-wide fold-and-thrust belt formed across the South China Block, the so-called Indosinian Orogen (Li and Li, 2007). Li et al. (2006) proposed that compressive tectonics initiated at ~265 Ma, based on the ages of arc-related, calc-alkaline granites in Hainan Island. This onset of compression is consistent with the change from Middle Permian marine limestones to Upper Permian-Lower Triassic siliciclastic sedimentary rocks close to the coastal zone, which has been interpreted to record formation of a foreland basin (e.g., Liu and Xu, 1994; Li et al., 2006b; Li and Li, 2007). From ~250 Ma, thrusting, metamorphism, and syn-orogenic magmatism migrated into the continental interior, and by ~235 Ma the orogenic front had propagated about 600 km into central South China (Li and Li, 2007). The orogeny resulted in continental uplift and depositional hiatuses in southeastern South China during the Middle Triassic, and was succeeded by a broad T_3-J_1 sedimentary basin that developed on top of the orogen (Li and Li, 2007; **Fig. 3.1A**). The basin was interpreted as an intracontinental sag basin by Li and Li (2007), because there is seemingly no stratigraphic response to bounding faults.

It has been suggested that the orogeny ended at about 195 Ma, as recorded by the youngest Ar-Ar ages from thrust zones in central South China (Wang et al., 2005e; **Fig. 3.1A**), and the onset of the anorogenic magmatism in northeastern Guangdong Province and adjacent regions including ~190 Ma A-type granites and volcanic rocks (GBGMR, 1996; Li et al., 2007a; Gong and Wu, 2010; Zhu et al., 2010). The Indosinian Orogeny thus may have lasted from ≥265 Ma to ~195 Ma. After the inversion of the T_3-J_1 basin, a basin-and-range magmatic province developed in southeastern South China during the Late Mesozoic (Gilder et al., 1991; Li et al., 2007a).

The studied sections are located in the Daxi-Zhuyuan area in the Xinfeng-Lianping region of northern Guangdong Province, which is about 200 km north of Hong Kong (**Fig. 3.1A, B**). In this area, the T_3-J_1 strata, initially designated as the Lantang Group (GBGMR, 1964; **Fig. 3.1C**), overlie Lower Triassic and older rocks on an angular unconformity. The Group comprises mudstone, siltstone, fine- to coarse-grained sandstone, and conglomerate. Palaeontological data (Fan, 1963a; Yin et al., 1964; Fan et al., 1965; Sun et al., 1980; Wang and Li, 1983; Wang and Smith, 1986; Qian et al., 1987) imply a terrestrial to shallow-marine depositional environment for the Lantang Group, which has not been formally divided into formations in the Daxi section. Early Jurassic basalts and tuffs are present in the middle and upper parts of the Lantang Group in the Shangping section ('3' in **Fig. 3.1B**; GBGMR, 1964, 1996; Sun, 1989), although their precise ages are not known. The lower part of the Lantang Group was intruded by a late-Early Jurassic granite (~186 Ma; unpublished SHRIMP [Sensitive High-Resolution Ion Microprobe] U-Pb zircon age of C-J P.), whereas the upper part is overlain unconformably by Middle Jurassic sedimentary rocks (the Malong Formation; **Fig. 3.1B, C**) (GBGMR, 1988). The lower, middle and upper parts of the Lantang Group are correlated respectively with: 1) the Carnian to Rhaetian Genkou Group (which is divided into the Hongweikeng, Xiaoshui and Toumuchong formations), 2) the Hettangian to early Pliensbachian Jinji Formation, and 3) the late Pliensbachian to Toarcian Qiaoyuan Formation in the Shaoguan region in northern Guangdong Province (e.g., GBGMR, 1988, 1996; **Fig. 3.1**).

Table 3. 1 Lithology, facies codes, sedimentary structures, geometry, and related depositional processes of the Daxi-Zhuyuan sections

Facies codes	Lithology	Sedimentary structures	Geometry	Depositional processes
C	Dark to dark grey carbonaceous mudstone, siltstone, coals, with plant fossils, and nodules of siderite and pyrite	Structureless	Tabular bedsets, beds range from 1 to tens of centimetres	Suspension deposition, high water table, relatively low sediment supply
Mm	Dark grey shale, siltstone, and mudstone, with sandstone pebbles, fossils, and nodules of pyrite and organic matter	Structureless	Tabular bedsets; beds range from millimetre to metre in thickness.	Suspension deposition with little or no current activity
Mh	Dark grey to yellow grey siltstone, silty mudstone, with nodules of pyrite and organic matter	Horizontal lamination	Tabular bedsets; beds range from 5 to tens of centimetres in thickness.	Suspension settling from low-density currents in subaqueous environment
MSm	Dark grey to yellowish mixed interbedded silty mudstone, siltstone, and fine-grained sandstone, with nodules of pyrite and organic matter	Structureless	Tabular to slightly wavy bedsets; beds range from 5 to 20 centimetres in thickness.	Rhythmic density-current deposition below wave base
MSr	Dark grey mixed interbedded silty mudstone, siltstone, and fine-grained sandstone	Starved ripple marks, lenticular bedding	Tabular to wavy bedsets; beds range from 1 to 3 centimetres.	Slow suspension fallout and varied current strength, limited sand supply
Sm	Muddy to well-sorted, very fine to coarse-grained sandstone, with fossils, and nodules of pyrite and organic matter	Structureless	Tabular bedsets; beds range from 5 centimetres to several metres in thickness.	Rapid deposition from sand-laden currents
Sp	Very fine to fine-grained sandstone	Planar cross-lamination	Tabular bedsets; beds are tens of centimetres thick.	Deposition from straight-crested dunes or sand waves
Sd	Dark grey very fine-grained sandstone	Convolute bedding	Tabular bedsets; beds are tens of centimetres thick.	Formed by gravity loading and dewatering
Sh	Muddy to well-sorted, yellow to white, very fine to medium-grained sandstone	Horizontal lamination	Tabular bedsets; beds range from millimetre to tens of centimetres.	Traction deposition within upper flow regime on plane beds
Sr	Muddy to well-sorted, fine to coarse-grained sandstone	Ripple marks, mostly straight-crested with asymmetrical to near-symmetrical shapes	Wavy bedsets; beds range from 5 to tens of centimetres in thickness.	Formed by shoaling waves or by an interaction of waves and currents of similar directions
St	Muddy to sorted, fine to coarse-grained sandstone	Trough cross-bedding, trough cross-lamination, channel-shaped bedding	Tabular to trough bedsets; beds are tens of centimetres thick.	Deposition within lower flow regime dunes in channels, and varied current strength
Sbio	Muddy fine-grained sandstone	Bioturbation	Tabular bedsets; bed vary from 5 to tens of centimetres.	Activities of organisms
Gm	Matrix-rich conglomerates; the average size of pebbles is 3 centimetres.	Weak grading and stratification	Tabular bed; bed is 20 centimetres thick.	Deposition of mixed pebble and sand load either within channels

3.3. Methodology

The Daxi section ('1' in **Fig. 3.1B**) is located along a county road between the Daxi and the Matou townships in Xinfeng County. Strata dip generally to the southwest, at between 20 ° and 40 °, and are not structurally complicated. However, stratification has been obliterated in some exposures due to modern weathering, and soil or vegetation cover. Strata were measured in the field using a tape measure and a compass, but lateral exposures are limited by dense vegetation cover on steep slopes. Because good exposures generally extend only 5 to 20 m distance from roads, this study relies primarily on vertical variations of sedimentary facies and palaeontology. Fossils found in the section were identified in the Nanjing Institute of Geology and Palaeontology, Chinese Academy of Sciences.

Over 2000 m of siliciclastic sedimentary rocks were measured in the Daxi section (**Fig. 3.1B**). However, the lowermost part of the Daxi section is not everywhere exposed. The Zhuyuan section located ~25 km to the north of the Daxi section ('2' in **Fig. 3.1B**) records the lowermost part of the T_3-J_1 succession and comprises more than 500 m of sedimentary rocks (Qian et al., 1987; GBGMR, 1988). Sedimentary rocks (the Hongweikeng and Xiaoshui formations) in the Zhuyuan section overlie Lower Triassic limestones and mudstones on an angular unconformity (Qian et al., 1987), and have been used to establish missing parts of the Daxi section.

3.4. Facies associations and depositional environments

Thirteen lithofacies are recognised (**Table 3.1**), and grouped into four facies associations based on interpreted depositional settings (e.g., Reading, 1986). We describe below the associations (**Figs 3.2-3.5**), with field locations marked in the lithostratigraphic columns in **Figures 3.6B** and **3.7**. The upper-case letters or letter prefixes in the lithofacies codes each designates a textual class, for instance, 'C' represents carbonaceous mudrock and coal, 'M' for mudrock (siltstone, shale, and mudstone), 'S' for sandstone, 'MS' for mixed mudrock and sandstone, and 'G' for conglomerate. The lower-case letters or letter suffixes each designates a qualifying

structure, where ‘bio’ is for bioturbation, ‘d’ for convolute bedding, ‘h’ for horizontal lamination, ‘m’ for massive/structureless, ‘p’ for planar cross-lamination, ‘r’ for ripple marker, and ‘t’ for trough cross-lamination and cross-bedding.

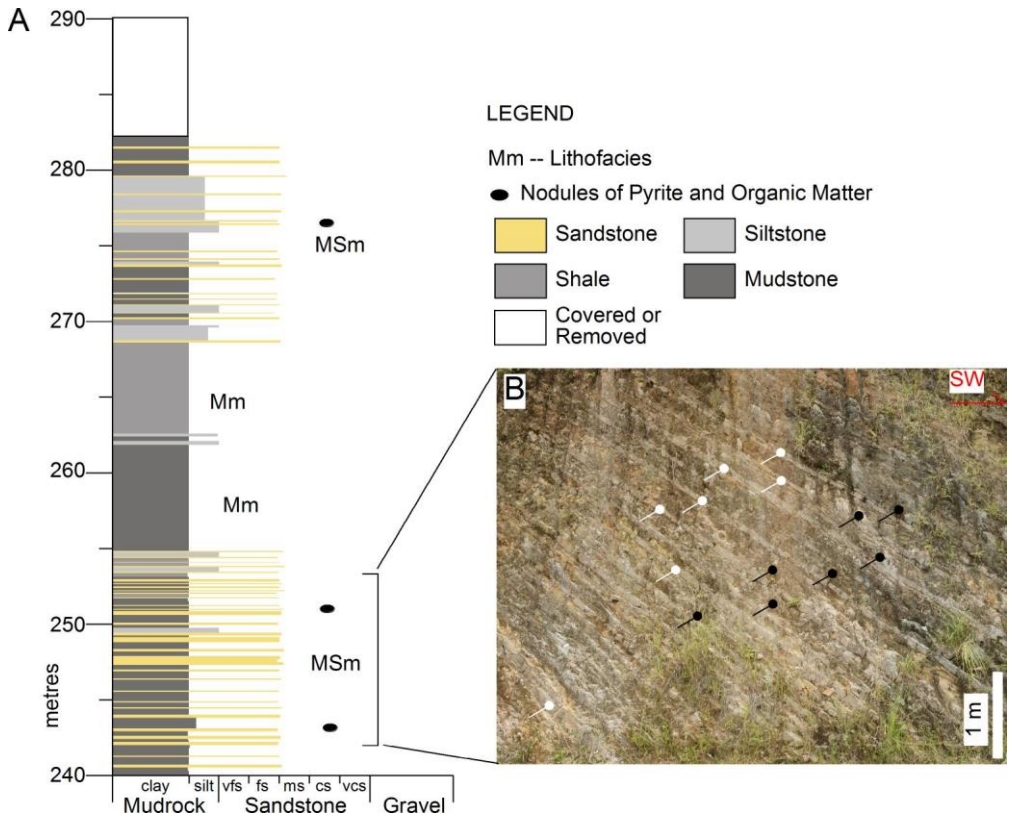

Figure 3.2 Details of prodelta facies association. (A) Vertical profile of massive mudrock (Mm), and mixed, interbedded mudrock and sandstone (MSm) (see **Figure 3.6B** for position). vfs = very fine-grained sandstone; fs = fine-grained sandstone; ms = middle-grained sandstone; cs = coarse-grained sandstone; vcs = very coarse-grained sandstone. (B) Outcrop photographs of MSm. White arrows show sandstones; black arrows show mudrocks.

3.4.1. Prodelta facies association

This association is dominated by Mm (**Fig. 3.2A**) and Mh (**Fig. 3.3A**), along with subordinate amounts of MSm (**Fig. 3.2A, B**), MSr (**Fig. 3.3B**), Sd, Sp, Sh and Sm (**Table 3.1**). It generally comprises tabular to wavy bedsets, with pebbles of sandstone, and nodules of pyrite and organic matter (**Figs 3.2A, 3.3C**). Planar cross-bedding within sandstone beds is rare, being present in only the uppermost parts of the association. Horizontal lamination within sandstone beds is also preserved in this part, in which laminae are marked by variations of grain size and colour (**Fig. 3.3D**).

Massive beds of sandstone intercalated with massive mudstone make up rare bedsets (**Fig. 3.4A**).

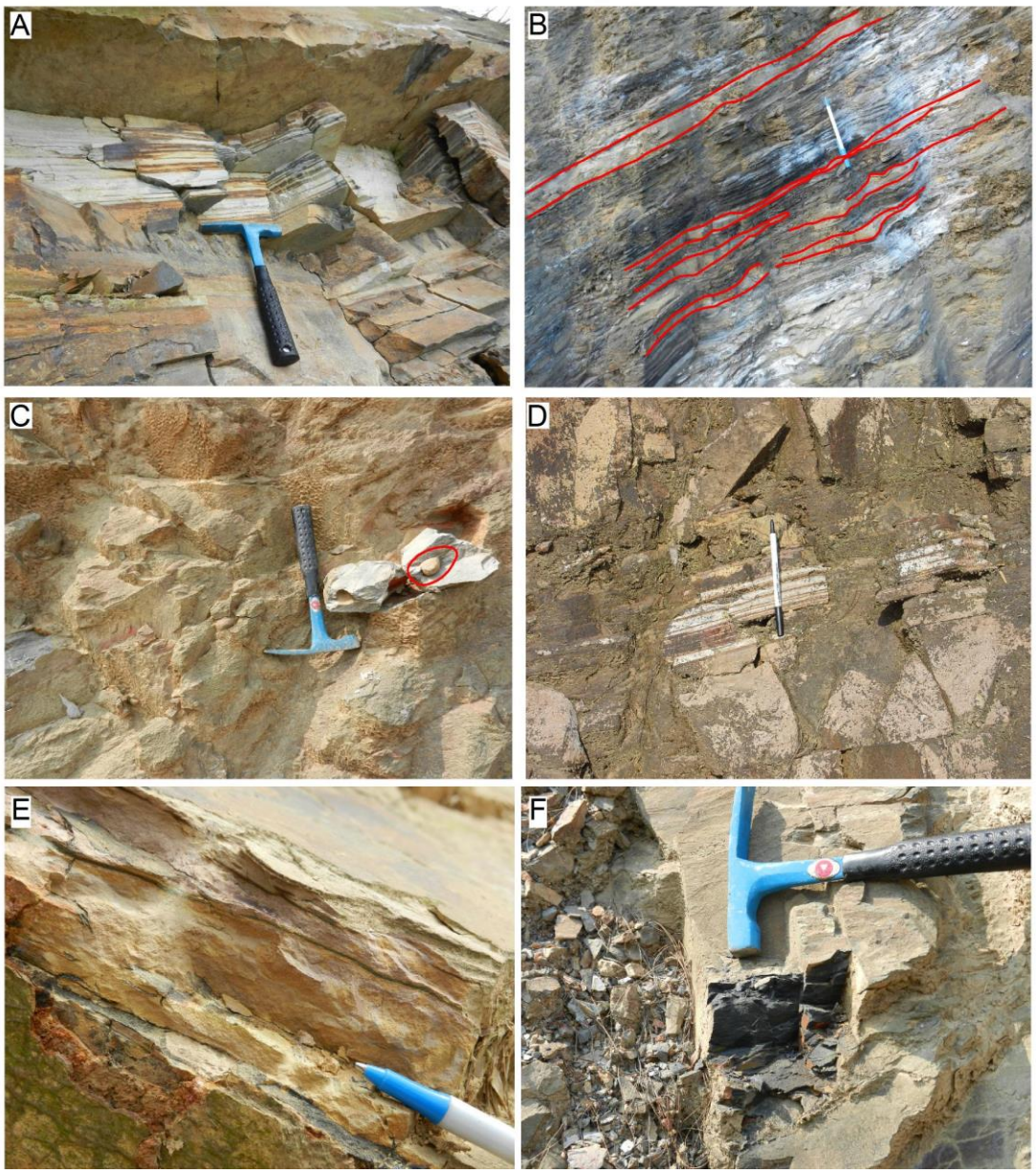

Figure 3.3 Outcrop photographs of lithofacies in prodelta and fluvial facies association. (A) Horizontal lamination in mudstone beds (Mh). (B) Starved ripple marks and lenticular bedding in MSr. (C) Sandstone pebbles in grey massive mudstones (Mm). (D) Horizontal laminations in fine-grained sandstones (Sh), separated by variations of grain size and colours. (E) Dark coloured mud drapes and clasts in yellow, muddy siltstones and very fine-grained sandstones. (F) Dark coloured, massive and carbonaceous mudrock (Mm and C).

Structureless to horizontally laminated mudrocks are interpreted to record suspension deposition from subaqueous density currents (e.g., Lowe, 1982), and

represent the most distal deposits of the Daxi section. MSm (**Fig. 3.2**), which is unique to this association, records the episodic introduction of sand (e.g., Gani and Bhattacharya, 2007). In contrast, MSr (**Fig. 3.3B**), which is similar to lenticular bedding as described by Collinson et al. (2006), implies that deposition formed under slow suspension fallout and varied traction conditions with limited supply of sand. Starved ripples in MSr in places (**Fig. 3.3B**) indicate that the currents or waves were relatively strong, i.e., exceeding the critical erosional velocity (Collinson et al., 2006). Sd is interpreted to be related to gravity loading and dewatering after deposition (Gani and Bhattacharya, 2007).

Plant fragments are sporadic and poorly preserved, whereas bivalves and ammonites in this facies association indicate an open marine environment. These deposits are interpreted to represent a marine prodelta environment (e.g., Gani and Bhattacharya, 2007). The interbedded sandstone layers are interpreted to record flood events that spread sand over the prodelta.

3.4.2. Delta-front facies association

Overlying prodelta mudrocks, this facies association is made up of 10 lithofacies, three of which are unique to the association. The dominant lithofacies are: Sm, St, Sr, Sp, Sbio and Gm, together with subordinate Sh, MSr, Mm and Mh (**Table 3.1**; **Figs 3.4B, 3.4D, 3.5A**). Sandstones are poorly to well sorted, with individual bed thickness up to 5 m. Sandstones and mudrocks are arranged into upward-thickening, upward-coarsening packages, in which individual beds of sandstone also thicken upwards within bedsets (**Fig. 3.4B**). However, in some of those packages the contact between mudrocks and overlying sandstones is sharp (**Fig. 3.4B-D**). Sedimentary structures are abundant in sandstones (**Fig. 3.5**), including bioturbation, asymmetrical to near-symmetrical ripple marks, planar cross-lamination, horizontal lamination and trough cross-bedding. Sandstone beds have tabular, wavy or channel-shaped geometries, showing variations from laminated beds up to thick, channel-shaped sandstone bodies in places resembling side-bar structures (e.g., Miall, 1985) (**Fig. 3.4**). Mud drapes up to 4 cm-thick are preserved within channel-shaped sandstone bedsets (**Fig. 3.4D**). Beds of Gm (20 cm-thick and average pebble size ~30 mm) (**Fig. 3.7A**) are matrix-rich, weakly graded and pinch out laterally.

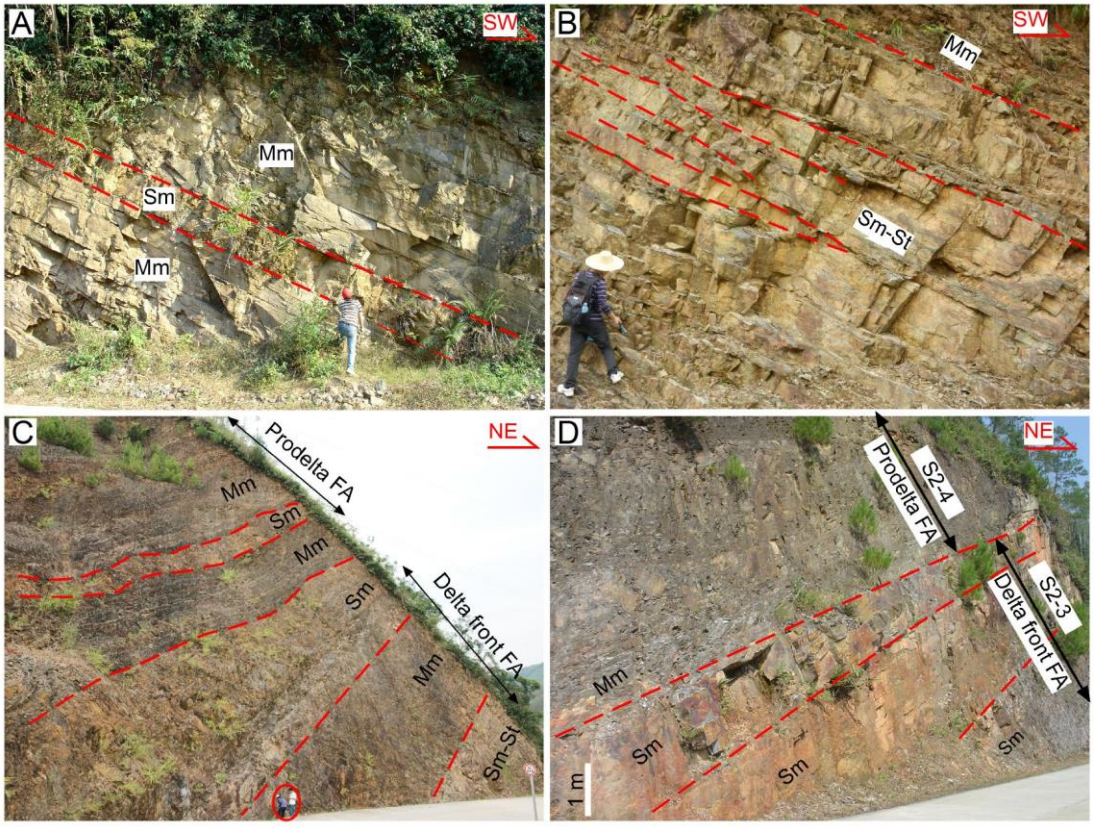

Figure 3.4 Outcrop photographs of prodelta and delta-front facies associations. (A) Thick and massive mudstone bedsets (Mm) and interbedded sandstone bed (Sm) of prodelta facies association. (B) Lateral pinched-out and upward-thickening sandstone beds (Sm and St) of delta-front facies association, overlain by thin mudstone beds (Mm) with erosional contacts. (C) Sandstone bedsets of delta-front facies association, overlain by massive mudrocks (Mm) and sandstones of prodelta facies association. (D) Lateral pinched-out and upward-thickening sandstone beds (Sm) of delta-front facies association, overlain by massive mudrocks (Mm) of prodelta facies association.

Thick bedsets of sandstone possibly resulted from rapid deposition from sand-rich currents, without wave or tide reworking. Bioturbation (**Fig. 3.5B**) implies organic activity during and after deposition. The asymmetrical straight-crested ripple marks (**Fig. 3.5C**) are interpreted to record shoaling waves or an interaction of waves and currents of similar directions (e.g., Collinson et al., 2006), whereas near-symmetrical ripple marks record wave processes (**Fig. 3.5D**). Varied scales of sets of trough cross-bedding (**Fig. 3.5E**) are interpreted to represent deposits of lower flow regime dunes in channels with fluctuating current strengths. In addition, massive conglomerates and mudrocks imply a fluvial, rather than a shoreface, setting. Based on the above criteria, this sandstone-dominated association is interpreted to record a fluvial-dominated delta-front setting (e.g., Dreyer et al., 1999; Bhattacharya, 2010).

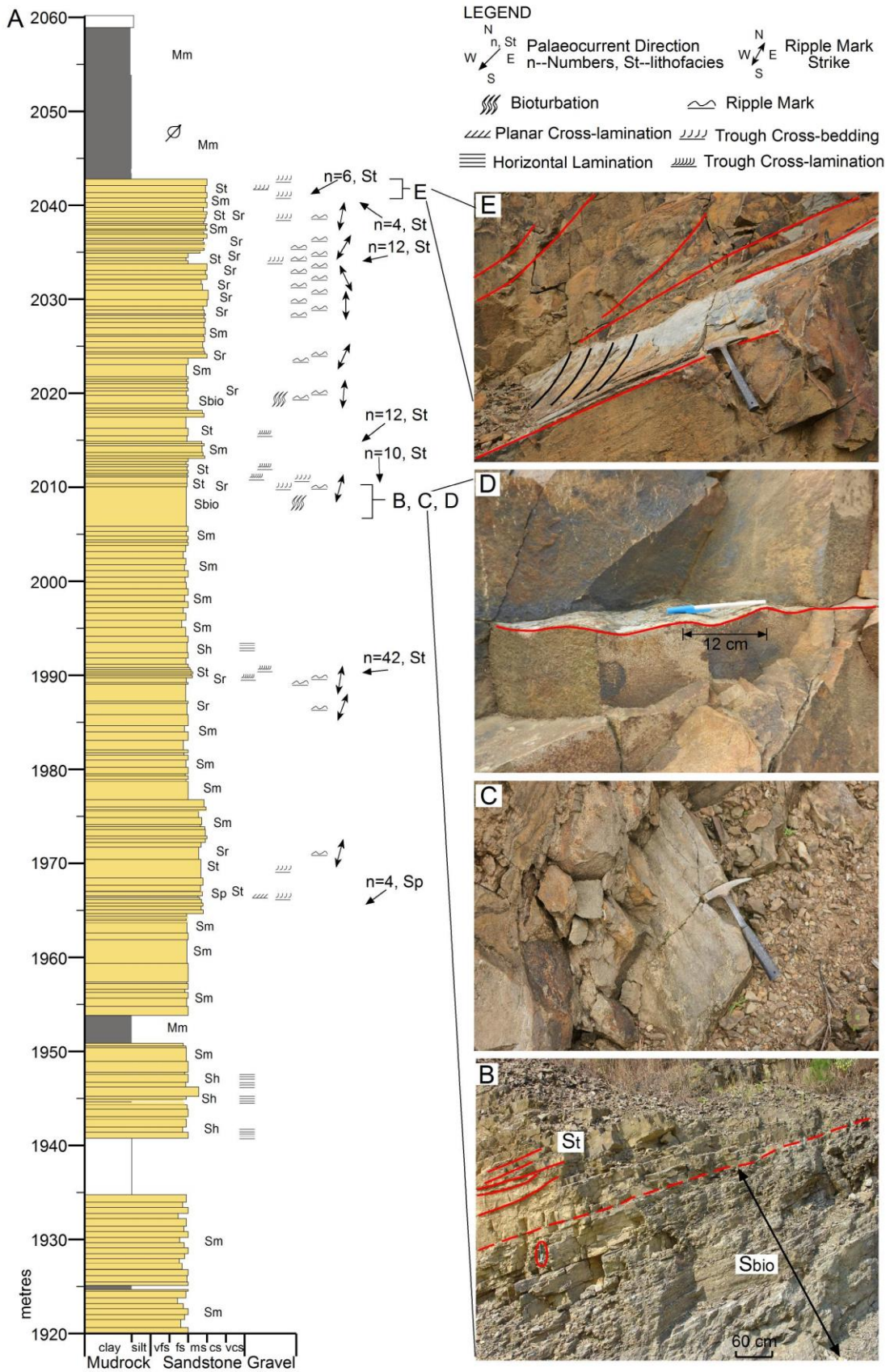
A
2060
2050
2040
2030
2020
2010
2000
1990
1980
1970
1960
1950
1940
1930
1920
metres
clay silt vfs fs ms cs vcs
Mudrock Sandstone Gravel
LEGEND
Palaeocurrent Direction
n--Numbers, St--lithofacies
Ripple Mark Strike
Bioturbation
Ripple Mark
Planar Cross-lamination
Trough Cross-bedding
Horizontal Lamination
Trough Cross-lamination
n=6, St
E
n=4, St
n=12, St
n=12, St
n=10, St
B, C, D
n=42, St
n=4, Sp
Mm
Sm
St
Sr
Sbio
Sh
Sp
E
D
12 cm
C
B
St
Sbio
60 cm

Figure 3.5 Details of delta-front facies association. (A) Vertical profile and sedimentary structures, along with the measured palaeocurrent data (see **Figure 3.7** for position). Mean vector azimuth of palaeocurrent is calculated after Bass (2000). (B) Bioturbated muddy (Sbio) and trough cross-bedded sandstone bedsets (St). (C) Near-asymmetrical ripple marks. (D) Asymmetrical ripple marks with wave lengths of 12 cm developed at the top of a sandy bed. (E) Trough cross-bedding in the uppermost sandstone beds.

The thickening-upward trend of sandstone beds indicates that river discharges gradually increased and water depths shallowed, implying a shoal-water type delta system (e.g., Postma, 1990). The sharp contact between delta-front sandstones and prodelta mudrocks possibly implies that subaqueous delta channels locally migrated into the prodelta setting.

3.4.3. Delta-plain facies association

This facies association is probably under-represented in the Daxi section because of poor exposures. Overlying delta-front sandstones, it generally comprises fining-upward units involving Sm and Mm. Sandstones are medium- to coarse-grained, and moderately to well sorted, in tabular beds or bedsets. Dark coloured mud drapes and mud clasts are present in yellow, muddy siltstones and very fine-grained sandstones (**Fig. 3.3E**). Fossil plants are present, but are scarce in mudrocks. Sedimentation units are interpreted to represent a delta-plain distributary system, although more field data are required to better establish this interpretation.

3.4.4. Fluvial facies association

This association comprises Mm, C, Sm and Gm (**Table 3.1**). Massive mudrocks (Mm) are generally dark grey with little organic matter, whereas carbonaceous mudrocks (C) are black and organic-rich. Two types of vertical facies associations are recognised. Type 1 deposits are dominated by Gm and Sm, with minor interbedded mudstones and coal seams, and are described mainly from the Zhuyuan section by Qian et al. (1987). Fining-upward trends from conglomerate to mudstone are typical of Type 1 deposits. Conglomerates and sandstones are interpreted to be the products of fluvial channels, whereas the interbedded mudstones and coal seams were likely formed in overbank setting (e.g., Miall, 1985; Ghazi and Mountney, 2009).

Type 2 deposits comprise mainly Mm and C, with minor Sm and Mh (**Fig. 3.3F**), and overlie Type 1 deposits. Small-scale coarsening-upward trends from mudstones to sandstones are present. Coals and fossil plants are most abundant in Type 2 deposits. Brackish-water bivalves (*Bakevelloides hekiensis* and *Modiolus* sp.; Qian et al., 1987) are present in mudrocks. Massive, carbonaceous mudrocks are attributed to deposition from overbank suspension, whereas massive sandstones were formed due to crevasse splay (e.g., Miall, 1996; Corbett et al., 2011). Based on fossils and component lithofacies, a coastal-plain fluvial overbank setting with swamps is interpreted for Type 2 deposits (e.g., Corbett et al., 2011).

3.5. Sequences

For the Daxi section, two coarsening-upward packages are present in the lower and the upper parts of the succession; these are named respectively Sequence 1 (S1), and Sequence 3 (S3). The intermediate Sequence 2 (S2) comprises four, nested coarsening-upward rhythms, and these are named, from lower to upper, Sequences 2-1, 2-2, 2-3 and 2-4 (**Figs 3.6, 3.7**). The large-scale coarsening-upward packages and the smaller, nested coarsening-upward rhythms are interpreted to have been produced by progradation and retrogradation of a deltaic depositional system (e.g., Bhattacharya, 2010). By combining the Daxi and the Zhuyuan sections, a complete depositional history is presented.

3.5.1. Basal coal-bearing fluvial deposits

Basal deposits were documented in the Zhuyuan section (**Fig. 3.1B**), and assigned to the Hongweikeng Formation, which unconformably overlies Lower Triassic and older rocks and is the oldest unit of the T_3-J_1 basin in Guangdong Province (Qian et al., 1987; GBGMR, 1988). Three cycles are recognised (**Fig. 3.6A**), each of which is made up of fluvial-channel and overbank associations. In the first cycle, fluvial-channel deposits are up to 50 m-thick, and are overlain by ~150 m of overbank deposits, showing a fining- to coarsening-upward trend (Qian et al., 1987; **Fig. 3.6A**). Fossil plants (e.g., *Pterophyllum sinense, Ptilozamites chinensis*, and *Nilssonian furcate*) and brackish-water bivalves (e.g., *B. hekiensis* and *Modiolus* sp.)

are present (ZY01-03 in **Table 3.2**; Qian et al., 1987). Nodules of pyrite and siderite, and minable coal seams are also preserved in the lower part of the first cycle (Qian et al., 1987; **Fig. 3.6A**).

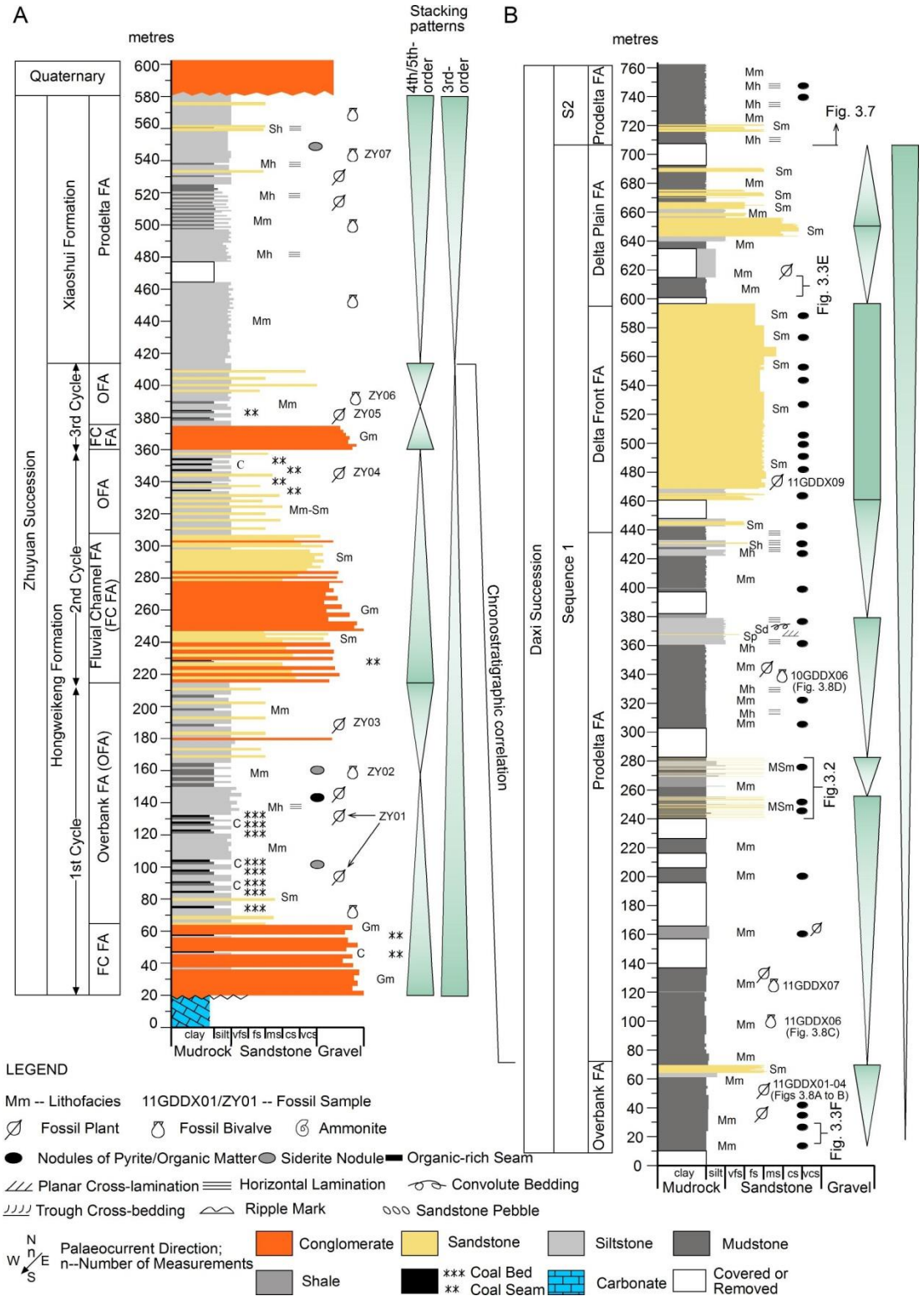

Figure 3.6 Stratigraphic columns of the Daxi and the Zhuyuan successions. (A) Vertical profile, facies associations and stratigraphic stacking patterns of the Zhuyuan succession (from Qian et al., 1987). The section is covered by Quaternary sediments, and lacks the top part. Fossils, sedimentary structures, coal seams, and nodules of siderite and pyrite are marked along with the lithofacies. FA = Facies association. (B) Vertical profile, facies associations and stratigraphic stacking patterns of Sequence 1 (S1) of the Daxi succession. Fossils, sedimentary structures and nodules of pyrite and organic matters are plotted along with the lithofacies. Positions of the outcrop and fossil photographs presented are also marked.

The second cycle comprises up to 90 m of fluvial-channel deposits and 55 m-thick overbank deposits, whereas fluvial-channel deposits are only 15 m-thick in the third cycle, and overbank deposits are 35 m-thick (Qian et al., 1987; **Fig. 3.6A**). A fining-upward trend is present in the second cycle, whereas a fining- to coarsening-upward trend is present in the third cycle (**Fig. 3.6A**). Coals are common in both cycles (Qian et al., 1987; **Fig. 3.6A**). Fossil plants (e.g., *Anthrophyopsis tuberculata, Pterophyllum aequale*, *Pterophyllum ptilum* and *Sinoctenis calophylla*) are present in the second and third cycles (ZY 04-05 in **Table 3.2**; Qian et al., 1987), whereas shallow-marine bivalves (e.g., *Unionites*? *concentrica, Unionites* cf. *dubia* and *Myophoriopis* cf. *acyrus*; ZY06 in **Table 3.2**) are present in the uppermost part of the overbank unit in the third cycle (Qian et al., 1987; **Fig. 3.6A**), implying a marine influence. Sedimentological and palaeontological data imply that the depositional environment changed from fluvial to marine-influenced coastal plain.

The cyclic upward-fining patterns were possibly generated by the lateral migration of river channels and the gradual abandonment of channel systems, whereas the upward-coarsening patterns in the overbank deposits of the first and third cycles may have been formed by crevasse splaying. The overall fining-upward (retrogradational) trend of the Hongweikeng Formation (**Fig. 3.6A**) implies that accommodation creation outstripped sediment supply.

3.5.2. Sequence 1 (S1)

Sequence 1 is well defined in the lower part of the Daxi section, where it is over 700 m-thick, and has an overall upward-coarsening trend from fluvial-overbank or prodelta facies to delta-front or delta-plain facies (**Fig. 3.6B**).

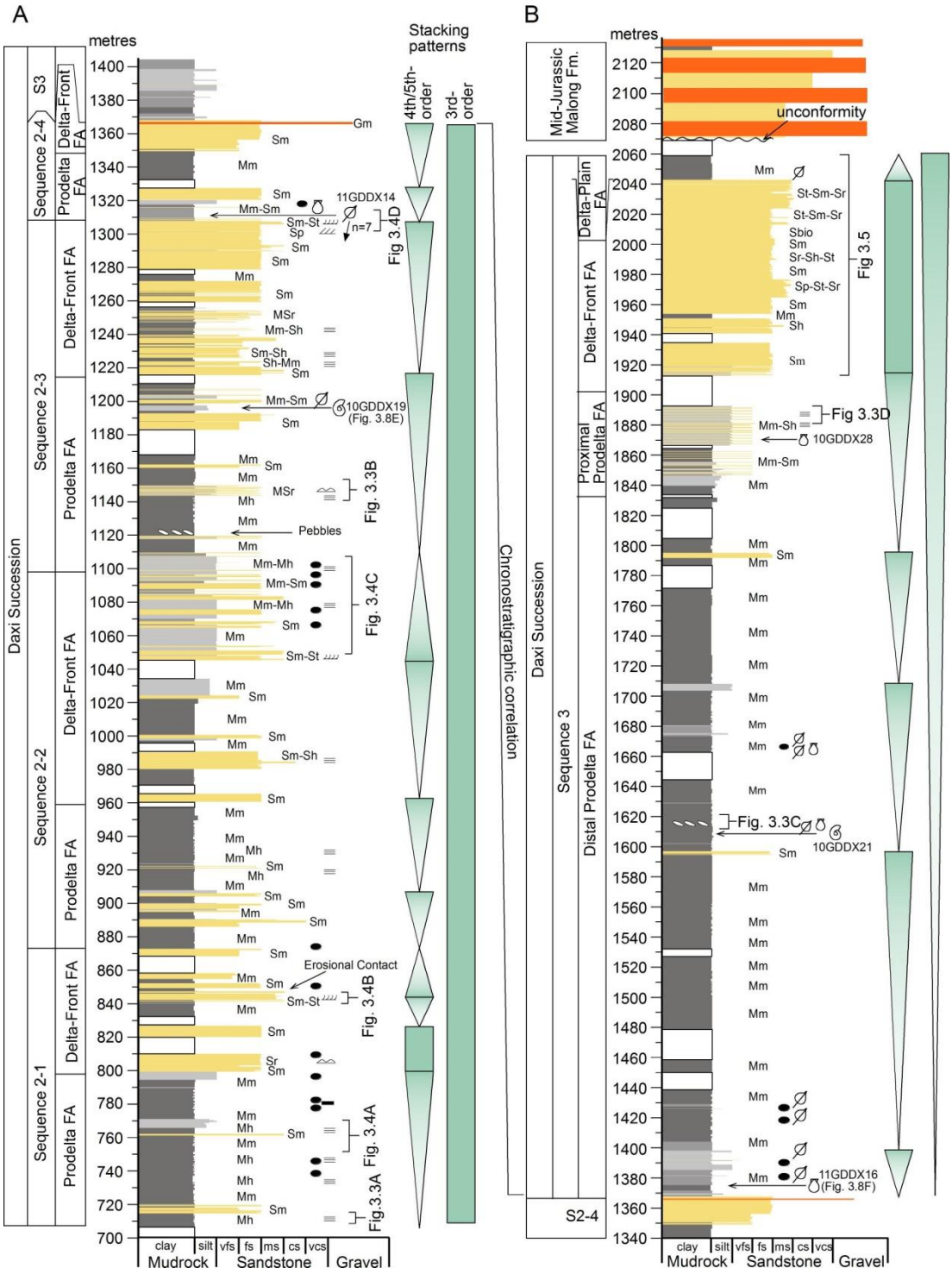

Figure 3.7 Stratigraphic columns of the Daxi succession. (A) Vertical profile, facies associations and stratigraphic stacking patterns of Sequence 2 (S2). Fossils, sedimentary structures and nodules of pyrite and organic matters are plotted along with the lithofacies. Positions of the outcrop and fossil photographs presented are also marked. (B) Vertical profile, facies associations and stratigraphic stacking patterns of Sequence 3 (S3). Legend is same as in **Figure 3.6**.

The base of S1 is characterised by 60 m-thick overbank deposits, with abundant well-preserved fossil plants and nodules of pyrite and organic matter (**Fig. 3.6B**). Fossil plants, such as *Neocalamites* cf. *hoerensis* (Schimper) Halle, *Todites* cf. *scoresbyensis*, *Pityophyllum* sp., and *Elatocladus* sp. (**Table 3.2**; **Fig. 3.8A-B**), are present in dark silty mudstones. Well-preserved fossil plants in mudrocks indicate that the overbank floodplain area was colonised by vegetation, whereas massive sandstone bedsets are interpreted to have formed by crevasse splay (**Fig. 3.6B**). A shallowing-upward stacking (0-70 m) is observed in this sedimentation unit.

Overbank deposits pass upwards into prodelta deposits, which are at least 400 m thick (**Fig. 3.6B**), reporting a rapid drowning. Plant debris is poorly preserved, whereas shallow-marine bivalves (Fan, 1963a; Yin et al., 1964; Chen, 1987a) such as *Pleuromya elongate* Agassiz, *Liotrigonia yanshouensis* J. Chen and *Pleuromya oblonga* Fan, are present in mudrocks (10GDDX06, 11GDDX06, 11GDDX07 in **Table 3.2**; **Fig. 3.8C-D**). Four coarsening-upward cycles are present, from 70 to 250 m, 250 to 280 m, 280 to 380 m, and 380 to 460 m on the measured section (**Fig. 3.6B**).

Similar lithologies and fossils are present the Zhuyuan section, where the Xiaoshui Formation comprises mudrocks with siderite nodules and interbedded horizontal laminated sandstones up to 170 m-thick (Qian et al., 1987; **Fig. 3.6A**). Shallow-marine bivalves, such as *Plagiostoma xiaoshuiensis, Oxytoma dabashanensis, Pleuromya* cf. *oblonga,* are abundant (ZY07 in **Table 3.2**; Qian et al., 1987; **Fig. 3.6A**), implying a marginal-marine environment, possibly an interdistributary bay or prodelta. Based on the lithofacies and fossils, the prodelta deposits of S1 are correlated with the Xiaoshui Formation, whereas the underlying overbank sediments of S1 are equivalent to the upper part of the Hongweikeng Formation (**Fig. 3.6**).

The delta-front facies association of S1 is mainly made up of massive sandstone overlying prodelta mudrocks (**Fig. 3.6B**). Tabular beds have a thickness from 30 cm to several metres and are laterally continuous. Pyrite nodules are extremely common and comprise isolated drusy masses and reddish clays in the cores. Fossil plants (*Neocalamites*? sp.; 10GDDX09 in **Table 3.2**) are present but

scattered in the sandstone. Unlike the prodelta units, vertical stacking of delta-front deposits is aggradational (**Fig. 3.6B**).

Figure 3.8 Fossils collected in the Daxi section. (A) Fossil plant (*Todites* cf. *scoresbyensis*). (B) Fossil plant (*Pityophyllum* sp.). (C) Shallow-marine bivalve (*Pleuromya elongate* Agassiz). (D) Shallow-marine bivalve (*Pleuromya oblonga* Fan). (E) Ammonite (*Hongkongites hongkongensis* Buchman). (F) Shallow-marine bivalve (*Retroceramus subinconditus* J. Chen). See **Table 3.2** for details.

The upper part of S1 is made up of a 100 m-thick delta-plain unit, which overlies the delta-front deposits (**Fig. 3.6B**). Poorly preserved plant debris is present. Because of poor exposure, details of sedimentary structures are not available, but

several fining-upward cycles in grain sizes are recognised. Vertical stacking of this unit varies from progradational (lower part, 595-650 m) to retrogradational (upper part, 650-700 m) (**Fig. 3.6B**). Overall, the upward change from fluvial to prodelta, and then back to delta-plain deposits in S1 reflects a transgression-regression cycle of basin filling (**Fig. 3.6B**).

3.5.3. Sequence 2 (S2)

Sequence 2 is at least 600 m-thick, consisting of four nested coarsening-upward cycles (S2-1, 2-2, 2-3 and 2-4) (**Fig. 3.7A**). Prodelta and delta-front facies associations are recognised in each cycle.

The thickness of the prodelta association varies from 40 to 110 m, and is made up of monotonous 1 cm to m thick tabular bedsets of mudrock and sandstone. Nodules of pyrite and organic-matter are commonly distributed along bedding planes, particularly in S2-1. An organic-rich seam in dark silty mudstone is present in S2-1. No fossils were found in the prodelta deposits of S2-1 and S2-2, whereas fossils of plants, ammonites and bivalves are preserved in S2-3 and S2-4. In particular, ammonites such as *Hongkongites hongkongensis* Buchman and *Arietites* sp. (10GDDX19 in **Table 3.2**; **Fig. 3.8E**), are preserved in the thick silty mudstone in S2-3 (**Fig. 3.7A**), indicating an open-marine environment (Fan et al., 1965; Sun et al., 1980; Wang and Smith, 1986; Wang and Li, 1983). Fossil plant (e.g., *Neocalamites*? sp.; 11GDDX14 in **Table 3.2**) and bivalve fragments are present but are poorly preserved in S2-4.

Overlying the prodelta deposits, delta-front units generally vary from 20 to 140 m in thickness. Individual beds range from 1 cm to several m in thickness. Erosional contacts between sandstones and overlying mudstones are observed in S2-1 (**Fig. 3.7A**). Palaeocurrent data indicate a south-southeast palaeoflow (**Fig. 3.7A**), although data are sporadic. Many parts of the lower half of the delta-front units of S2-2 are weathered and poorly exposed, but exposures suggest that it comprises mostly massive, thin-bedded mudrock and sandstone. These rocks pass upwards into thick channel-shaped and lenticularly bedded sandstones, which in turn are overlain by prodelta massive mudrocks (**Fig. 3.4C**).

Table 3. 2 Fossil samples in the Daxi and the Zhuyuan sections. Sample ZY 01, 02, 03, 04, 05, 06, and 07 from Qian et al. (1987); others were collected in this study. See **Figures 3.6** and **3.7** for sample positions.

Sample	Flora/Fauna	Species	Stage/Age	Sample Position	Photograph
ZY01	Plant	*Podozamites lanceolatus*; *Pterophyllum sinense*; *P. ptilum*; *P. aequale*; *P. exhibens*; *Thinnfeldia* sp.; *Neocalamites* sp.; *Ctenis* sp.; *Pseudoctenis* sp.; *Marattia* sp.; *Baiera* sp.; *Ptilozamites chinensis*; *Nilssonia furcata*; *Anthrophyopsis crassinervis*; *Otozamites* sp.	Late Triassic	Hongweikeng Formation	
ZY02	Bivalve	*Bakevelloides hekiensis; Modiolus* sp.	Carnian	Hongweikeng Formation	
ZY03	Plant	*Sinoctenis calophylla*; *Pterophyllum sinense*; *Clathropteris* sp.	Late Triassic	Hongweikeng Formation	
ZY04	Plant	*Sinoctenis calophylla*; *Pterophyllum aequale*; *P. ptilum*; *Anthrophyopsis tuberculata*	Late Triassic	Hongweikeng Formation	
ZY05	Plant	*Pterophyllum ptilum; P. angustum*; *P.aequale*; *P. subaequale*; *Anthrophyopsis tuberculata*; *A. vanulosa*; *Clathropteris* sp.	Late Triassic	Hongweikeng Formation	
ZY06	Bivalve	*Unionites*? *Concentrica*; *U.* cf. *dubia*; *Myophoriopis* cf. *acyrus*	Carnian	Hongweikeng Formation	
ZY07	Bivalve	*Plagiostoma xiaoshuiensis*; *Oxytoma zhuyuanensis*; *O.* aff. *Mojsisovicsa zhongguoensis*; *Chlamys similis*; *Entolium kolymensis*; *Palaeopharus huagushanensis*; *Bakevelloides hekiensis*; *Modiolus paronaiformis*; *Nanlingella niugudunensis*; *Plicatula* cf. *carinata*; *Isognomon (Mytiloperna) Nanlingensis*; *Isocardioides yini*; *Pteria frechii*; *Homomya matsuoensis*; *Pleuromya triangularis*; *P.* cf. *oblonga*; *Unionites*? cf. *dandunensis*; *Myophoria* sp.; *Krumberckia lanpingensis*; *Palaeocardita* sp.	Carnian-Norian	Xiaoshui Formation	
11GDDX01	Plant	*Neocalamites* cf. *hoerensis* (Schimper) Halle	Late Triassic	S1	
11GDDX02	Plant	*Todites* cf. *scoresbyensis*	Late Triassic	S1	Fig. 3.8A
11GDDX03	Plant	*Pityophyllum* sp.	Late Triassic to Early Jurassic	S1	Fig. 3.8B
11GDDX04	Plant	*Elatocladus* sp.	Late Triassic to Early Jurassic	S1	
11GDDX09	Plant	*Neocalamites*? sp.	Late Triassic to Early Jurassic	S1	
11GDDX06	Bivalve	*Pleuromya elongate* Agassiz	Late Triassic	S1	Fig. 3.8C
11GDDX07	Bivalve	*Liotrigonia yanshouensis* J.Chen	Late Triassic to Early Jurassic	S1	
10GDDX06	Bivalve	*Pleuromya oblonga* Fan	Late Triassic to Early Jurassic	S1	Fig. 3.8D
10GDDX19	Ammonite	*Hongkongites hongkongensis* Buchman*; Arietites* sp.	Lower Sinemurian	S2-3	Fig. 3.8E
11GDDX14	Plant	*Neocalamites*? sp.	Late Triassic to Early Jurassic	S2-4	
11GDDX16	Bivalve	*Pseudomytiloides dubius (*J. deC. Sowerby*); Retroceramus subinconditus* J.Chen	Sinemurian-Pliensbachian	S3	Fig. 3.8F
11GDDX21	Ammonite	*Ammonoid* gen. st. ind	Sinemurian-Pliensbachian	S3	
10GDDX28	Bivalve	*Chlamys* cf. *tenuistrianta* Fan	Sinemurian-Pliensbachian	S3	

Based on sedimentary characteristics, the vertical stacking of each cycle from prodelta to delta-front facies association is progradational, whereas stacking patterns within delta-front deposits vary from cycle to cycle. For instance, aggradational stacking is present in S2-1 from 800 to 830 m on the measured section, which is followed by progradational and then retrogradational stacking between 840 and 860 m (**Fig. 3.7A**). Progradation (960-1080 m) and retrogradation (1080-1100 m) are observed in the delta-front facies association of S2-2, but only progradational stacking is present in S2-3 and S2-4. Nevertheless, the long-term stacking pattern of S2 is aggradational, within which each upward change from delta front to prodelta unit records a back-stepping of facies tracts. An abrupt upward change from delta front to prodelta facies is generally observed, however, one exception is that the upward change from the delta front unit of S2-2 to the prodelta unit of S2-3 is gradual (**Fig. 3.7A**). The implication is that most back-stepping events were due to rapid drowning.

3.5.4. Sequence 3 (S3)

The upper part of the Daxi section, or Sequence 3, is overwhelmingly upward-coarsening, from prodelta to delta-front to delta-plain facies associations, with a total thickness of about 700 m (**Fig. 3.7B**).

The prodelta unit in the lower part of S3 is ~530 m-thick, and can be divided into two parts. The lower part (1370-1830 m) is dominated by mudrock, with rounded sandstone pebbles and eroded nodules of pyrite and organic matter (**Fig. 3.7B**), ranging from 10 cm to several metres in bed thickness. Shallow-marine bivalves, such as *Pseudomytiloides dubius* J.deC.Sowerby and *Retroceramus subinconditus* J. Chen (11GDDX16 in **Table 3.2**; Chen, 1987; **Fig. 3.8F**), are preserved in this unit. Fragments of ammonites (*Ammonoid* gen. st. ind.; 10GDDX21 in **Table 3.2**) and plants are also present in silty mudstones. The predominance of mudrocks implies that the lower part formed either in a prodelta or a distal-bay environment. In contrast, the upper part (1830-1900 m) consists of interbedded laminated sandstone and mudrock bedsets (**Fig. 3.7B**), varying from ~3 to 10 cm in bed thickness. Minor organic-rich shale layers are present. Shallow-marine bivalves (Fan, 1963; Yin et al., 1964), such as *Chlamys* cf. *tenuistrianta* Fan (10GDDX28 in **Table 3.2**), are present. The upward-increasing proportion of sandstone in the upper

part implies that it was deposited in a proximal prodelta environment. Five nested (smaller-scale) progradational stacking (coarsening-upward units) are present in the prodelta unit (**Fig. 3.7B**), suggesting that the delta periodically underwent progradation and subsequent backstepping.

The delta-front unit in the upper part (1910-2045 m) of S3 is dominated by sandstone, and has an approximate thickness of 135 m (**Figs 3.5, 3.7B**). Palaeocurrent data show that palaeoflows varied between south, southwest and northwest (**Fig. 3.5A**), all within the western hemisphere ($Vector_{mean}$ = 246, calculated using EZ-ROSE program (Baas, 2000), implying that the regional source area may have been to the east or northeast. The vertical stacking of this unit is aggradational and progradational, with upward changes to a more proximal facies association (delta plain) (**Fig. 3.7B**).

Overlying the delta-front sandstones, the delta-plain unit comprises massive mudrock and is about 20 m-thick in the uppermost of S3 (**Fig. 3.7B**). Beds range from several to tens of centimetres in thickness. Plant fragments are preserved in the dark grey mudstones, but are not well-enough preserved to enable classification. This unit is interpreted to have been deposited in a distributary overbank environment of a delta-plain (**Fig. 3.7B**), although data are limited. The top of this unit is truncated by a modern valley, which makes the contact between this unit and the overlying younger sedimentary rocks unclear. However, an angular unconformity is recognised regionally between the T_3-J_1 Lantang Group and the overlying Malong Formation (GBGMR, 1988, 1996; **Fig. 3.7B**). The precise depositional age of the Malong Formation is poorly constrained, although it is suggested to be Middle Jurassic age (GBGMR, 1988, 1996). Overall, the vertical stacking of S3 is progradational and records the shallowing of the T_3-J_1 basin.

3.6. Timing of deposition

The basal deposit (the Hongweikeng Formation) is considered to be of Carnian age according to the fossil record (Qian et al., 1987; GBGMR, 1988; GBGMR, 1996; **Figs 3.6A, 3.9**; **Table 3.2**). In this study, the Late Triassic fossil

plants in the Hongweikeng Formation, such as *Neocalamites* cf. *hoerensis* (Schimper) Halle and *Todites* cf. *scoresbyensis*, were found in the lowermost part of S1 in the Daxi section (**Fig. 3.6B**; **Table 3.2**). In the Zhuyuan section, the Hongweikeng Formation is conformably overlain by the Xiaoshui Formation, which has abundant shallow-marine bivalves of late Carnian to early Norian age (Qian et al., 1987; GBGMR, 1988; GBGMR, 1996; **Figs 3.6A, 3.9**; **Table 3.2**). Bivalves in the Xiaoshui Formation such as *P. oblonga* Fan, are also present in the lower part of S1 in the Daxi section (**Figs 3.6B, 3.8D**). Thus, the lowest part of S1 was probably deposited between the late Carnian and the early Norian (**Fig. 3.9**). The upper part of S1 is probably late Norian to Rhaetian in age (**Fig. 3.9**), consistent with the Late Triassic age assigned to the lower part of the Lantang Group (S1, here) (GBGMR, 1996). Recently, Lucas et al. (2012) redefined the boundary between the Carnian and the Norian at ~220 Ma. In that case, the Hongweikeng Formation may have deposited from ~235 to ~220 Ma, whereas the Xiaoshui Formation may range from ~220 to ~215 Ma (**Fig. 3.9**). The upper part of S1 possibly formed between ~215 and ~200 Ma (**Fig. 3.9**).

In the upper part of S2, the ammonites *H. hongkongensis* Buchman and *Arietites* sp. in S2-3 (**Figs 3.7A, 3.8E**), are interpreted to appear in earliest Sinemurian in South China (Yin et al., 1964; Fan et al., 1965; Wang and Smith, 1986). The shallow-marine bivalves, such as *Chlamys* cf. *tenuistriata* Fan and *Retroceramus subinconditus* J. Chen, in the lower part of S3 (**Figs 3.7B, 3.8F**), also appeared exclusively during the Sinemurian to the Pliensbachian (Fan, 1963a; Chen, 1987a). Therefore, S2 to the lower part of S3 probably formed between the Hettangian and the early Pliensbachian (**Fig. 3.9**). In addition, detrital zircon U-Pb ages of a medium-grained sandstone sample from the upper part of S2 obtained a maximum depositional age of ~192 Ma (**Chapter 6**). Thus, the boundary between S2 and S3 is placed at ~192 Ma or younger (**Fig. 3.9**). The depositional age of the uppermost part of S3 is poorly constrained due to the poor preservation of fossils. However, previous studies (GBGMR, 1988, 1996) suggested that this unit is the equivalent of the Qiaoyuan Formation, which was suggested to be late Pliensbachian to the Toarcian age (Qian et al., 1987; GBGMR, 1988; GBGMR, 1996). In addition, zircon U-Pb ages from a sandstone sample indicate a maximum depositional age of ~182 Ma for the uppermost part of the Qiaoyuan Formation (**Chapter 6**). Therefore,

it is suggested here that the Daxi-Zhuyuan sedimentary succession was deposited between the Carnian and the early Toarcian (~235 to ~180 Ma), lasting about 55 Myrs (**Fig. 3.9**).

As noted earlier, the Indosinian Orogeny in South China may have lasted from ~265 Ma to ~195 Ma (**Fig. 3.9**). Thus, the Daxi-Zhuyuan succession appears to span the late stage of the orogeny and the early stage of post-orogenic events, as defined by Li and Li (2007).

3.7. Discussion

3.7.1. Controls on basin filling

To understand forcing on sedimentation, allogenic controlling factors (e.g., eustasy, climate, and tectonics, e.g., Devlin et al., 1993; Blum and Törnqvist, 2000; Hampson et al., 2012), and autogenic controls (e.g., delta-lobe switching, and channel migration and avulsion, e.g., Johnson and Graham, 2004; Stouthamer and Berendsen, 2007; Hajek et al., 2012) are discussed.

The Late Triassic to the Early Jurassic eustatic curve of Haq et al. (1987) is used to estimate the influence of global sea level on the formation of the Daxi-Zhuyuan succession. Long-term global sea level rose to a maximum at ~223 Ma, and then fell to a minimum at ~205 Ma (Haq et al., 1987; **Fig. 3.9**). Sea level rose subsequently to a maximum at ~192 Ma and then fell slightly to a minimum at ~187 Ma, followed by rising to a maximum at ~182 Ma (Haq et al., 1987; **Fig. 3.9**). Recent study (Lucas et al., 2012) suggests that the Carnian-Norian boundary could be at about 220 Ma. In that case, the basal terrestrial sediments (Carnian-aged Hongweikeng Formation) were deposited during rising global sea level, whereas marine sedimentation (late Carnian-early Norian Xiaoshui Formation and lower part of S1) occurred during falling global sea level (**Fig. 3.9**). Global sea level rose gradually during the deposition of S2 (~201-192 Ma), which comprises stacked transgressive-regressive cycles with a long-term progradational pattern (**Fig. 3.9**). For the early Pliensbachian, there is a similar mismatch between falling global sea level and an aggradational stacking of mudrocks in the lower part of S3 (**Fig. 3.9**).

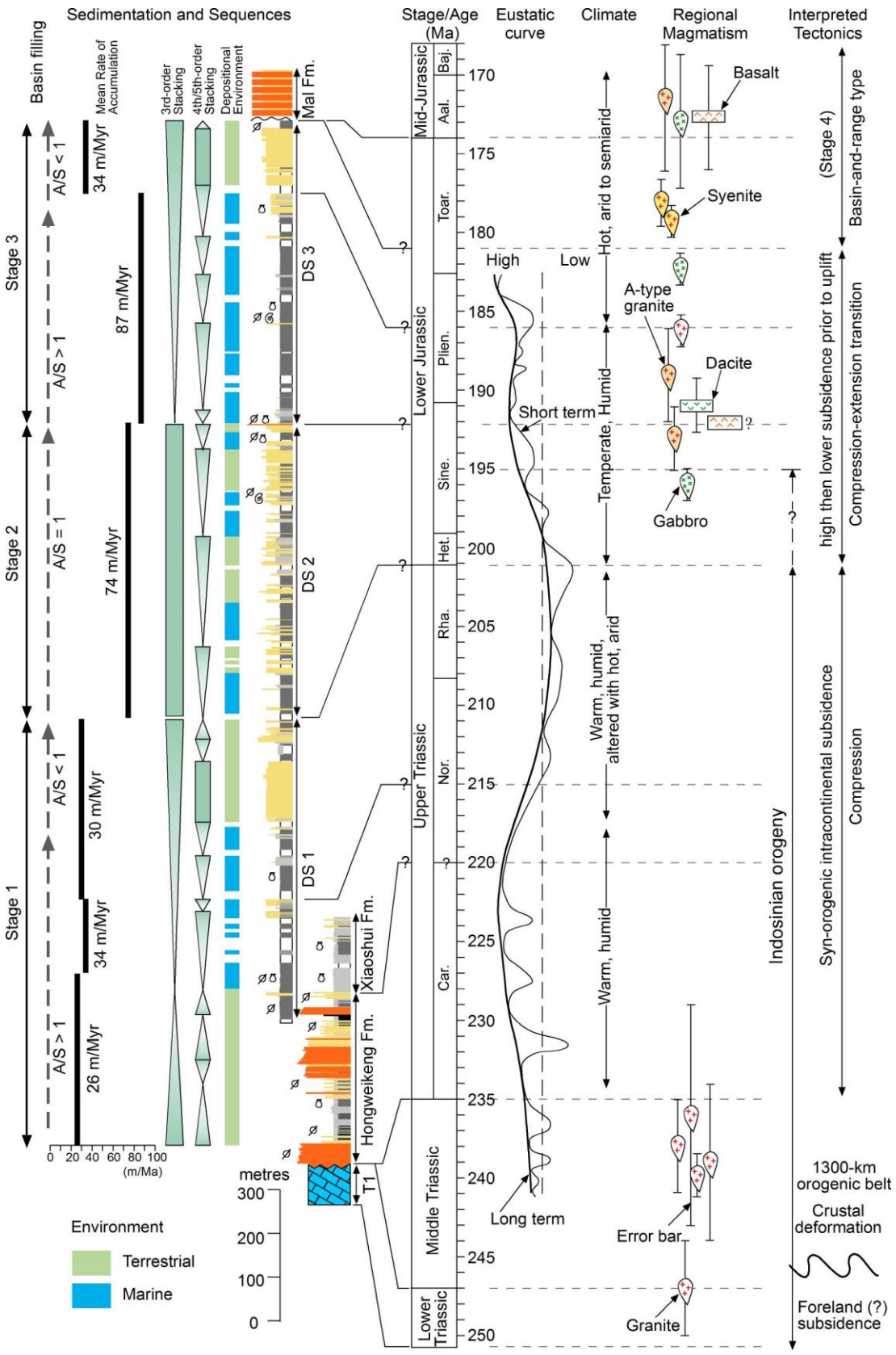

Figure 3.9 Stratigraphic synthesis of the Daxi-Zhuyuan succession. The depositional ages are based on fossils and regional stratigraphic correlation. Depositional environments, stacking patterns, average sediment accumulation rate (uncorrected for decompaction) are plotted along with the stratigraphic column. Eustatic curve

(after Haq et al., 1987), palaeoclimate (after Qian et al., 1987), regional magmatism (**Table 3.3**), and interpreted tectonics are also shown. Four stages are divided to depict the depositional history of the Daxi-Zhuyuan deltaic succession. Geological time scale is after the International Commission on Stratigraphy (2012). The age of the Carnian-Norian boundary (~220 Ma) follows Lucas et al. (2012). A = Accommodation; S = Sediment supply; Mal Fm = Malong Formation; T1 = Lower Triassic; Car. = Carnian; Nor. = Norian; Rha. = Rhaetian; Het. = Hettangian; Sine. = Sinemurian; Plien. = Pliensbachian; Toar. = Toarcian; Aal. = Aalenian; Baj. = Bajocian.

A tropical to subtropical climate with warm and humid conditions is interpreted during the Early-Late Triassic in South China, which became warm and humid alternating with hot and arid during the late-Late Triassic on the basis of fossil plants (Qian et al., 1987; **Fig. 3.9**). The warm and humid climate is consistent with the presence of coal deposits in the Hongweikeng Formation of the Zhuyuan section, as well as coal formation during the Late Triassic elsewhere in South China (e.g., Qian et al., 1987). As a result, palaeoclimate may have played an important role on vegetation and sedimentation by stabilising catchment areas as well as on floodplains, thereby reducing river sediment discharge. A temperate and humid palaeoclimate is interpreted during the early-Early Jurassic, followed by a hot and arid climate during the late-Early Jurassic (Qian et al., 1987; **Fig. 3.9**). Due to poor age constraints, the role of climatic influences on sedimentation stacking patterns may be underestimated here, and more details are required to better understand those influences.

Taking into account the long-term deposition of the Daxi-Zhuyuan deltaic succession, tectonic activity is interpreted to be the first-order allogenic factor that controlled sediment supply, accommodation and sedimentary stacking patterns, although autogenic deposition processes may also have been locally important. Overall, the long-term stratigraphic pattern is consistent with subsidence increasing through time, as discussed below.

3.7.2. Deposition and subsidence rates

Four depositional stages of the Daxi-Zhuyuan deltaic succession are interpreted.

3.7.2.1. Stage 1

This stage corresponds to the basal deposits (the Hongweikeng Formation) and overlying Xiaoshui Formation in the Zhuyuan section, and S1 in the Daxi section (**Figs 3.9, 3.10**). It records a retrogradation-progradation cycle formed during the Carnian to the Rhaetian. There are three divisions to the stage, each of which relates to three different sectors of the global sea-level curve (**Fig. 3.9**).

The first division is made up of three fining-upward cycles in the basal deposits, which overall show a retrogradational trend (A/S >1; **Fig. 3.9**). This implies that the overall rate of accommodation generation (A) outstripped the rate of sediment supply (S) (e.g., Catuneanu et al., 2009). During this interval, depositional environments cyclically shifted from fluvial channel to overbank, and finally to a marginal marine or prodelta environment (**Fig. 3.10**), signifying transgression. The three fining-upward sedimentary cycles correspond to a period of increasing global sea-level (to the maximum at ~223 Ma), and correlate to three shorter-term sea-level cycles (**Fig. 3.9**). The low overall sedimentation rate and the correlation of the three sedimentary cycles to shorter-term sea-level cycles indicate that the role of subsidence on sedimentation patterns was much less than the influence of global sea level. The implication is that initial basin subsidence rates were low.

The second division corresponds to the lower part of S1 and the Xiaoshui Formation, and is marked by an aggradational stacking of prodeltaic mudrocks with minor sandstones. Overall sedimentation rates were low during this time (34 m/Myr; **Fig. 3.9**), and the stratigraphic geometry is consistent with underfilling. Global sea-level was falling during this period, to a minimum at ~205 Ma (Haq et al., 1987), thereby generating a mismatch with the sedimentary response because an offshore shift in facies tracts is predicted. Rather, an increasing subsidence rate is interpreted to be the major control on the sedimentary response.

The third division, corresponding to the upper, sandstone-rich, part of S1, is characterised by low-sedimentation rates (30 m/Myr) and aggradational facies stacking (**Fig. 3.9**). However, this period corresponds to gradually increasing global sea level, which would predict gradual back-stepping of the facies tracts. Rather, there was an initial progradational jump from prodelta mudrocks to delta-front

sandstones, and then a return to aggradation. The initial change is interpreted to relate to delta progradation, and thereafter maintenance of the balance between sediment flux and subsidence-driven accommodation.

The interpretation of subsidence rates during Stage 1 is not typical of foreland basins, which initiate with very high rates of subsidence. Instead, Stage 1 shows low subsidence rates following initiation and increasing subsidence rates through time, but overall low sedimentation rates (**Fig. 3.9**). In fact, to maintain aggradational stacking of delta-front facies in the upper division while the global sea-level was rising, slightly decreasing subsidence rates can be envisaged towards to end of the stage.

3.7.2.2. Stage 2

This stage is defined by S2. It is made up of four Hettangian to late Sinemurian transgressive-regressive packages (**Fig. 3.9**), which are overall aggradationally stacked. The change from the uppermost delta-plain unit of S1 to the lowermost prodelta unit of S2 establishes a rapid back-stepping of facies tracts (**Fig. 3.10**). The change corresponds to the onset of rising global sea level at ~201 Ma, but the overall doubling of the sedimentation rate of Stage 2 relative to Stage 1 (~74 m/Myr versus ~30 m/Myr; **Fig. 3.9**) appears to be at odds with rising sea level. An explanation for the higher sedimentation rate is possibly that the basin and its source area increased in size, and at the same time there was uplift of the source area relative to global sea-level. The implication of increasing basin size is increasing basin subsidence. Aggradational stacking of the four transgressive-regressive packages appears to be at odds with combined long-term global sea-level rise and increasing subsidence, which predicts drowning. Furthermore, increasing sedimentation rates predict progradation. Neither factor alone can explain the transgressive-regressive packages or their aggradational stacking. Rather, Stage 2 is concluded to record a cyclical interplay between basin subsidence, sea-level change and uplift-related increasing sedimentation.

3.7.2.3. Stage 3

Stage 3 corresponds to a late Sinemurian to early Toarcian, retrogradation-progradation cycle (S3) recorded in the Daxi deltaic succession (**Figs 3.9, 3.10**). The dramatic change from fluvial conglomerates at the top of S2-4 to marine mudrocks at the base of S3 (**Fig. 3.10**), is interpreted to represent rapidly increasing accommodation at ~192 Ma (**Fig. 3.9**). As gradual sea-level fall began at the same time, rejuvenated subsidence probably caused the stratigraphic change. The subsequent long-lasting aggradational stacking of prodelta mudrocks (lower part of S3) occurred during global sea-level fall, while at the same time sediment accumulation rates were high (~87 m/Myr; **Fig. 3.9**). The cause of the aggradational stacking of mudrocks is interpreted to have been tectonic. As sedimentation rates were high, but progradation did not occur during globally falling sea level, it is probable that the long-term controlling factor was increasing subsidence. The change from prodelta mudrocks of the lower part of S3 to delta-front sandstones of the upper part of S3 records a progradational jump, but the change corresponds to the onset of globally rising sea level at ~187 Ma (**Fig. 3.9**). Sedimentation rates also fell dramatically (to 34 m/Myr, **Fig. 3.9**). The upper part of S3 ends in fluvial conglomerates, which is contrary to the predicted response to rising sea level. It is possible therefore that the influence of subsidence was low towards the end of Stage 3, and possibly the aggradational-progradational stacking was caused by relative sea-level fall due to regional uplift.

3.7.2.4. Stage 4

The basin was gradually shallowing between the early Toarcian and the Aalenian, as shown by the stacking pattern, and the angular unconformable relationship with the overlying Malong Formation (**Fig. 3.9**). As stated above, the age of the Malong Formation is poorly constrained although it has been assigned a Middle Jurassic age (GBGMR, 1988, 1996). Taking the Malong Formation to be of Middle Jurassic age, there would be a ~7 Myr lacuna between the early Toarcian and the Aalenian. However, regional analysis shows that to the northeast (~150 km) of the study area, the Middle Jurassic deposits (the Zhangping Formation) conformably overlies the T_3-J_1 strata (GBGMR, 1988, 1996), suggesting continuous deposition elsewhere in the basin during the early Toarcian–Aalenian. The depositional gap in

the studied area could have been caused by a local uplift. Shallowing and uplift of the basin culminated with the formation of a basin-and-range province from the late-Early to the Middle Jurassic (**Fig. 3.9**), as defined by Gilder et al. (1991) and Li and Li (2007). The original, broad sag-like basin was broken up into NE-trending graben, accompanied by widespread bimodal magmatism, including basalts, A-type granites and mafic intrusions (Li et al., 2007a; Li and Li, 2007; Meng et al., 2012; **Fig. 3.9**).

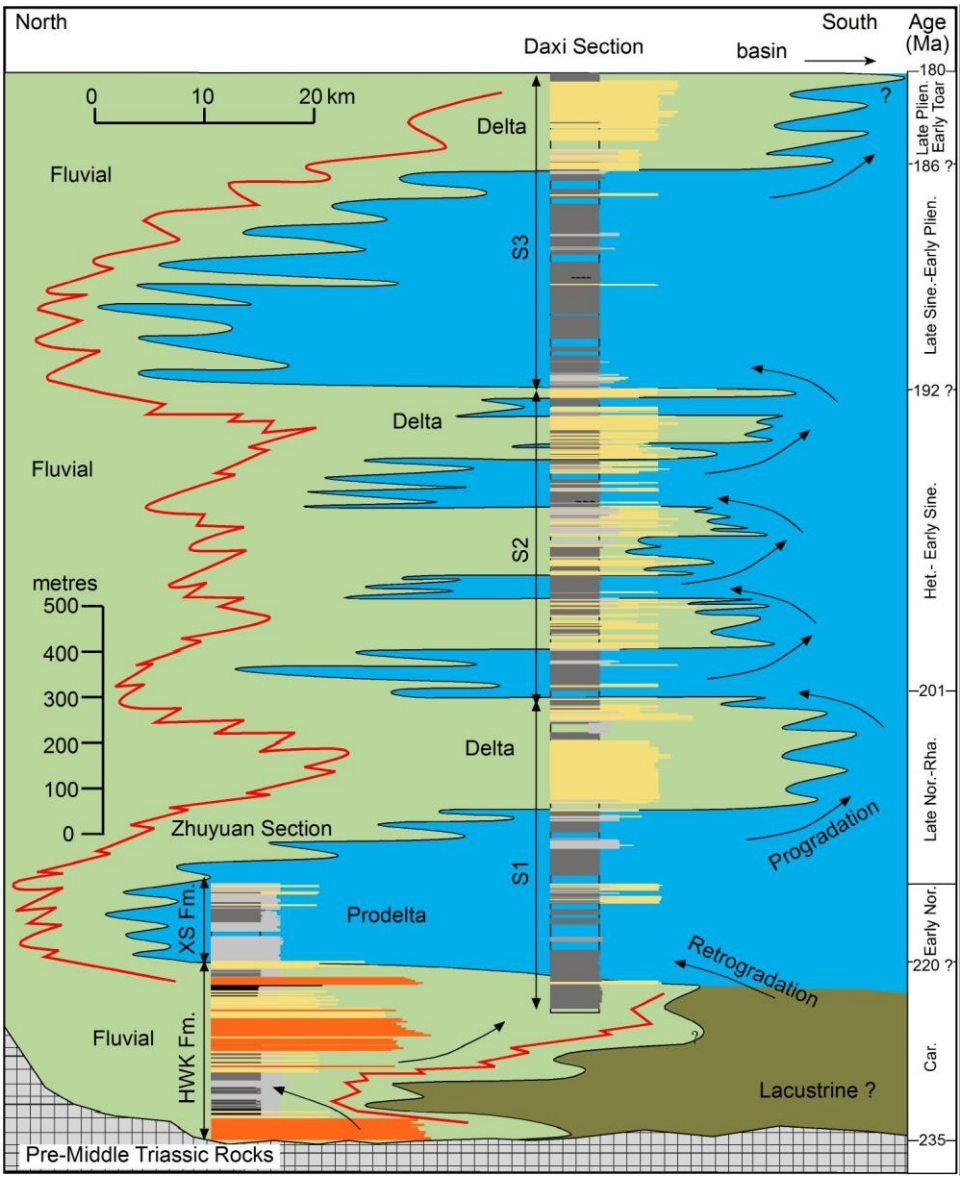

Figure 3.10 A schematic anatomy of the T_3-J_1 marine-influenced deltaic system in the Daxi-Zhuyuan area. An inferred boundary between fluvial and deltaic deposits is traced by the red line.

3.7.3. Regional spatial and temporal evolution of the basin

The Daxi-Zhuyuan succession provides a unique insight into local depositional processes of the T_3-J_1 sedimentary basin. To better understand the basin evolution and its geodynamic implications, we present a ~350 km-long basin-scale NW-SE stratigraphic cross section, consisting of composite stratigraphic columns from the Shaoguan, Xinfeng-Lianping, Huidong, and Huilai regions respectively marked as 1, 2, 3 and 4 (**Figs 3.1A, 3.11**). These sections are correlated on the basis of sedimentology and biostratigraphy, as determined by GBGMR (1973, 1988) and Qian et al. (1987).

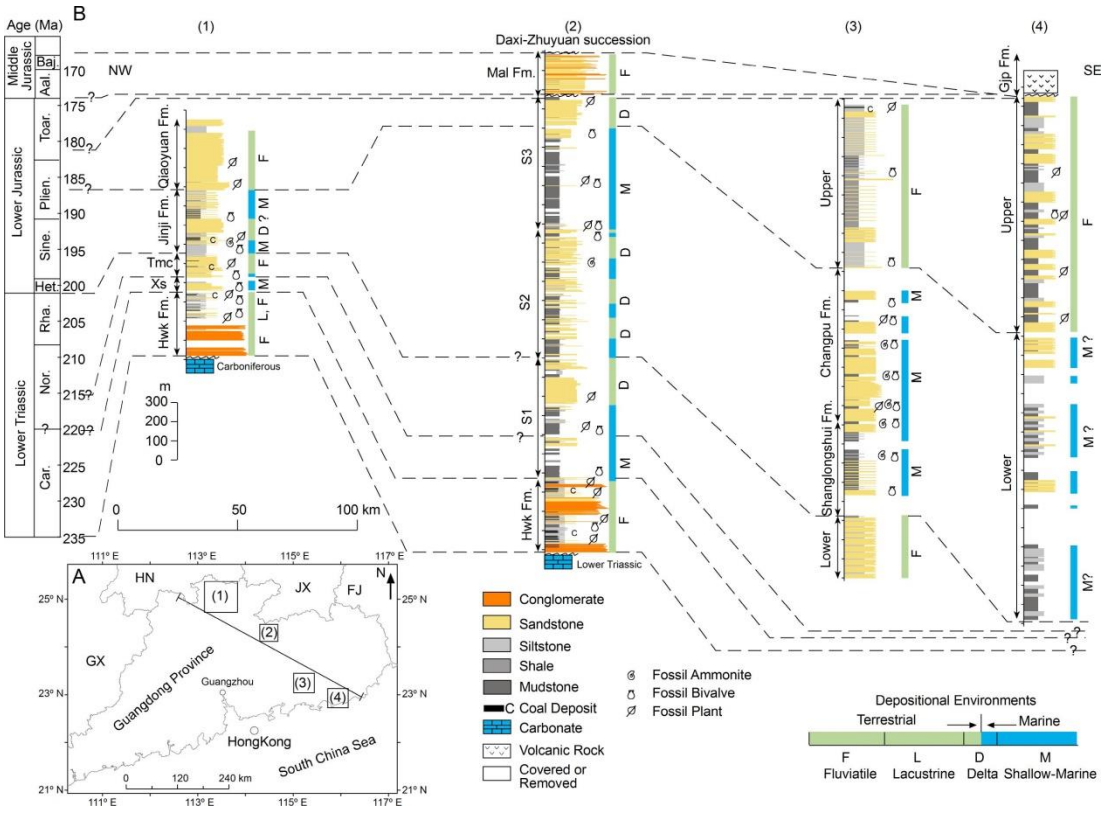

Figure 3.11 A stratigraphic cross section from northwestern to southeastern Guangdong Province. (A) Locations of the presented sections. (1) = section 1 in the Shaoguan region; (2) = section 2 in the Xinfeng-Lianping region; (3) = section 3 in the Huidong region; (4) = section 4 in the Huilai region. GX = Guangxi Province; HN = Hunan Province; JX = Jiangxi Province; FJ = Fujian Province. (B) Composite stratigraphic columns from the northwest to the southeast. Complied sections include: the Hulukou section (modified after Qian et al. 1987), and the Qujiang section (modified after GBGMR, 1996) in the Shaoguan region; the Daxi and the Zhuyuan sections in the Xinfeng-Lianping region; the Shanglongshui section in the Huidong region (modified after GBGMR, 1973, 1996); and the Kuitan section in the Huilai region (modified from GBGMR, 1973). Hwk Fm = Hongweikeng Formation; Xs =

Xiaoshui Formation; Tmc = Toumuchong Formation; Gjp Fm = Gaojiping Formation. Age abbreviations are the same as in **Figure 3.9**.

As shown in Sections 1 and 2, the basin began to subside during the Carnian, and received the early Carnian coal-bearing fluvial and lacustrine deposits (Qian et al., 1987), which are succeeded by the late Carnian-early Norian bivalve-bearing mudrocks and sandstones, and the late Norian-Rhaetian coal-bearing fluvial and deltaic deposits (Qian et al., 1987; GBGMR, 1988, 1996; **Fig. 3.11B**). Stratigraphic analyses here indicate that the basin underwent a retrogradation-progradation (deepening-shallowing) cycle during the Late Triassic (**Figs 3.9–3.11**). Deposition processes are best represented by the Daxi-Zhuyuan succession (Section 2; **Figs 3.10, 3.11**), implying that the basin experienced initially increasing but then slightly decreasing subsidence during the Late Triassic as discussed above.

During the early-Early Jurassic, the basin underwent an episode of rapid subsidence resulting in the onset of a broader shallow-marine environment, with abundant bivalves and ammonites (the Jinji Formation and equivalents; Sun et al., 1980; Chen et al., 1987; Qian et al., 1987; GBGMR, 1988, 1996; **Figs 3.10, 3.11**). As documented by the Daxi-Zhuyuan succession (Section 2), the subsidence rate of the basin could have increased prior to a slowing down in subsidence, corresponding to uplift during the late-Early Jurassic (**Figs 3.9, 3.11**). Shallowing and uplift of the basin are also recorded in Sections 1, 3 and 4, where deposition was dominated by fluvial sedimentation (the Qiaoyuan Formation and equivalents) during the late-Early Jurassic (GBGMR, 1973, 1988, 1996; Qian et al., 1987; **Fig. 3.11B**).

The long-term basin evolution from shallow-marine to fluvial environments was accompanied by the change of the depocentre during the Early Jurassic. For the Hettangian to the early Pliensbachian, stratal thicknesses increase from the northwest (~300 m in Section 1) to the south and southeast (~1200-1500 m in Sections 2, 3 and 4; GBGMR, 1973, 1988, 1996; **Fig. 3.11B**), implying that the depocentre was located in the south and southeast (i.e., the Xinfeng-Lianping to the Huilai regions; **Fig. 3.11**). However, during the late Pliensbachian to the early Toarcian, the depositional thickness increased from Section 2 (140 m) to Section 1 (350-500 m), and to Sections 3 and 4 (~800-1200 m) (**Fig. 3.11B**), indicating the basin was segmented by an intrabasinal high in the Xinfeng-Lianping region. This is consistent

with west to northwest palaeoflow directions (**Fig. 3.5A**), and the interpreted shallowing and uplift of the basin in the Xinfeng-Lianping region. Thus, it is suggested that the basin experienced a retrogradation-progradation (deepening-shallowing) cycle as well as shift in the depocentre during the late-Early Jurassic prior to the development of a basin-and-range province (**Fig. 3.11**).

The South China basin is a time equivalent to the basins (e.g., the Jeanne D′Arc and Lusitanian basins) in the Newfoundland and Iberian regions of the North Atlantic. The Lusitanian and Jeanne D′Arc basins accumulated siliciclastic red-bed sediments during the Carnian, and these were succeeded by evaporate deposits that reached into the Hettangian (Sinclair, 1995; Driscoll et al., 1995; Rasmussen et al., 1998; Alves et al., 2003; Tucholke et al., 2007; Alves et al., 2009; Leleu and Hartley, 2010). The Sinemurian-Callovian marine sandstones, shales and carbonates that are widely deposited in the North Atlantic, were followed by a regional unconformity spanning the Callovian-Oxfordian (Sinclair, 1995; Driscoll et al., 1995; Rasmussen et al., 1998; Alves et al., 2003; Tucholke et al., 2007; Alves et al., 2009; Leleu and Hartley, 2010). The North Atlantic basins evolved from fluvial to marine environments, and then to basin uplift during the Late Triassic-Middle Jurassic, thereby showing a similar evolutionary pattern to the South China basin. Nevertheless, the following discussion based on regional geological observations implies that basin formation mechanisms may have been different.

Table 3. 3 Magmatism of Middle Triassic to Early-Middle Jurassic age adjacent to the Daxi-Zhuyuan area.

Location	Lithology	Igneous classification	Age (Ma)	Method	Reference
Syn-orogenic					
Xiazhuang, Guidong	Two-mica granite		236 ±7	LAICPMS zircon U-Pb	Xu et al., 2003
Luxi, Guidong	Biotite granite		239 ±5	LAICPMS zircon U-Pb	Xu et al., 2003
Longyuanba, Longnan	Biotite granite	S-type	240 ±1.4	LAICPMS zircon U-Pb	He et al., 2010
Guidong	Monzogranite	I-type	238 ±3	LAICPMS zircon U-Pb	Li and Li, 2007
Sanbiao, Anyuan	Biotite granite	I-type	247 ±3	SHRIMP zircon U-Pb	Li and Li, 2007
Stage 2					
Hanhu, Longnan	Granodiorite	A-type	193 ±2	SHRIMP zircon U-Pb	Yu et al., 2010
Hanhu, Longnan	Gabbro-Diabase		196 ±1	SHRIMP zircon U-Pb	Yu et al., 2010
Stage 3					
Shibei, Lianping	Granite		186 ±2	SHRIMP zircon U-Pb	C-J P's unpublished data
Keshubei, Anyuan	Alkaline granite	A-type	189 ±3	SHRIMP zircon U-Pb	Li and Li, 2007
Liren, Longnan	Dacite		191 ±1.7	SHRIMP zircon U-Pb	Gong and Wu, 2010
Shangping, Lianping	Basalt		Early		GBGMR, 1996

			Jurassic?		
Stage 4					
Tabei, Longnan	Syenite	Shoshonitic	178.2 ±1.5	LAICPMS zircon U-Pb	He et al., 2010
Huangbu, Longnan	Syenite	Shoshonitic	179.3 ±1	LAICPMS zircon U-Pb	He et al., 2010
Chenglong, Longnan	Gabbro		182.3 ±1	LAICPMS zircon U-Pb	He et al., 2010
Zhaibei, Longnan	Granite	A-type	171.6 ±4.6	SHRIMP zircon U-Pb	Li et al., 2003
Baimianshi, Xunwu	Basalt		172.7 ±3.3	K-Ar	Wang et al., 2003
Chebu, Longnan	Gabbro		173 ±4	SHRIMP zircon U-Pb	Li et al., 2003

3.7.4. Geodynamic implications

During the Middle Triassic, the 1300 km-wide southeastern South China was uplifted, deformed and intruded by granites related to the Indosinian Orogeny (**Fig. 3.9**), and explained as the cratonward migration of flat subduction of an oceanic plateau (Li and Li, 2007, Li et al., 2012). The T_3-J_1 basin is interpreted to have initiated on the orogenic belt as a sag basin (Li and Li, 2007), and underwent a relatively steady episode of subsidence during the Late Triassic (Stage 1; **Fig. 3.9**). Subsidence is interpreted to have been caused by gravitational pull driven by the basalt to eclogite facies metamorphism of the subducted flat-slab (Li and Li, 2007). Such a phase transformation-driven subsidence could explain why the T_3-J_1 basin initiated on the orogenic belt and evolved into a terrestrial to shallow-marine basin from the Carnian to the early Norian (**Figs 3.9–3.11**). Dynamic modelling (Liu et al., 2010) also suggests that the surface could have been dragged downward by both the overall negative slab density anomaly and enhanced plate coupling during shallow subduction in the Cretaceous western North America.

Although lithospheric stretching could have caused regional subsidence, this contradicts the compressive tectonic scenario interpreted for South China (late Indosinian Orogeny; Wang et al., 2005e; Li and Li, 2007; **Fig. 3.9**). If so, then initiating tectonic drivers for the South China and North Atlantic basins were different. The Late Triassic North Atlantic basins originated as half-graben and graben due to intracontinental lithospheric extension (e.g., Driscoll et al., 1995; Rasmussen et al., 1998; Alves et al., 2003; Tucholke et al., 2007; Alves et al., 2009). Notwithstanding the possible difference in tectonic initiation, the North Atlantic basins formed on a Palaeozoic-aged orogen (Caledonian-Hercynian orogenic events; e.g., Færseth, 1996), whereas the Late Triassic basin in southeastern South China initiated on a Middle Triassic orogen. The timing of basin formation relative to

preceding orogeny, and thereby the thermal state of the lithosphere, is dissimilar. Nevertheless, the evolution of the North Atlantic and South China basins follow a similar pattern in terms of basin-filling patterns, implying comparable long-term tectonic processes.

The basin in southeastern South China was subjected to a rejuvenated subsidence at the beginning of the Early Jurassic (Stages 2 and 3; **Figs 3.9, 3.10**). Such a rapid subsidence could be due to a number of factors, such as (1) sediment gravity loading, (2) lithospheric stretching, and (3) increased gravitational pulling force (see figure 4E of Li and Li, 2007). From the early Pliensbachian to the early Toarcian, however, subsidence gradually decreased and the basin became increasingly shallow (**Figs 3.9–3.11**) in the Xinfeng-Lianping region, that is, uplift occurred near the estimated depocentre (**Fig. 3.11**). This is consistent with predicted basin termination, in which the depocentre started to uplift first due to the break-off and foundering of the underlying subducted flat-slab there causing local lithospheric rebound (Li and Li, 2007).

The change of vertical crustal movement from subsidence-driven basin deepening to uplift and basin shallowing (late Stage 3 to Stage 4, **Fig. 3.9**) coincides with the occurrence of anorogenic magmatism in this region (Li et al., 2007a; Li and Li, 2007; He et al., 2010; Yu et al., 2010c; **Table 3.3**; **Fig. 3.9**). Known magmatism of this age in the region ~90 to 130 km north of the Daxi Town includes gabbro, A-type granite, basalt and dacite (**Table 3.3**; **Fig. 3.9**). Li and Li (2007) interpreted this increase in high-temperature magmatism and the end of rapid subsidence to be due to the delamination of an eclogitised flat-slab and subsequent asthenospheric upwelling (see figures 4E to F of Li and Li, 2007).

Since the Middle Jurassic, the broad T_3-J_1 basin gave way to a basin-and-range province throughout all of China (Gilder et al., 1991; Tian et al., 1992; Ren et al., 2002; Li and Li, 2007; Stage 4 in **Fig. 3.9**). A depositional hiatus occurred during this time interval (**Figs 3.9, 3.11**), implying widespread uplift and erosion of the T_3-J_1 deposits. Both the regional uplift and the development of the basin-and-range province are consistent with the break-up and foundering of an eclogitised flat-slab (Li and Li, 2007).

3.8. Conclusions

Over 2000 m of siliciclastic sedimentary rocks are measured in the Daxi section in northern Guangdong Province and are correlated with the published Zhuyuan section and other three sections. Thirteen lithofacies are summarised based on lithology, sedimentary structures and palaeontology, and are grouped into four facies associations: prodelta, delta-front, delta-plain and fluvial.

A fining-upward basal unit and three coarsening-upward sequences are defined for the Daxi-Zhuyuan succession, representing a Carnian to early Toarcian marine-influenced deltaic succession, lasting ~55 Myrs. A fluvially dominated deltaic setting is interpreted to explain the origin of the sequences. A retrogradational stratal pattern is identified for the basal unit, suggesting that the subsidence rate outstripped the sediment supply rate, whereas a progradational stacking pattern is recognised for the overlying Sequence 1. An aggradational stacking pattern is present in Sequence 2, reflecting a sediment supply balanced with accommodation generation, whereas a progradational stacking pattern is shown in Sequences 3, indicating that the sediment supply rate was gradually higher than the accommodation creation rate.

Tectonic controls played a primary role on the basin filling, rather than eustasy and climate. Four tectonostratigraphic stages are defined for the Daxi-Zhuyuan succession, and these identify Late Triassic to early-Middle Jurassic depositional cycles. Stage 1 records a retrogradation-progradation cycle associated with an increasing to a slowly decreasing subsidence rate, apparently in a compressive tectonic setting. Stage 2 documents a mainly aggradation cycle responding to a complex interplay between moderate subsidence rates, high sedimentation rates and eustasy, whereas Stage 3 records a retrogradational-aggradational-progradational cycle reflecting changes of high sedimentation and subsidence rates to lower subsidence and sedimentation rates prior to the intracontinental uplift. Stage 4 records the continental uplift and subsequent development of a Late Jurassic-Cretaceous basin-and-range province.

The ~350 km-wide basin-scale stratigraphic analysis establishes a temporal-spatial evolution that has been interpreted to fit a sag basin related to flat-slab subduction. The basin initiated by sagging on the orogenic belt, evolved from fluvial to shallow-marine to fluvial again, and eventually became shallow and uplifted from the Late Triassic to the Early Jurassic, which was followed by the development of a basin-and-range style magmatic province. Basin evolution and associated magmatism have been interpreted by the gravitational pull, and later the break-up and foundering of a flat-subducted oceanic slab beneath southeastern South China.

Chapter 4: Climatic and tectonic controls on the Gaosi-Songxi succession in northeastern Guangdong Province

This chapter has been removed due to copyright restrictions.

This chapter has been removed due to copyright restrictions.

This chapter has been removed due to copyright restrictions.

This chapter has been removed due to copyright restrictions.

This chapter has been removed due to copyright restrictions.

This chapter has been removed due to copyright restrictions.

This chapter has been removed due to copyright restrictions.

This chapter has been removed due to copyright restrictions.

This chapter has been removed due to copyright restrictions.

This chapter has been removed due to copyright restrictions.

This chapter has been removed due to copyright restrictions.

This chapter has been removed due to copyright restrictions.

This chapter has been removed due to copyright restrictions.

This chapter has been removed due to copyright restrictions.

This chapter has been removed due to copyright restrictions.

This chapter has been removed due to copyright restrictions.

This chapter has been removed due to copyright restrictions.

This chapter has been removed due to copyright restrictions.

This chapter has been removed due to copyright restrictions.

This chapter has been removed due to copyright restrictions.

This chapter has been removed due to copyright restrictions.

This chapter has been removed due to copyright restrictions.

This chapter has been removed due to copyright restrictions.

This chapter has been removed due to copyright restrictions.

This chapter has been removed due to copyright restrictions.

This chapter has been removed due to copyright restrictions.

This chapter has been removed due to copyright restrictions.

This chapter has been removed due to copyright restrictions.

This chapter has been removed due to copyright restrictions.

This chapter has been removed due to copyright restrictions.

This chapter has been removed due to copyright restrictions.

This chapter has been removed due to copyright restrictions.

This chapter has been removed due to copyright restrictions.

This chapter has been removed due to copyright restrictions.

This chapter has been removed due to copyright restrictions.

This chapter has been removed due to copyright restrictions.

Chapter 5: Stratigraphic and palaeogeographic evolution of the Late Triassic to Middle Jurassic basin

This chapter has been removed due to copyright restrictions.

This chapter has been removed due to copyright restrictions.

This chapter has been removed due to copyright restrictions.

This chapter has been removed due to copyright restrictions.

This chapter has been removed due to copyright restrictions.

This chapter has been removed due to copyright restrictions.

This chapter has been removed due to copyright restrictions.

This chapter has been removed due to copyright restrictions.

This chapter has been removed due to copyright restrictions.

This chapter has been removed due to copyright restrictions.

This chapter has been removed due to copyright restrictions.

This chapter has been removed due to copyright restrictions.

This chapter has been removed due to copyright restrictions.

This chapter has been removed due to copyright restrictions.

This chapter has been removed due to copyright restrictions.

This chapter has been removed due to copyright restrictions.

This chapter has been removed due to copyright restrictions.

This chapter has been removed due to copyright restrictions.

This chapter has been removed due to copyright restrictions.

This chapter has been removed due to copyright restrictions.

This chapter has been removed due to copyright restrictions.

This chapter has been removed due to copyright restrictions.

This chapter has been removed due to copyright restrictions.

This chapter has been removed due to copyright restrictions.

This chapter has been removed due to copyright restrictions.

This chapter has been removed due to copyright restrictions.

This chapter has been removed due to copyright restrictions.

This chapter has been removed due to copyright restrictions.

This chapter has been removed due to copyright restrictions.

This chapter has been removed due to copyright restrictions.

This chapter has been removed due to copyright restrictions.

This chapter has been removed due to copyright restrictions.

This chapter has been removed due to copyright restrictions.

This chapter has been removed due to copyright restrictions.

This chapter has been removed due to copyright restrictions.

This chapter has been removed due to copyright restrictions.

This chapter has been removed due to copyright restrictions.

This chapter has been removed due to copyright restrictions.

This chapter has been removed due to copyright restrictions.

This chapter has been removed due to copyright restrictions.

This chapter has been removed due to copyright restrictions.

This chapter has been removed due to copyright restrictions.

This chapter has been removed due to copyright restrictions.

This chapter has been removed due to copyright restrictions.

This chapter has been removed due to copyright restrictions.

Chapter 6: Provenance Analysis: records from detrital zircon U-Pb ages

This chapter has been removed due to copyright restrictions.

This chapter has been removed due to copyright restrictions.

This chapter has been removed due to copyright restrictions.

This chapter has been removed due to copyright restrictions.

This chapter has been removed due to copyright restrictions.

This chapter has been removed due to copyright restrictions.

This chapter has been removed due to copyright restrictions.

This chapter has been removed due to copyright restrictions.

This chapter has been removed due to copyright restrictions.

This chapter has been removed due to copyright restrictions.

This chapter has been removed due to copyright restrictions.

This chapter has been removed due to copyright restrictions.

This chapter has been removed due to copyright restrictions.

This chapter has been removed due to copyright restrictions.

This chapter has been removed due to copyright restrictions.

This chapter has been removed due to copyright restrictions.

This chapter has been removed due to copyright restrictions.

This chapter has been removed due to copyright restrictions.

This chapter has been removed due to copyright restrictions.

This chapter has been removed due to copyright restrictions.

This chapter has been removed due to copyright restrictions.

.

This chapter has been removed due to copyright restrictions.

This chapter has been removed due to copyright restrictions.

This chapter has been removed due to copyright restrictions.

This chapter has been removed due to copyright restrictions.

This chapter has been removed due to copyright restrictions.

This chapter has been removed due to copyright restrictions.

This chapter has been removed due to copyright restrictions.

This chapter has been removed due to copyright restrictions.

This chapter has been removed due to copyright restrictions.

This chapter has been removed due to copyright restrictions.

Chapter 7: Basin Record of Mesozoic Tectonic Events in southeastern South China: A Synthesis

This chapter has been removed due to copyright restrictions.

This chapter has been removed due to copyright restrictions.

This chapter has been removed due to copyright restrictions.

This chapter has been removed due to copyright restrictions.

This chapter has been removed due to copyright restrictions.

This chapter has been removed due to copyright restrictions.

This chapter has been removed due to copyright restrictions.

This chapter has been removed due to copyright restrictions.

This chapter has been removed due to copyright restrictions.

This chapter has been removed due to copyright restrictions.

This chapter has been removed due to copyright restrictions.

This chapter has been removed due to copyright restrictions.

This chapter has been removed due to copyright restrictions.

References

Allen, J.P., Fielding, C.R., Rygel, M.C., Gibling, M.R., 2013. Deconvolving Signals of Tectonic and Climatic Controls From Continental Basins: An Example From the Late Paleozoic Cumberland Basin, Atlantic Canada. Journal of Sedimentary Research 83(10), 847-872.

Allen, J.R.L., 1964. Primary Current Lineation in The Lower Old Red Sandstone (Devonian), Anglo-Welsh Basin. Sedimentology 3(2), 89-108.

Allen, P.A., Allen, J.R., 2005. Bain Analysis; Principles and Application. Blackwell Publishing, 549 pp.

Allmendinger, R.W., Jordan, T.E., Kay, S.M., Isacks, B.L., 1997. The Evolution of the Altiplano-Puna Plateau of the Central Andes. Annual Review of Earth and Planetary Sciences 25(1), 139-174.

Alves, T.M., Manuppella, G., Gawthorpe, R.L., Hunt, D.W., Monteiro, J.H., 2003. The depositional evolution of diapir- and fault-bounded rift basins: examples from the Lusitanian Basin of West Iberia. Sedimentary Geology 162(3–4), 273-303.

Alves, T.M. et al., 2009. Diachronous evolution of Late Jurassic–Cretaceous continental rifting in the northeast Atlantic (west Iberian margin). Tectonics 28(4), TC4003.

Armitage, J.J., Duller, R.A., Whittaker, A.C., Allen, P.A., 2011. Transformation of tectonic and climatic signals from source to sedimentary archive. Nature Geosci 4(4), 231-235.

Axen, G.J., Taylor, W.J., Bartley, J.M., 1993. Space-time patterns and tectonic controls of Tertiary extension and magmatism in the Great Basin of the western United States. Geological Society of America Bulletin 105(1), 56-76.

Baas, J.H., 2000. EZ-ROSE: a computer program for equal-area circular histograms and statistical analysis of two-dimensional vectorial data. Computers & Geosciences 26(2), 153-166.

Bhattacharya, J.P., 2010. Deltas. In: N.P. James, R.W. Dalrymple (Eds.), Facies models 4. Geological Association of Canada, St John's, Newfoundland, pp. 233-264.

Black, L.P. et al., 2003. TEMORA 1: a new zircon standard for Phanerozoic U–Pb geochronology. Chemical Geology 200(1–2), 155-170.

Blum, M.D., Törnqvist, T.E., 2000. Fluvial responses to climate and sea-level change: a review and look forward. Sedimentology 47, 2-48.

Bonis, N.R., Ruhl, M., Kürschner, W.M., 2010. Climate change driven black shale deposition during the end-Triassic in the western Tethys. Palaeogeography, Palaeoclimatology, Palaeoecology 290(1–4), 151-159.

Cao, B., 1982. The Discovery of Early Jurassic Marine Strata in Fujian. Geological Review 28(5), 490-491.

Catuneanu, O. et al., 2009. Towards the standardization of sequence stratigraphy. Earth-Science Reviews 92(1-2), 1-33.

Cecca, F., 1992. Ammonite habitats in the Early Tithonian of Western Tethys. Lethaia 25(3), 257-267.

Chen, C.-H., Lin, W., Lan, C.-Y., Lee, C.-Y., 2004. Geochemical, Sr and Nd isotopic characteristics and tectonic implications for three stages of igneous rock in the Late Yanshanian (Cretaceous) orogeny, SE China. Earth and Environmental Science Transactions of the Royal Society of Edinburgh 95(1-2), 237-248.

Chen, J.-h., 1982a. Liassic Bivalve fossils from Mt. Jinji of Guangdong. Acta Palaeontologica Sinica 21(4), 404-416.

Chen, J., 1982b. Mesozoic Transgressions, Regressions and Bivalve Province in China. Acta Geologica Sinica 56(4), 334-346.

Chen, J., 1987a. Early Jurassic marine bivalves from Guangdong-Nanling district, southern China. Bull. Nanjing Inst. Geol. & Palaeont., Acad. Sinica 0(12), 23-94.

Chen, J., 1987b. Early Jurassic marine bivalves from Guangdong-Nanling district, southern China. Bulletin Nanjing Institue Geology and& Palaeontology, Academy Sinica 0(12), 23-94.

Chen, K. et al., 2013. 2.6–2.7 Ga crustal growth in Yangtze craton, South China. Precambrian Research 224(0), 472-490.

Chen, X., Zhang, Y., Fan, J., Cheng, J., Li, Q., 2010. Ordovician graptolite-bearing strata in southern Jiangxi with a special reference to the Kwangsian Orogeny. Science China Earth Sciences 53(11), 1602-1610.

Cloetingh, S., Ziegler, P.A., 2007. Tectonic Models for the Evolution of Sedimentary Basins. In: G. Schubert (Ed.), Treatise on Geophysics. Elsevier, Amsterdam, pp. 485-611.

Colgan, J.P., John, D.A., Henry, C.D., Fleck, R.J., 2008. Large-magnitude Miocene extension of the Eocene Caetano caldera, Shoshone and Toiyabe Ranges, Nevada. Geosphere 4(1), 107-130.

Collinson, J.D., Mountney, N.P., Thompson, D., 2006. Sedimentary Structures. Terra Publishing, 292 pp.

Coney, P.J., Reynolds, S.J., 1977. Cordilleran Benioff zones. Nature 270(5636), 403-406.

Corbett, M.J., Fielding, C.R., Birgenheier, L.P., 2011. Stratigraphy of a Cretaceous Coastal-Plain Fluvial Succession: The Campanian Masuk Formation, Henry Mountains Syncline, Utah, U.S.A. Journal of Sedimentary Research 81(2), 80-96.

Cross, T.A., Pilger, R.H., 1978. Tectonic controls of late Cretaceous sedimentation, western interior, USA. Nature 274(5672), 653-657.

Cui, S., Li, J., 1983. On the indosinian Orogeny along the Chinese western Pacific Belt. Acta Geological Sinica 57, 51-61.

Dalmayrac, B., Molnar, P., 1981. Parallel thrust and normal faulting in Peru and constraints on the state of stress. Earth and Planetary Science Letters 55(3), 473-481.

Dalrymple, R.W., 2010. Interpreting Sedimentary Successions: Facies, Facies Analysis and Facies Models. In: N.P. James, R.W. Dalrymple (Eds.), Facies models 4. Geological Association of Canada, St John's, Newfoundland, pp. 3-18.

DeCelles, P.G., 2004. Late Jurassic to Eocene evolution of the Cordilleran thrust belt and foreland basin system, western U.S.A. American Journal of Science 304(2), 105-168.

DeCelles, P.G., Giles, K.A., 1996. Foreland basin systems. Basin Research 8(2), 105-123.

DeCelles, P.G. et al., 1991. Controls on synorogenic alluvial-fan architecture, Beartooth Conglomerate (Palaeocene), Wyoming and Montana. Sedimentology 38(4), 567-590.

Dera, G. et al., 2011. Climatic ups and downs in a disturbed Jurassic world. Geology 39(3), 215-218.

Devlin, W.J., Rudolph, K.W., Shaw, C.A., Ehman, K.D., 1993. The Effect of Tectonic and Eustatic Cycles on Accommodation and Sequence-Stratigraphic

Framework in the Upper Cretaceous Foreland Basin of Southwestern Wyoming. In: H.W. Posamentier, C.P. Summerhayes, B.U. Haq, G.P. Allen (Eds.), Sequence Stratigraphy and Facies Associations. Blackwell Scientific Publications, pp. 501-520.

Dickinson, W., 2002. The Basin and Range Province as a Composite Extensional Domain. International Geology Review 44(1), 1 - 38.

Dickinson, W.R., Gehrels, G.E., Marzolf, J.E., 2010. Detrital zircons from fluvial Jurassic strata of the Michigan basin: Implications for the transcontinental Jurassic paleoriver hypothesis. Geology 38(6), 499-502.

Dickinson, W.R. et al., 1988. Paleogeographic and paleotectonic setting of Laramide sedimentary basins in the central Rocky Mountain region. Geological Society of America Bulletin 100(7), 1023-1039.

Dickinson, W.R., Suczek, C.A., 1979. Plate tectonics and sandstone compositions. Aapg Bulletin 63(12), 2164-2182.

Dreyer, T., Corregidor, J., Arbues, P., Puigdefabregas, C., 1999. Architecture of the tectonically influenced Sobrarbe deltaic complex in the Ainsa Basin, northern Spain. Sedimentary Geology 127(3–4), 127-169.

Driscoll, N.W., Hogg, J.R., Christie-Blick, N., Karner, G.D., 1995. Extensional tectonics in the Jeanne d'Arc Basin, offshore Newfoundland: implications for the timing of break-up between Grand Banks and Iberia. In: R.A. Scrutton, G.B. Shimmield, A.W. Tudhope (Eds.), The Tectonics, Sedimentation and Palaeoceanography of the North Atlantic Region. Geological Society, London, Special Publications, pp. 1-28.

Druschke, P., Hanson, A.D., Wells, M.L., 2009a. Structural, stratigraphic, and geochronologic evidence for extension predating Palaeogene volcanism in the Sevier hinterland, east-central Nevada. International Geology Review 51(7), 743 - 775.

Druschke, P. et al., 2009b. Synconvergent surface-breaking normal faults of Late Cretaceous age within the Sevier hinterland, east-central Nevada. Geology 37(5), 447-450.

Elliott, T., 1974. Interdistributary bay sequences and their genesis. Sedimentology 21(4), 611-622.

Elliott, T., 1986. Deltas. In: H.G. Reading (Ed.), Sedimentary Environment and Facies. Blackwell, Oxford, pp. 113-154.

Færseth, R.B., 1996. Interaction of Permo-Triassic and Jurassic extensional fault-blocks during the development of the northern North Sea. Journal of the Geological Society 153(6), 931-944.

Fan, J.-s., 1963a. On Loewr Liassic Lamllibranchiata From Guangdong (Kuangtung). Acta Palaeontologica Sinica 11(04), 508-543.

Fan, J.-s., 1963b. On Lower Liassic Lamellibranchiata From Guangdong (Kuangtung). Acta Palaeontologica Sinica 11(04), 508-543.

Fan, J.-s., Lao, C.-y., Zhu, M., 1965. On the Stratigraphical Sequence and the Geological Age of the Lantang Group, Boluo District, Guangtong. Acta Geological Sinica 45(2), 143-152.

Fan, W., Wang, Y., Zhang, A., Zhang, F., Zhang, Y., 2010. Permian arc–back-arc basin development along the Ailaoshan tectonic zone: Geochemical, isotopic and geochronological evidence from the Mojiang volcanic rocks, Southwest China. Lithos 119(3–4), 553-568.

FBGMR, 1972a. Regional Geological Investigation Report of 1: 200,000 Guangze Sheet (F-50-4).

FBGMR, 1972b. Regional Geological Investigation Report of 1: 200,000 Ninghua Sheet (F-50-15).

FBGMR, 1985. Regional Geology of Fujian Province, People's Republic of China, (in Chinese with detailed English abstract). Geological Publishing House, Beijing, 671 pp.

FBGMR, 1997. Stratigraphy (Lithostratic) of Fujian Province. Multiple Classification and Correlation of the Stratigraphy of China. China University of Geosciences Press, Wuhan, 216 pp.

Fedo, C.M., Sircombe, K.N., Rainbird, R.H., 2003. Detrital Zircon Analysis of the Sedimentary Record. Reviews in Mineralogy and Geochemistry 53(1), 277-303.

Fielding, C.R., 2006. Upper flow regime sheets, lenses and scour fills: Extending the range of architectural elements for fluvial sediment bodies. Sedimentary Geology 190(1–4), 227-240.

Foreman, B.Z., Heller, P.L., Clementz, M.T., 2012. Fluvial response to abrupt global warming at the Palaeocene/Eocene boundary. Nature advance online publication.

Fouch, T.D., 1979. Character and paleogeographic distribution of Upper Cretaceous(?) and Paleogene nonmarine sedimentary rocks in east-central Nevada. In: J.M. Armentrout, M.R. Cole, H. Terbest (Eds.), Cenozoic paleogeography and of the western United States: Pacific Coast Paleogeographic Symposium 3: Pacific Section. SEPM, pp. 97-111.

Gani, M.R., Bhattacharya, J.P., 2007. Basic Building Blocks and Process Variability of a Cretaceous Delta: Internal Facies Architecture Reveals a More Dynamic Interaction of River, Wave, and Tidal Processes Than Is Indicated by External Shape. Journal of Sedimentary Research 77(4), 284-302.

Gao, S. et al., 2011. Age and growth of the Archean Kongling terrain, South China, with emphasis on 3.3 ga granitoid gneisses. American Journal of Science 311(2), 153-182.

GBGMR, 1964. Regional Geological Investigation Report of 1: 200,000 Lianping Sheet (G-50-31).

GBGMR, 1965. Regional Geological Investigation Report of 1: 200,000 Huizhou Sheet (F-50-7) and Bao'an Sheet (F-50-13).

GBGMR, 1969. Regional Geological Investigation Report of 1: 200,000 Yangchun Sheet (F-49-16).

GBGMR, 1971a. Regional Geological Investigation Report of 1: 200,000 Haifeng Sheet (F-50-8).

GBGMR, 1971b. Regional Geological Investigation Report of 1: 200,000 Meixian Sheet.

GBGMR, 1973. Regional Geological Investigation Report of 1: 200,000 Haifeng Sheet (G-50-8).

GBGMR, 1988. Regional Geology of Guangdong Province, People's Republic of China. Geological Publishing House, Beijing, 941 pp.

GBGMR, 1996. Stratigraphy (Lithostratic) of Guangdong Province. Multiple Classification and Correlation of the Stratigraphy of China. China University of Geosciences Press, Wuhan, 262 pp.

Gehrels, G.E. et al., 2011. Detrital zircon U-Pb geochronology of Paleozoic strata in the Grand Canyon, Arizona. Lithosphere 3(3), 183-200.

Ghazi, S., Mountney, N.P., 2009. Facies and architectural element analysis of a meandering fluvial succession: The Permian Warchha Sandstone, Salt Range, Pakistan. Sedimentary Geology 221(1–4), 99-126.

Gilder, S.A., Keller, G.R., Luo, M., Goodell, P.C., 1991. Eastern Asia and the Western Pacific timing and spatial distribution of rifting in China. Tectonophysics 197(2–4), 225-243.

Gómez-Paccard, M. et al., 2012. Tectonic and climatic controls on the sequential arrangement of an alluvial fan/fan-delta complex (Montserrat, Eocene, Ebro Basin, NE Spain). Basin Research 24(4), 437-455.

Gong, C., Wu, J.-h., 2010. The SHRIMP Zircon U-Pb Dating of Felsic Volcanic Rocks and Its Geological Significance from Yutian Group in Southern Jiangxi. Journal of East China Institute of Technology 33(2), 131-138.

Good, S.C., 1987. Mollusc-based interpretations of lacustrine paleoenvironments of the Sheep Pass Formation (latest Cretaceous to Eocene) of east central Nevada. Palaios 2(5), 467-478.

Guo, F. et al., 2012. Multi-stage crust–mantle interaction in SE China: Temporal, thermal and compositional constraints from the Mesozoic felsic volcanic rocks in eastern Guangdong–Fujian provinces. Lithos 150(0), 62-84.

Hajek, E.A., Heller, P.L., Schur, E.L., 2012. Field test of autogenic control on alluvial stratigraphy (Ferris Formation, Upper Cretaceous–Paleogene, Wyoming). Geological Society of America Bulletin 124(11-12), 1898-1912.

Hampson, G.J. et al., 2012. Controls on large-scale patterns of fluvial sandbody distribution in alluvial to coastal plain strata: Upper Cretaceous Blackhawk Formation, Wasatch Plateau, Central Utah, USA. Sedimentology 59(7), 2226-2258.

Haq, B.U., Hardenbol, J., Vail, P.R., 1987. Chronology of Fluctuating Sea Levels Since the Triassic. Science 235(4793), 1156-1167.

Haynes, S.R., 2003. Development of the Eocene Elko Basin, Northeastern Nevada: Implications for Paleogenography and Regional Tectonsim. Master. thesis, 1-171.

HBGMR, 1984. Regional Geology of Hunan Province, People's Republic of China, (in Chinese with detailed English abstract). Geological Publishing House, Beijing, 719 pp.

HBGMR, 1997. Stratigraphy (Lithostratic) of Hunan Province. Multiple Classification and Correlation of the Stratigraphy of China. China University of Geosciences Press, Wuhan, 292 pp.

He, B. et al., 2007. Age and duration of the Emeishan flood volcanism, SW China: Geochemistry and SHRIMP zircon U-Pb dating of silicic ignimbrites, post-volcanic Xuanwei Formation and clay tuff at the Chaotian section. Earth and Planetary Science Letters 255(3-4), 306-323.

He, Z.-Y., Xu, X.-S., Niu, Y., 2010. Petrogenesis and tectonic significance of a Mesozoic granite-syenite-gabbro association from inland South China. Lithos 119(3-4), 621-641.

Hickson, T.A., Sheets, B.A., Paola, C., Kelberer, M., 2005. Experimental test of tectonic controls on three-dimensional alluvial facies architecture. Journal of Sedimentary Research 75(4), 710-722.

HIGS, 1977. Palaeontological Altas of Central South China (3)-Mesozoic and Cenozoic. Geological Publishing House, Beijing.

Hsieh, P.S., Chen, C.H., Yang, H.J., Lee, C.Y., 2008. Petrogenesis of the Nanling Mountains granites from South China: Constraints from systematic apatite geochemistry and whole-rock geochemical and Sr-Nd isotope compositions. Journal of Asian Earth Sciences 33(5-6), 428-451.

Hsu, K.J. et al., 1990. Tectonics of South China: Key to understanding West Pacific geology. Tectonophysics 183(1-4), 9-39.

Huerta, P., Armenteros, I., Silva, P.G., 2011. Large-scale architecture in non-marine basins: the response to the interplay between accommodation space and sediment supply. Sedimentology 58(7), 1716-1736.

Ingersoll, R.V., 1988. Tectonics of sedimentary basins. Geological Society of America Bulletin 100(11), 1704-1719.

Ingersoll, R.V., 1990. Actualistic Sandstone Petrofacies - Discriminating Modern and Ancient Source Rocks. Geology 18(8), 733-736.

Ingersoll, R.V., 2012. Tectonics of sedimentary basins, with revised nomenclature. In: C.J. Busby, A. Azor (Eds.), Tectonics of Sedimentary Basins: Recent Advance. Wiley-Blackwell, pp. 3-43.

Ingersoll, R.V. et al., 1984. The effect of grain size on detrital modes; a test of the Gazzi-Dickinson point-counting method. Journal of Sedimentary Research 54(1), 103-116.

JBGMR, 1964. Regional Geological Investigation Report of 1: 200,000 Dongxiang Sheet (H-50-30).

JBGMR, 1970. Regional Geological Investigation Report of 1: 200,000 Longnan Sheet (G-50-25).

JBGMR, 1977. Regional Geological Investigation Report of 1: 200,000 Xingan Sheet (G-50-2).

JBGMR, 1984. Regional Geology of Jiangxi Province, People's Republic of China, (in Chinese with detailed English abstract). Geological Publishing House, Beijing, 921 pp.

JBGMR, 1997. Stratigraphy (Lithostratic) of Jiangxi Province. Multiple Classification and Correlation of the Stratigraphy of China. China University of Geosciences Press, Wuhan, 375 pp.

Jian, P. et al., 2009. Devonian to Permian plate tectonic cycle of the Paleo-Tethys Orogen in southwest China (I): Geochemistry of ophiolites, arc/back-arc assemblages and within-plate igneous rocks. Lithos 113(3–4), 748-766.

Jiao, W., Wu, Y., Yang, S., Peng, M., Wang, J., 2009. The oldest basement rock in the Yangtze Craton revealed by zircon U-Pb age and Hf isotope composition. Science in China Series D: Earth Sciences 52(9), 1393-1399.

Johnson, C.L., Graham, S.A., 2004. Cycles in Perilacustrine Facies of Late Mesozoic Rift Basins, Southeastern Mongolia. Journal of Sedimentary Research 74(6), 786-804.

Kane, I.A., McCaffrey, W.D., Martinsen, O.J., 2009. Allogenic vs. Autogenic Controls on Megaflute Formation. Journal of Sedimentary Research 79(9), 643-651.

Kellogg, H.E., 1964. Cenozoic Stratigraphy and Structure of the Southern Egan Range, Nevada. Geological Society of America Bulletin 75(10), 949-968.

Krapez, B., 1989. Depositional Styles and Geotectonic Settings of Archean Metasedimentary Sequences: Evidence from the Lalla Rookh Basin, Pilbara Block, Western Australia Ph.D. thesis Thesis, The University of Western Australia, Perth.

Krapez, B., 1996. Sequence stratigraphic concepts applied to the identification of basin-filling rhythms in Precambrian successions. Australian Journal of Earth Sciences 43(4), 355-380.

Krapez, B., Barley, M.E., 2008. Late Archaean synorogenic basins of the Eastern Goldfields Superterrane, Yilgarn Craton, Western Australia: Part III.

Signatures of tectonic escape in an arc-continent collision zone. Precambrian Research 161(1-2), 183-199.

Krapez, B., Barley, M.E., Brown, S.J.A., 2008. Late Archaean synorogenic basins of the Eastern Goldfields Superterrane, Yilgarn Craton, Western Australia: Part I. Kalgoorlie and Gindalbie Terranes. Precambrian Research 161(1-2), 135-153.

Krapez, B., Brown, S.J.A., Hand, J., Barley, M.E., Cas, R.A.F., 2000. Age constraints on recycled crustal and supracrustal sources of Archaean metasedimentary sequences, Eastern Goldfields Province, Western Australia: evidence from SHRIMP zircon dating. Tectonophysics 322(1-2), 89-133.

Kustatscher, E., van Konijnenburg-van Cittert, J.H.A., Roghi, G., 2010. Macrofloras and palynomorphs as possible proxies for palaeoclimatic and palaeoecological studies: A case study from the Pelsonian (Middle Triassic) of Kühwiesenkopf/Monte Prà della Vacca (Olang Dolomites, N-Italy). Palaeogeography, Palaeoclimatology, Palaeoecology 290(1–4), 71-80.

Lallemand, S., Heuret, A., Boutelier, D., 2005. On the relationships between slab dip, back-arc stress, upper plate absolute motion, and crustal nature in subduction zones. Geochemistry, Geophysics, Geosystems 6(9), Q09006.

Leeder, M.R., 2011. Tectonic sedimentology: sediment systems deciphering global to local tectonics. Sedimentology 58(1), 2-56.

Leleu, S., Hartley, A.J., 2010. Controls on the stratigraphic development of the Triassic Fundy Basin, Nova Scotia: implications for the tectonostratigraphic evolution of Triassic Atlantic rift basins. Journal of the Geological Society 167(3), 437-454.

Li, W., Zhao, X., Xing, G., Cen, T., Tao, J., 2013a. Geochronology of the Betrital Zircons from Early Jurassic Sedimentary Rocks from the Dongkeng Basin and its Geological Implications. Geotectonica et Metallogenia 37(1), 78-86.

Li, W.X., Li, X.H., Li, Z.X., 2010a. Ca. 850 Ma bimodal volcanic rocks in northeastern Jiangxi Province, South China: Initial extension during the breakup of Rodinia? Am J Sci 310(9), 951-980.

Li, X.-h., 2000. Cretaceous magmatism and lithospheric extension in Southeast China. Journal of Asian Earth Sciences 18(3), 293-305.

Li, X.-H. et al., 2012a. The Early Permian active continental margin and crustal growth of the Cathaysia Block: In situ U–Pb, Lu–Hf and O isotope analyses of detrital zircons. Chemical Geology 328(0), 195-207.

Li, X.-H., Li, Z.-X., Li, W.-X., 2014a. Detrital zircon U–Pb age and Hf isotope constrains on the generation and reworking of Precambrian continental crust in the Cathaysia Block, South China: A synthesis. Gondwana Research 25(3), 1202-1215.

Li, X.-H., Li, Z.-X., Li, W.-X., Wang, X.-C., Gao, Y., 2013b. Revisiting the "C-type adakites" of the Lower Yangtze River Belt, central eastern China: In-situ zircon Hf–O isotope and geochemical constraints. Chemical Geology 345(0), 1-15.

Li, X.-H., McCulloch, M.T., 1998. Geochemical Characteristics of Cretaceous Mafic Dikes from Northern Guangdong, SE China: Age, Origin and Tectonic Significance. In: M.F.J. Flower, S.-L. Chung, C.-H. Lo, T.-Y. Lee (Eds.), Mantle Dynamics and Plate Interactions in East Asia. American Geophysical Union, Washington, D.C., pp. 405-419.

Li, X.H., Chen, Z., Liu, D.Y., Li, W.X., 2003a. Jurassic gabbro-granite-syenite suites from Southern Jiangxi province, SE China: Age, origin, and tectonic significance. International Geology Review 45(10), 898-921.

Li, X.H. et al., 2009a. Amalgamation between the Yangtze and Cathaysia Blocks in South China: Constraints from SHRIMP U-Pb zircon ages, geochemistry and Nd-Hf isotopes of the Shuangxiwu volcanic rocks. Precambrian Research 174(1-2), 117-128.

Li, X.H. et al., 2009b. Role of mantle-derived magma in genesis of early Yanshanian granites in the Nanling Range, South China: in situ zircon Hf-O isotopic constraints. Science in China Series D-Earth Sciences 52(9), 1262-1278.

Li, X.H. et al., 2007a. U-Pb zircon, geochemical and Sr-Nd-Hf isotopic constraints on age and origin of Jurassic I- and A-type granites from central Guangdong, SE China: A major igneous event in response to foundering of a subducted flat-slab? Lithos 96(1-2), 186-204.

Li, X.H., Li, Z.X., Li, W.X., Wang, Y., 2006a. Initiation of the Indosinian Orogeny in South China: Evidence for a Permian Magmatic Arc on Hainan Island. The Journal of Geology 114(3), 341-353.

Li, X.H., Li, Z.X., Li, W.X., Wang, Y.J., 2006b. Initiation of the Indosinian Orogeny in South China: Evidence for a Permian magmatic arc on Hainan Island. Journal of Geology 114(3), 341-353.

Li, Z.-X., 1998a. Tectonic history of the major East Asian lithospheric blocks since the mid-Proterozoic-A synthesis. In: M.F.J. Flower, S.L. Chung, C.H. Lo, T.Y. Lee (Eds.), Mantle Dynamics and Plate Interactions in East Asia. American Geophysical Union Series, pp. 221-243.

Li, Z.-X., 1998b. Tectonic history of the major East Asian lithospheric blocks since the mid-Proterozoic-A synthesis. American Geophysical Union Series 27, 221-243.

Li, Z.-X., Li, X.-H., 2007. Formation of the 1300-km-wide intracontinental orogen and postorogenic magmatic province in Mesozoic South China: A flat-slab subduction model. Geology 35(2), 179-182.

Li, Z.-X. et al., 2012b. Magmatic switch-on and switch-off along the South China continental margin since the Permian: Transition from an Andean-type to a Western Pacific-type plate boundary. Tectonophysics 532–535(0), 271-290.

Li, Z.-X. et al., 2010b. Magmatic and metamorphic events during the early Paleozoic Wuyi-Yunkai orogeny, southeastern South China: New age constraints and pressure-temperature conditions. Geological Society of America Bulletin 122(5-6), 772-793.

Li, Z.-X., Li, X.-H., Zhou, H., Kinny, P.D., 2002. Grenvillian continental collision in south China: New SHRIMP U-Pb zircon results and implications for the configuration of Rodinia. Geology 30(2), 163-166.

Li, Z.-X. et al., 2007b. Early history of the eastern Sibao Orogen (South China) during the assembly of Rodinia: New mica 40Ar/39Ar dating and SHRIMP U-Pb detrital zircon provenance constraints. Precambrian Research 159(1-2), 79-94.

Li, Z.X. et al., 2008. Assembly, configuration, and break-up history of Rodinia: A synthesis. Precambrian Research 160(1-2), 179-210.

Li, Z.X., Chen, H.L., Li, X.H., Zhang, F.Q., 2014b. Tectonics of the South China Block — Interpreting the Rock Record. Chinese Science Press, Beijing.

Li, Z.X. et al., 2003b. Geochronology of Neoproterozoic syn-rift magmatism in the Yangtze Craton, South China and correlations with other continents: evidence

for a mantle superplume that broke up Rodinia. Precambrian Research 122(1-4), 85-109.

Liu, B., Xu, X., 1994. Altas of Lithofacies and Palaeogeography of South China. Beijing, Science Press, 188 pp.

Liu, L. et al., 2010. The role of oceanic plateau subduction in the Laramide orogeny. Nature Geosci 3(5), 353-357.

Liu, X., Gao, S., Diwu, C., Ling, W., 2008. Precambrian crustal growth of Yangtze Craton as revealed by detrital zircon studies. American Journal of Science 308(4), 421-468.

Livaccari, R.F., Burke, K., Sengor, A.M.C., 1981. Was the Laramide orogeny related to subduction of an oceanic plateau? Nature 289(5795), 276-278.

Lopez-Blanco, M., 1993. Stratigraphy and sedimentary development of the Sant Llorenc del Munt fan-delta complex (Eocene, southern Pyrenean foreland basin, northeast Spain). In: L.E. Frostick, R.J. Steel (Eds.), Tectonics Controls and Signatures in Sedimentary Successions. Blackwell Scientific Publications, pp. 67-89.

Lowe, D.R., 1982. Sediment gravity flows; II, Depositional models with special reference to the deposits of high-density turbidity currents. JOURNAL OF SEDIMENTARY RESEARCH 52(1), 279-297.

Lucas, S.G., Tanner, L.H., Kozur, H.W., Weems, R.E., Heckert, A.B., 2012. The Late Triassic timescale: Age and correlation of the Carnian–Norian boundary. Earth-Science Reviews 114(1–2), 1-18.

Ludwig, K.R., 2008. User Manual for Isoplot/Ex Rev. 3.7: A Geochronological Toolkit for Microsoft Excel. Berkeley Geochronology Center Special Publication(4), 77 p.

Ludwig, K.R., 2009. SQUID 2: A User's Manual, rev. Berkeley Geochronology Center Special Publication(5), 110 p.

McCabe, P.J., 1984. Depositional Environments of Coal and Coal-Bearing Strata. In: R.A. Rahmani, R.M. Flores (Eds.), Sedimentology of Coal and Coal-Bearing Sequences. Blackwell Scientific Publications, Oxford, pp. 11-42.

McElwain, J.C., Beerling, D.J., Woodward, F.I., 1999. Fossil Plants and Global Warming at the Triassic-Jurassic Boundary. Science 285(5432), 1386-1390.

McElwain, J.C., Popa, M.E., Hesselbo, S.P., Haworth, M., Surlyk, F., 2007. Macroecological responses of terrestrial vegetation to climatic and

atmospheric change across the Triassic/Jurassic boundary in East Greenland. Paleobiology 33(4), 547-573.

McKenzie, D., 1981. The variation of temperature with time and hydrocarbon maturation in sedimentary basins formed by extension. Earth and Planetary Science Letters 55(1), 87-98.

Meng, L., Li, Z.-X., Chen, H., Li, X.-H., Wang, X.-C., 2012. Geochronological and geochemical results from Mesozoic basalts in southern South China Block support the flat-slab subduction model. Lithos 132–133(0), 127-140.

Miall, A.D., 1985. Architectural-element analysis: A new method of facies analysis applied to fluvial deposits. Earth-Science Reviews 22(4), 261-308.

Miall, A.D., 1996. The Geology of Fluvial Deposits. Spring, 582 pp.

Miall, A.D., 2010. Alluvial Deposits. In: N.P. James, R.W. Dalrymple (Eds.), Facies models 4. Geological Association of Canada, St John's, Newfoundland, pp. 105-137.

Mills, P.C., 1983. Genesis and diagnostic value of soft-sediment deformation structures--A review. Sedimentary Geology 35(2), 83-104.

Muto, T., Steel, R.J., 1997. Principles of regression and transgression; the nature of the interplay between accommodation and sediment supply. Journal of Sedimentary Research 67(6), 994-1000.

Pang, C.-J. et al., 2014. Stratigraphic evolution of a Late Triassic to Early Jurassic intracontinental basin in southeastern South China: A consequence of flat-slab subduction? Sedimentary Geology 302(0), 44-63.

Plummer, P.S., Gostin, V.A., 1981. Shrinkage cracks; desiccation or synaeresis? Journal of Sedimentary Research 51(4), 1147-1156.

Posamentier, H.W., Jervey, M.T., Vail, P.R., 1988. Eustatic Controls on Clastic Depostion I-Conceptual Framework. In: C.K. Wilgus et al. (Eds.), Sea-level Changes: An Integrated Approach. Society of Economic Paleontologists and Mineralogists, pp. 109-124.

Postma, G., 1990. An analysis of the variation in delta architecture. Terra Nova 2(2), 124-130.

Potter, C.J., Dubiel, R.F., Snee, L.W., Good, S.C., 1995. Eocene Extension of Early Eocene Lacustrine Strata in a Complexly Deformed Sevier-Laramide Hinterland, Northwest Utah and Northeast Nevada. Geology 23(2), 181-184.

Preto, N., Kustatscher, E., Wignall, P.B., 2010. Triassic climates - State of the art and perspectives. Palaeogeography Palaeoclimatology Palaeoecology 290(1-4), 1-10.

Price, G.D., 1999. The evidence and implications of polar ice during the Mesozoic. Earth-Science Reviews 48(3), 183-210.

Qian, L. et al., 1987. Mesozoic coal-bearing sequences in South China. China Coal Industry Publishing House, Beijing, 322 pp.

Qiu, Y.M., Gao, S., McNaughton, N.J., Groves, D.I., Ling, W., 2000. First evidence of >3.2 Ga continental crust in the Yangtze craton of south China and its implications for Archean crustal evolution and Phanerozoic tectonics. Geology 28(1), 11-14.

Ramos, V.A., Folguera, A., 2009. Andean flat-slab subduction through time. Geological Society, London, Special Publications 327(1), 31-54.

Rasmussen, E.S., 2004. The interplay between true eustatic sea-level changes, tectonics, and climatic changes: what is the dominating factor in sequence formation of the Upper Oligocene-Miocene succession in the eastern North Sea Basin, Denmark? Global and Planetary Change 41(1), 15-30.

Rasmussen, E.S., Lomholt, S., Andersen, C., Vejbæk, O.V., 1998. Aspects of the structural evolution of the Lusitanian Basin in Portugal and the shelf and slope area offshore Portugal. Tectonophysics 300(1–4), 199-225.

Reading, H.G., 1986. Facies. In: H.G. Reading (Ed.), Sedimentary Environment and Facies. Blackwell, Oxford, pp. 4-19.

Ren, J.S., 1991. On the Geotectonics of Southern China. Acta Geologica Sinica-English Edition 4(2), 111-136.

Ren, J.Y., Tamaki, K., Li, S.T., Junxia, Z., 2002. Late Mesozoic and Cenozoic rifting and its dynamic setting in Eastern China and adjacent areas. Tectonophysics 344(3-4), 175-205.

Renaut, R.W., Gierlowski-Kordesch, E.H., 2010. Lakes. In: N.P. James, R.W. Dalrymple (Eds.), Facies models 4. Geological Association of Canada, St John's, Newfoundland, pp. 541-575.

Schlager, W., 1993. Accommodation and supply—a dual control on stratigraphic sequences. Sedimentary Geology 86(1–2), 111-136.

Sdrolias, M., Müller, R.D., 2006. Controls on back-arc basin formation. Geochemistry, Geophysics, Geosystems 7(4), Q04016.

She, Z. et al., 2012. An Early Mesozoic transcontinental palaeoriver in South China: evidence from detrital zircon U–Pb geochronology and Hf isotopes. Journal of the Geological Society 169(3), 353-362.

Shu, L.S. et al., 2009. Mesozoic tectonic evolution of the Southeast China Block: New insights from basin analysis. Journal of Asian Earth Sciences 34(3), 376-391.

Sinclair, I.K., 1995. Transpressional inversion due to episodic rotation of extensional stresses in Jeanne d'Arc Basin, offshore Newfoundland. In: J.G. Buchanan, P.G. Buchanan (Eds.), Bains Inversion. Geological Society, London, Special Publications, pp. 249-271.

Sircombe, K.N., 2004. AgeDisplay: an EXCEL workbook to evaluate and display univariate geochronological data using binned frequency histograms and probability density distributions. Computers & Geosciences 30(1), 21-31.

Smith, G.A., 1994. Climatic influences on continental deposition during late-stage filling of an extensional basin, southeastern Arizona. Geological Society of America Bulletin 106(9), 1212-1228.

Stern, R.A., 2001. A new isotopic and trace-element standard for ion microprobe: preliminary thermal ionization mass spectrometry (TIMS) U–Pb and electron-microprobe data. Geological Survey of Canada, Radiogenic Age and Isotopic Studies(Report 14, Current Research 2001-F1), 1-7.

Stouthamer, E., Berendsen, H.J.A., 2007. Avulsion: The relative roles of autogenic and allogenic processes. Sedimentary Geology 198(3-4), 309-325.

Stratigraphy, I.C.o., 2012. International Chronostratigraphic Chart.

Sun, G., Meng, F.S., Qian, L., Ouyang, S., 1995. Triassic Floras. In: X. Li (Ed.), Fossil Floras of China Through the Geological Ages. Guangdong Science and Technology Press, Guangzhou, pp. 229-259.

Sun, S. et al., 1989. Mesozoic and Cenozoic sedimentary history of South China. AAPG Bulletin 73(10), 1247-1269.

Sun, T., 2006. A new map showing the distribution of granites in South China and its explanatory notes. Geological Bulletin of China 25(3), 332-335.

Sun, Y.-z., Zhu, G.-m., Liu, G.-f., Sheng, H.-b., 1980. Studies on lower Jurassic Ammonites from Kaiping-Enping Area, Guangdong. Acta Palaeontologica Sinica 19(2), 68-78.

Thomas, W.A., 2011. Detrital-zircon geochronology and sedimentary provenance. Lithosphere 3(4), 304-308.

Tian, Z.Y., Han, P., Xu, K.D., 1992. The Mesozoic Cenozoic East China Rift System. Tectonophysics 208(1-3), 341-363.

Ting, W.K., 1929. The orogenic movement in China. Bulletin of the Geological Society of China 8(1), 151-170.

Tong, J., Liu, Z., 2000. The Middle Triassic Straitgraphy and Sedimentary Paleogeography of South China. Albertiana 20, 33-42.

Torsvik, T.H., Van der Voo, R., Meert, J.G., Mosar, J., Walderhaug, H.J., 2001. Reconstructions of the continents around the North Atlantic at about the 60th parallel. Earth and Planetary Science Letters 187(1–2), 55-69.

Tucholke, B.E., Sawyer, D.S., Sibuet, J.-C., 2007. Breakup of the Newfoundland–Iberia rift. In: G.D. Karner, G. Manatschal, L.M. Pinheiro (Eds.), Imaging, Mapping and Modelling Continental Lithosphere Extension and Breakup. Geological Society, London, Special Publications, pp. 9-46.

Van Konijnenburg-Van Cittert, J.H.A., 2002. Ecology of some Late Triassic to Early Cretaceous ferns in Eurasia. Review of Palaeobotany and Palynology 119(1–2), 113-124.

Van Wagoner, J.C., Mitchum, R.M., Campion, K.M., Rahmanian, V.D., 1990. Siliciclastic sequence stratigraphy in well logs, cores, and outcrops: concepts for high-resolution correlation of time and facies, AAPG methods in exploration series, No. 7. Tulsa, OK (USA); American Association of Petroleum Geologists, 55 pp.

Vandenberghe, J., 2003. Climate forcing of fluvial system development: an evolution of ideas. Quaternary Science Reviews 22(20), 2053-2060.

Vandervoort, D.S., Schmitt, J.G., 1990. Cretaceous to early Tertiary paleogeography in the hinterland of the Sevier thrust belt, east-central Nevada. Geology 18(6), 567-570.

Vauchez, A., Barruol, G., Tommasi, A., 1997. Why do continents break-up parallel to ancient orogenic belts? Terra Nova 9(2), 62-66.

Volynets, E., Shorokhova, S., 2007. Late Triassic (Mongugai) flora of the Primorye region and its position among coeval floras of Eurasia. Russian Journal of Pacific Geology 1(5), 482-494.

Walker, T.R., 1967. Formation of Red Beds in Modern and Ancient Deserts. Geological Society of America Bulletin 78(3), 353-368.

Wan, Y. et al., 2010. Evolution of the Yunkai Terrane, South China: Evidence from SHRIMP zircon U–Pb dating, geochemistry and Nd isotope. Journal of Asian Earth Sciences 37(2), 140-153.

Wan, Y. et al., 2007. SHRIMP U–Pb zircon geochronology and geochemistry of metavolcanic and metasedimentary rocks in Northwestern Fujian, Cathaysia block, China: Tectonic implications and the need to redefine lithostratigraphic units. Gondwana Research 12(1–2), 166-183.

Wang, G.-s., He, F.-b., Zhu, W.-p., Ma, W.-p., 2009a. U-Pb Dating of Detrital Zircons from Late Triassic Wenbinshan Formation in Southwestern Fujian and Its Geological Significance. Geoscience 23(2), 246-255.

Wang, H., 1985. Altas of the Palaeogeography of China. Cartographic Publishing House, Beijing, 143 pp.

Wang, J., Li, Z.-X., 2003. History of Neoproterozoic rift basins in South China: implications for Rodinia break-up. Precambrian Research 122(1-4), 141-158.

Wang, L.-J., Griffin, W.L., Yu, J.-H., O'Reilly, S.Y., 2010a. Precambrian crustal evolution of the Yangtze Block tracked by detrital zircons from Neoproterozoic sedimentary rocks. Precambrian Research 177(1–2), 131-144.

Wang, N., 1977. Fish fossils in Coal-bearing Jurassic Strata in Hunan Province (1): Discovery and significance of the Pholidophoriformes in the Yumushan area, Hengyang city. Vertebrata Palasiatica 15(3), 177-183.

Wang, Q. et al., 2005a. Alkaline syenites in eastern Cathaysia (South China): link to Permian-Triassic transtension. Earth and Planetary Science Letters 230(3-4), 339-354.

Wang, X.-C., Li, X.-H., Li, W.-X., Li, Z.-X., 2007a. Ca. 825 Ma komatiitic basalts in South China: First evidence for >1500 {degrees}C mantle melts by a Rodinian mantle plume. Geology 35(12), 1103-1106.

Wang, X.-C., Li, X.-H., Li, W.-X., Li, Z.-X., 2009b. Variable involvements of mantle plumes in the genesis of mid-Neoproterozoic basaltic rocks in South China: A review. Gondwana Research 15(3-4), 381-395.

Wang, X.-C. et al., 2012. Episodic Precambrian crust growth: Evidence from U-Pb ages and Hf-O isotopes of zircon in the Nanhua Basin, central South China. Precambrian Research 222, 386-403.

Wang, X.-C., Li, Z.-X., Li, X.-H., Li, Q.-L., Zhang, Q.-R., 2011. Geochemical and Hf-Nd isotope data of Nanhua rift sedimentary and volcaniclastic rocks indicate a Neoproterozoic continental flood basalt provenance. Lithos 127(3-4), 427-440.

Wang, X.-L. et al., 2007b. Detrital zircon geochronology of Precambrian basement sequences in the Jiangnan orogen: Dating the assembly of the Yangtze and Cathaysia Blocks. Precambrian Research 159(1–2), 117-131.

Wang, X.C. et al., 2008. The Bikou basalts in the northwestern Yangtze block, South China: Remnants of 820-810 Ma continental flood basalts? Geological Society of America Bulletin 120(11-12), 1478-1492.

Wang, Y.-G., Smith, P.L., 1986. Sinemurian (Early Jurassic) Ammonite Fauna from the Guangdong Region of Southern China. Journal of Paleontology 60(5), 1075-1085.

Wang, Y., Cao, Z., Thévenard, F., 2005b. Additional data on Todites (Osmundaceae) from the Lower Jurassic—with special references to the paleogeographical and stratigraphical distributions in China. Geobios 38(6), 823-841.

Wang, Y., Fan, W., Peng, T., Guo, F., 2005c. Elemental and Sr–Nd isotopic systematics of the early Mesozoic volcanic sequence in southern Jiangxi Province, South China: petrogenesis and tectonic implications. International Journal of Earth Sciences 94(1), 53-65.

Wang, Y., Fan, W., Zhang, G., Zhang, Y., 2013. Phanerozoic tectonics of the South China Block: Key observations and controversies. Gondwana Research 23(4), 1273-1305.

Wang, Y., Li, S., 1983. A survey of the Jurassic System of China. Canadian Journal of Earth Sciences 20(11), 1646-1656.

Wang, Y., Mosbrugger, V., Zhang, H., 2005d. Early to Middle Jurassic vegetation and climatic events in the Qaidam Basin, Northwest China. Palaeogeography, Palaeoclimatology, Palaeoecology 224(1–3), 200-216.

Wang, Y. et al., 2010b. Tectonic setting of the South China Block in the early Paleozoic: Resolving intracontinental and ocean closure models from detrital zircon U-Pb geochronology. Tectonics 29(6), TC6020.

Wang, Y., Zhang, Y., Fan, W., Peng, T., 2005e. Structural signatures and 40Ar/39Ar geochronology of the Indosinian Xuefengshan tectonic belt, South China Block. Journal of Structural Geology 27(6), 985-998.

Ward, P.D., Montgomery, D.R., Smith, R., 2000. Altered River Morphology in South Africa Related to the Permian-Triassic Extinction. Science 289(5485), 1740-1743.

Wells, M.L., Hoisch, T.D., 2008. The role of mantle delamination in widespread Late Cretaceous extension and magmatism in the Cordilleran orogen, western United States. Geological Society of America Bulletin 120(5-6), 515-530.

Winfrey, W.M., 1960. Stratigraphy, Correlation, and Oil Potential of the Sheep Pass Formation, East-Central Nevada, Intermountain Association of Petroleum Geologists Eleventh Annual Field Conference Salt Lake City, Utah, pp. 126-132.

Wingate, F.H., 1983. Palynology and Age of the Elko Formation (Eocene) near Elko, Nevada. Palynology 7(ArticleType: primary_article / Full publication date: 1983 / Copyright © 1983 American Association of Stratigraphic Palynologists, Inc.), 93-132.

Wu, L., Jia, D., Li, H., Deng, F., Yiquan, L., 2010. Provenance of detrital zircons from the late Neoproterozoic to Orovician sandstones of South China: implications fro its continental affinity. Geological Magazine 147(6), 974-980.

Xie, C. et al., 2006. Identification of Hercynian shoshonitic intrusive rocks in central Hainan Island and its geotectonic implications. Chinese Science Bulletin 51(20), 2507-2519.

Xie, X., Heller, P.L., 2009. Plate tectonics and basin subsidence history. Geological Society of America Bulletin 121(1-2), 55-64.

Xu, X.S. et al., 2007. The crust of Cathaysia: Age, assembly and reworking of two terranes. Precambrian Research 158(1-2), 51-78.

Xu, Z.J., Cheng, R.H., Wang, L.L., Zhang, L., Li, F., 2010. Elemental geochemical characteristics of tuffaceous sediments and tectonic setting of Tangxia Formation of Middle Jurassic in Gongguan, Guangdong Province. Acta Petrologica Sinica 26(1), 352-360.

Yan, Y., Hu, X.-q., Lin, G., Santosh, M., Chan, L.-S., 2011. Sedimentary provenance of the Hengyang and Mayang basins, SE China, and implications for the Mesozoic topographic change in South China Craton: Evidence from detrital zircon geochronology. Journal of Asian Earth Sciences 41(6), 494-503.

Yang, W., Kominz, M.A., Major, R.P., 1998. Distinguishing the roles of autogenic versus allogenic processes in cyclic sedimentation, Cisco Group (Virgilian and Wolfcampian), north-central Texas. Geological Society of America Bulletin 110(10), 1333-1353.

Yang, Z., He, B., 2013. Transformation of Jurassic Tectonic COnfiguration of South China Block: Evidence from U-Pb Ages of Detrital Zircons. Geotectonica et Metallogenia 37(4), 580-591.

Yao, J., Shu, L., Santosh, M., 2011. Detrital zircon U–Pb geochronology, Hf-isotopes and geochemistry—New clues for the Precambrian crustal evolution of Cathaysia Block, South China. Gondwana Research 20(2–3), 553-567.

Yin, Z.-X. et al., 1964. The age relationships of the marine Lower Liassic of Guang-dong. Scientia Geologica Sinica 5(3), 203-210 (in Chinese with English abstract).

Yu, J.-H. et al., 2010a. Components and episodic growth of Precambrian crust in the Cathaysia Block, South China: Evidence from U-Pb ages and Hf isotopes of zircons in Neoproterozoic sediments. Precambrian Research 181(1-4), 97-114.

Yu, J.-H. et al., 2008. Where was South China in the Rodinia supercontinent?: Evidence from U–Pb geochronology and Hf isotopes of detrital zircons. Precambrian Research 164(1–2), 1-15.

Yu, J.-H. et al., 2010b. Components and episodic growth of Precambrian crust in the Cathaysia Block, South China: Evidence from U–Pb ages and Hf isotopes of zircons in Neoproterozoic sediments. Precambrian Research 181(1–4), 97-114.

Yu, J.-H. et al., 2009. A Paleoproterozoic orogeny recorded in a long-lived cratonic remnant (Wuyishan terrane), eastern Cathaysia Block, China. Precambrian Research 174(3–4), 347-363.

Yu, X.Q. et al., 2010c. The Early Jurassic tectono-magmatic events in southern Jiangxi and northern Guangdong provinces, SE China: Constraints from the SHRIMP zircon U-Pb dating. Journal of Asian Earth Sciences 39(5), 408-422.

Zhang, R., 1985. The general description of regional stratigraphy of China: The central South China region. In: S.-e. Wang, Z. Cheng, N. Wang (Eds.), The Jurassic system of China. Geological Publishing House, Beijing, China, pp. 189-204.

Zhang, S.B. et al., 2006a. Zircon isotope evidence for >= 3.5 Ga continental crust in the Yangtze craton of China. Precambrian Research 146(1-2), 16-34.

Zhang, S.B. et al., 2006b. Zircon U-Pb age and Hf-O isotope evidence for Paleoproterozoic metamorphic event in South China. Precambrian Research 151(3-4), 265-288.

Zhao, J.-H., Zhou, M.-F., Yan, D.-P., Zheng, J.-P., Li, J.-W., 2011. Reappraisal of the ages of Neoproterozoic strata in South China: No connection with the Grenvillian orogeny. Geology 39(4), 299-302.

Zhou, J.-C., Wang, X.-L., Qiu, J.-S., 2009. Geochronology of Neoproterozoic mafic rocks and sandstones from northeastern Guizhou, South China: Coeval arc magmatism and sedimentation. Precambrian Research 170(1–2), 27-42.

Zhou, T.-s., Zhou, H.-q., 1983. Triassic Non-Marine Strata and Flora of China. Acta Geoscientica Sinica 5(1), 95-110.

Zhou, X.M., Li, W.X., 2000. Origin of Late Mesozoic igneous rocks in Southeastern China: implications for lithosphere subduction and underplating of mafic magmas. Tectonophysics 326(3-4), 269-287.

Zhou, X.M., Sun, T., Shen, W.Z., Shu, L.S., Niu, Y.L., 2006. Petrogenesis of Mesozoic granitoids and volcanic rocks in South China: A response to tectonic evolution. Episodes 29(1), 26-33.

Zhou, Z., 1989. Late Triassic Plants from Shaqiao Hengyan, Hunan province. Palaeontologia Cathayana 0(4), 131-197.

Zhou, Z.Y., 1995. Jurassic Floras. In: X. Li (Ed.), Fossil Floras of China Through the Geological Ages. Guangdong Science and Technology Press, Guangzhou, pp. 343-410.

Zhu, K.-Y., Li, Z.-X., Xu, X.-S., Wilde, S.A., 2013. Late Triassic melting of a thickened crust in southeastern China: Evidence for flat-slab subduction of the Paleo-Pacific plate Journal of Asian Earth Sciences 74(25), 265-279.

Zhu, R.-X., Yang, J.-H., Wu, F.-Y., 2012. Timing of destruction of the North China Craton. Lithos 149(0), 51-60.

Zhu, W.-G. et al., 2010. The early Jurassic mafic-ultramafic intrusion and A-type granite from northeastern Guangdong, SE China: Age, origin, and tectonic significance. Lithos 119(3-4), 313-329.

Zi, J.-W. et al., 2012. Generation of Early Indosinian enriched mantle-derived granitoid pluton in the Sanjiang Orogen (SW China) in response to closure of the Paleo-Tethys. Lithos 140–141(0), 166-182.

Every reasonable effort has been made to acknowledge the owners of copyright material. I would be pleased to hear from any copyright owner who has been omitted or incorrectly acknowledged.

Chongjin Pang

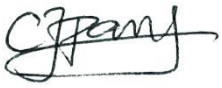

Date: 21-03-2014

Appendices

This chapter has been removed due to copyright restrictions.

This chapter has been removed due to copyright restrictions.

This chapter has been removed due to copyright restrictions.

This chapter has been removed due to copyright restrictions.

This chapter has been removed due to copyright restrictions.

This chapter has been removed due to copyright restrictions.

This chapter has been removed due to copyright restrictions.

This chapter has been removed due to copyright restrictions.

This chapter has been removed due to copyright restrictions.

This chapter has been removed due to copyright restrictions.

This chapter has been removed due to copyright restrictions.

This chapter has been removed due to copyright restrictions.

This chapter has been removed due to copyright restrictions.

This chapter has been removed due to copyright restrictions.

This chapter has been removed due to copyright restrictions.

This chapter has been removed due to copyright restrictions.

This chapter has been removed due to copyright restrictions.

This chapter has been removed due to copyright restrictions.

This chapter has been removed due to copyright restrictions.

This chapter has been removed due to copyright restrictions.

This chapter has been removed due to copyright restrictions.

This chapter has been removed due to copyright restrictions.

This chapter has been removed due to copyright restrictions.

This chapter has been removed due to copyright restrictions.

This chapter has been removed due to copyright restrictions.

This chapter has been removed due to copyright restrictions.

This chapter has been removed due to copyright restrictions.

This chapter has been removed due to copyright restrictions.

This chapter has been removed due to copyright restrictions.

This chapter has been removed due to copyright restrictions.

This chapter has been removed due to copyright restrictions.

This chapter has been removed due to copyright restrictions.

This chapter has been removed due to copyright restrictions.

This chapter has been removed due to copyright restrictions.

This chapter has been removed due to copyright restrictions.

This chapter has been removed due to copyright restrictions.

This chapter has been removed due to copyright restrictions.

This chapter has been removed due to copyright restrictions.

This chapter has been removed due to copyright restrictions.

This chapter has been removed due to copyright restrictions.

This chapter has been removed due to copyright restrictions.

This chapter has been removed due to copyright restrictions.

This chapter has been removed due to copyright restrictions.

This chapter has been removed due to copyright restrictions.

This chapter has been removed due to copyright restrictions.

This chapter has been removed due to copyright restrictions.

This chapter has been removed due to copyright restrictions.

This chapter has been removed due to copyright restrictions.

This chapter has been removed due to copyright restrictions.

Appendix Copyright Clearance

Statement of Individual Contributions to Published Papers

I, **Chongjin Pang**, contributed to all aspects of research including, but not limit to, primary data collection, data analysis, data interpretation, figure drawing, and writing for the publication of the paper entitled:

"Stratigraphic evolution of a Late Triassic to Early Jurassic intracontinental basin in southeastern South China: A consequence of flat-slab subduction?" (*Sedimentary Geology*, in-press 2014).

Chongjin Pang

Date: 21-03-2014

A realistic breakdown of the contribution by each author is as follows:

Chongjin Pang 70%

Bryan Krapež 10%

Zheng-Xiang Li 5%

Yi-Gang Xu 5%

Hai-Quan Liu 5%

Jun Cao 5%

I, as co-author and supervisor to Chongjin, endorse that the level of contributions indicated above are accurate.

Bryan Krapež

Date: 21-03-2014

I, as co-author and supervisor to Chongjin, endorse that the level of contributions indicated above are accurate. Furthermore, I endorse that the level of contribution from Yi-Gang Xu, Hai-Quan Liu and Jun Cao (Who is not contactable at the time of submission of this thesis) indicated above is accurate.

Zheng-Xiang Li

Date: 21-03-2014